NASA TECHNICAL NOTE

NASA TN D-3946

NASA TN D-3946

INVESTIGATION OF METHODS FOR PREDICTING FLOW IN THE SHOCK LAYER OVER BODIES AT SMALL ANGLES OF ATTACK

by William F. Gallo and John V. Rakich

Ames Research Center
Moffett Field, Calif.

NATIONAL AERONAUTICS AND SPACE ADMINISTRATION • WASHINGTON, D. C. • MAY 1967

NASA TN D-3946

INVESTIGATION OF METHODS FOR PREDICTING FLOW IN THE SHOCK LAYER OVER BODIES AT SMALL ANGLES OF ATTACK

By William F. Gallo and John V. Rakich

Ames Research Center
Moffett Field, Calif.

NATIONAL AERONAUTICS AND SPACE ADMINISTRATION

For sale by the Clearinghouse for Federal Scientific and Technical Information
Springfield, Virginia 22151 – CFSTI price $3.00

INVESTIGATION OF METHODS FOR PREDICTING FLOW IN THE SHOCK LAYER OVER BODIES AT SMALL ANGLES OF ATTACK

By William F. Gallo and John V. Rakich

Ames Research Center

SUMMARY

Two theoretical methods for predicting the flow field about axisymmetric bodies at small angles of attack are studied. The methods, the linearized characteristics method and the equivalent body method, are compared with experimental data for a blunted cone, an ogive cylinder, and an X-15 airplane model. Each theory was found superior in certain flow regions, neither being superior in all cases.

The linearized characteristic theory was found to be useful for predicting the flow fields about bodies of higher fineness ratio, such as an ogive cylinder and the X-15 at small angles of attack. Of particular interest was its ability to provide circumferential variations of certain flow quantities, especially flow angle, for bodies at angle of attack. Pressures were not predicted as well as flow angle and Mach number, however, for the limited cases studied. In regions dominated by blunt nose effects the linearized characteristic method did not agree well with experiment although a modification to the method improved the agreement close to the nose (less than 4 nose radii). The equivalent body method agreed well with experiment in this nose region and in regions further downstream dominated by the effects of the blunt nose (about 16 radii). The equivalent body method, however, is restricted in the present report to the plane of flow symmetry.

Additional theoretical predictions of parameters of interest to the X-15 flight test program are included. The parameters investigated are local Mach number, flow angle, and pitot pressure for three different free-stream Mach numbers and at angles of attack up to 10°.

INTRODUCTION

In design studies of hypersonic aircraft with airbreathing propulsion systems, the engine inlet is often well aft on the body. An inlet in this position would generally be completely in the shock layer, where the flow field is nonuniform, particularly at angle of attack. Theoretical predictions of these shock-layer flow fields are important in assessing the operating environment and in designing inlets.

Although the most accurate and complete method of calculating angle-of-attack effects in the shock layer would be to utilize a truly three-dimensional method of characteristics solution (refs. 1-3), it is often

necessary to use a simplified approach. This study, therefore, investigates two simplified methods, a linearized characteristics method and an equivalent body method, to predict the flow in the shock layer over bodies at angle of attack.

There are standard computer programs for applying method of characteristics to axisymmetric bodies at zero angle of attack (e.g., refs. 4,5). The linearized method of characteristics (refs. 6, 7) predicts flow at small angles of attack by perturbing the basic method of characteristics for axisymmetric flow and neglecting terms proportional to the square of angle of attack and higher. Another method, termed for purposes of discussion an equivalent body method, also makes use of the method of characteristics for axisymmetric flow. This method includes some of the nonlinear terms neglected by the linearized characteristics method, but completely neglects the crossflow velocity which is a first-order term. Both of these methods have previously been applied only to the calculation of surface pressures and resultant forces. This study is undertaken to investigate the applicability of these methods to the flow in the layer between the shock and the body (i.e., shock layer).

A secondary purpose of this study is to present the theoretical results from the linearized characteristics method for the flow region near the aft underside of the X-15 fuselage where an experimental scramjet engine is to be mounted. Local Mach number, pitot pressure, and flow angle are presented at angles of attack of -3°, 0°, 5°, and 10° and free-stream Mach numbers of 4, 6, and 8.

SYMBOLS

a speed of sound

C_p pressure coefficient, $\frac{p - p_\infty}{q_\infty}$

h enthalpy

H total enthalpy

j index for number of degrees of symmetry; $j = 0$ for plane flow, and $j = 1$ for axisymmetric flow

M Mach number

p pressure

q dynamic pressure, $\frac{1}{2}\rho V^2$

R nose radius

S entropy

u	velocity component in x direction
V	velocity
w	velocity component in circumferential direction (crossflow velocity)
x,r,z	cylindrical coordinates
x,y,z	rectangular coordinates
s,n,t	streamline coordinates (see fig. 1)
$\vec{s},\vec{n},\vec{t}$	unit vectors, streamline coordinates
α	angle of attack
β	$\sqrt{M^2 - 1}$
γ	specific heat ratio
ϵ	transformed flow angle (see eq. (20))
η	distance normal from the body surface
θ	flow angle measured from x axis in meridional plane
ξ	right-running characteristic coordinate
ρ	density
φ	crossflow angle
Φ	azimuthal coordinate, cylindrical coordinate system
Ψ	stream function

Subscripts

B	body conditions
m	coordinates fixed with the meridional plane (fig. 1)
t	total
∞	free stream
0	zero-order variable from solution of axisymmetric flow
1	first-order perturbation variable (see eq. (6))

THEORY

To illustrate the nature of the approximate methods used in this report it is pertinent to consider the inviscid gas dynamic equations for general three-dimensional flow. These equations are given below, in the form derived in reference 6, in terms of streamline coordinates s,n,t as independent variables (see fig. 1). The dependent variables in the momentum equations are the pressure, p, and the flow angles, θ and φ; continuity of mass is automatically satisfied by these equations.

Momentum equations:

Streamwise ($\vec{s}$)

$$\frac{\beta^2}{\rho V^2}\frac{\partial p}{\partial s} + \cos\varphi\,\frac{\partial \theta}{\partial n} + \frac{\partial \varphi}{\partial t} + j\,\frac{\cos\varphi\,\sin\theta}{r} = 0 \tag{1}$$

Radial-normal ($\vec{n}$)

$$\frac{1}{\rho V^2}\frac{\partial p}{\partial n} + \cos\varphi\,\frac{\partial \theta}{\partial s} - j\,\frac{\sin^2\varphi\,\cos\theta}{r} = 0 \tag{2}$$

Cross-normal ($\vec{t}$)

$$\frac{1}{\rho V^2}\frac{\partial p}{\partial t} + \frac{\partial \varphi}{\partial s} + j\,\frac{\sin\varphi\,\sin\theta}{r} = 0 \tag{3}$$

Entropy conservation:

$$\frac{\partial S}{\partial s} = 0 \tag{4}$$

Energy:

$$h + \frac{V^2}{2} = H = \text{constant} \tag{5}$$

The foregoing equations must be supplemented by equations of state relating the variables p, ρ, h, and S. It is only for the equations of state that the distinction between real and perfect gas must be made. Equations (1) - (5) therefore are applicable to equilibrium real-gas flow as well as to perfect gas.

The Linearized Characteristics Method

Description.- This method, which is more fully described in reference 6, determines the first derivative or linear change of the flow parameters with angle of attack, evaluated at zero angle of attack. The circumferential variation of the dependent variables is approximated by a trigonometric function. The crossflow parameters which vanish in the plane of symmetry vary as the sine, and the remaining parameters vary as the cosine. The following equations, then, express the variation of flow parameters as a function of angle of attack and circumferential angle.

$$\left.\begin{aligned} p &= p_o + p_1 \alpha \cos \Phi \\ \rho &= \rho_o + \rho_1 \alpha \cos \Phi \\ S &= S_o + S_1 \alpha \cos \Phi \\ h &= h_o + h_1 \alpha \cos \Phi \\ \varphi &= \varphi_1 \alpha \sin \Phi \\ &\text{etc.} \end{aligned}\right\} \tag{6}$$

The perturbation quantities p_1, ρ_1, etc. determine the slope of their respective quantities at zero angle of attack, that is, $(\partial p/\partial \alpha)_{\alpha=0} = p_1 \cos \Phi$. Substituting the series expansions (6) into equations (1) - (5), and retaining only terms of order α, one obtains the following set of perturbation equations.

Momentum:

$\vec{s}$ component

$$\frac{\beta_o^2}{\rho_o V_o^2} \frac{\partial p_1}{\partial s_o} + \frac{\partial \theta_1}{\partial n_o} = F(p_1, \theta_1, \varphi_1, h_1) \tag{7}$$

$\vec{n}$ component

$$\frac{1}{\rho_o V_o^2} \frac{\partial p_1}{\partial n_o} + \frac{\partial \theta_1}{\partial s_o} = G(p_1, \theta_1, \varphi_1, h_1) \tag{8}$$

$\vec{t}$ component

$$\frac{\partial \varphi_1}{\partial s_o} = \left(\frac{1}{\rho_o V_o^2} \frac{\partial p_o}{\partial s_o} - j \frac{\sin \theta_o}{r} \right) \varphi_1 + j \frac{p_1}{r \rho_o V_o^2} \tag{9}$$

where F and G are complicated expressions involving the perturbation variables linearly (see ref. 6).

Entropy:

$$\frac{\partial S_1}{\partial s_o} = -\theta_1 \frac{dS_o}{dn_o} \tag{10}$$

Energy:

$$h_1 + V_o V_1 = 0 \tag{11}$$

It is seen that these perturbation equations retain the fundamental three-dimensional nature of the flow over a body at angle of attack. The cross-normal ($\vec{t}$) component of momentum is coupled with the other equations and describes the variation of crossflow angle φ along the streamline s_o.

Second-order terms.- The perturbation equations neglect terms of order (α^2) and, therefore, apply only when the flow quantity variations are nearly linear with angle of attack. For some flows there will be limited regions in which the second-order terms are not negligible even for small angles of attack; the following sections will attempt to show, by comparison with data, where such regions may be encountered.

One cannot, in general, evaluate the relative magnitude of first- and second-order terms except by a more exact solution. However, it is possible to include some second-order terms in the calculation of pitot pressure and Mach number. This is accomplished by including the crossflow velocity w in the following way:

$$V^2 = (V_o + \alpha V_1 \cos \Phi)^2 + (\alpha w_1 \sin \Phi)^2 \tag{12}$$

where

$$w_1 = V_o \varphi_1$$

The velocity given by equation (12) and the linearized pressure and density

$$p = p_o + \alpha p_1 \cos \Phi \tag{13}$$

$$\rho = \rho_o + \alpha \rho_1 \cos \Phi \tag{14}$$

were used to calculate pitot pressure. Jump conditions across a normal shock and the subsequent isentropic compression are then computed with the aid of equilibrium real gas tables. Thus, to the extent of including velocity from equation (12), certain second-order effects are included in the pitot pressure.

Mach number can also be calculated with the aid of equations (12), (13), and (14), and with the speed of sound obtained from real gas tables. For a perfect gas, however, explicit dependence on pressure and density can be eliminated by the equation

$$a^2 = \gamma \frac{p}{\rho} = (\gamma - 1)h \quad \text{(perfect gas)} \tag{15}$$

Substituting (15) into the general form of the energy equation (5), one obtains the following expression for Mach number as a function of velocity.

$$M^2 = \frac{2/(\gamma-1)}{2H/V^2-1} \quad \text{(perfect gas)} \tag{16}$$

Thus, if V^2 from equation (12) is used, the second-order (α^2) terms are partially included. Equation (16) was used in calculating the Mach number distributions to be presented in a later section of the report.

Entropy perturbations.- In the course of this study it was found that certain quantities, derived from the entropy, were subject to sizable numerical errors as the calculations were extended far downstream on relatively slender bodies. To eliminate this source of error, it was found necessary to revise the numerical algorithm used in reference 6 for calculating the entropy perturbation (eq. (10)). While the original scheme provided exact results on the body, it did not adequately account for the discontinuous nature of the entropy layer for inviscid hypersonic flow. A new method for calculating the entropy perturbation was therefore developed and is described in the appendix. The new method makes use of the stream function in a manner similar to that described in reference 8 and permits the flow perturbations outside the entropy layer to be determined accurately. However, the thin layer near the body surface, which is commonly called the entropy layer, must be recognized as a region where the present linearized perturbation theory does not apply. This restriction becomes academic in many instances, since the viscous boundary layer tends to engulf the entropy layer.

Equivalent Body Method

One approach employed to obtain surface pressures of simple bodies at angle of attack has been to apply the method of characteristics to an equivalent shaped axisymmetric body at zero angle of attack which has one surface

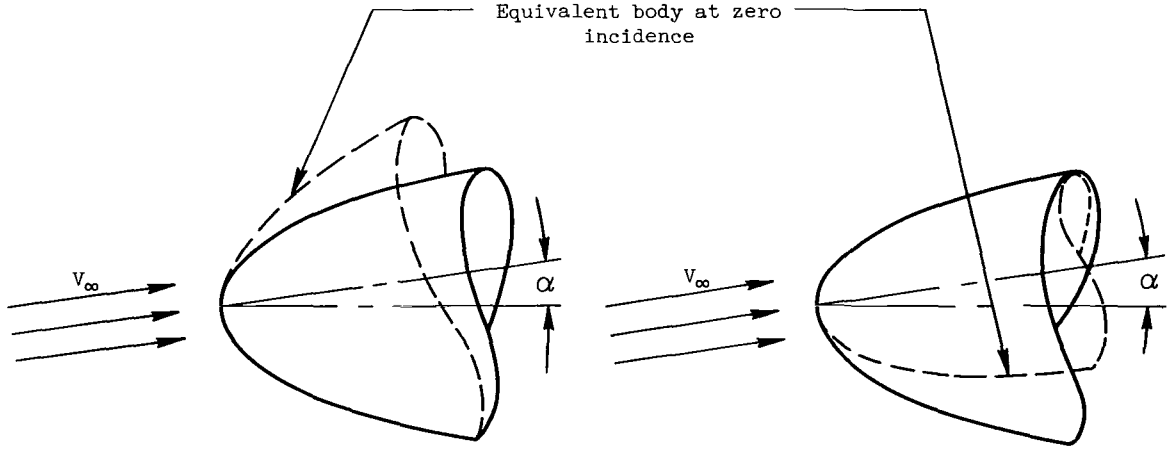

Sketch (a)

contour coincident with the inclined body. The pressures along the coincident contour line (e.g., the windward surface and plane) are then assumed to be the same as those obtained by the method of characteristics for the equivalent body at $\alpha = 0^{o}$. (For example, see refs. 5 and 9.) In like manner another equivalent body is used to approximate the flow in the leeward plane.

To determine what effect crossflow has on the applicability of the equivalent body method, the general equations of motion (1) - (5) are examined.

The assumption of an axisymmetric flow is equivalent to setting the crossflow angle $\varphi = 0$. Equations (1) and (2) then reduce to

$$\frac{\beta^2}{\rho V^2}\frac{\partial p}{\partial s} + \left(\frac{\partial \theta}{\partial n} + j\,\frac{\sin\theta}{r}\right) = 0 \tag{17}$$

$$\frac{1}{\rho V^2}\frac{\partial p}{\partial n} + \frac{\partial \theta}{\partial s} = 0 \tag{18}$$

These equations are now decoupled from equation (3) which described the circumferential momentum balance. In the plane of symmetry ($\Phi = 0,\pi$) the boundary conditions result in setting $\varphi = 0$; therefore, it is seen that only the term $\partial\varphi/\partial t$ in equation (1) is neglected in applying the equivalent body method. Thus in order to calculate the correct pressure gradient it is necessary that

$$\frac{\partial \varphi}{\partial t} \ll \left(\frac{\partial \theta}{\partial n} + j\,\frac{\sin\theta}{r}\right) \tag{19}$$

This approximation is similar to that used in reference 10 in deriving the shock expansion method. However, in shock expansion theory, disturbances reflected from the shock wave are neglected. These reflected waves are included in the present equivalent body method.

Away from the plane of symmetry the error of the equivalent body method is more difficult to assess since $\varphi \neq 0$, and the streamlines no longer lie in meridional planes. However, the method may still have some applicability provided $\cos\varphi \simeq 1$ and $\sin^2\varphi \simeq 0$. As is done in the linearized characteristic method, a cosine circumferential pressure variation could then be assumed. With this assumption equation (3), which was uncoupled in the equivalent body approximation, could then be integrated to give the crossflow angle φ. This modification to the method was not attempted at this time.

RESULTS AND DISCUSSION

Blunted 15° Cone

The two methods described above were applied to a spherically blunted 15° cone for which there are previously reported wind tunnel results (ref. 5). In figure 2, pitot pressure data for two body stations at $M_\infty = 10.6$ are compared with both the equivalent body method and the linearized method of characteristics. A modification to the linear method also shown is discussed later.

In figure 2 the equivalent body method shows agreement at $\alpha = 5^\circ$ to the same degree as exhibited by the method of characteristics at $\alpha = 0^\circ$.[1] The disagreement between data and the method of characteristics at $\alpha = 0^\circ$ and $x/R = 16.67$ (fig. 2(b)) is considered minor. Thus, for the prediction of pitot pressure in the shock layer of blunt-nosed bodies in the plane of symmetry the equivalent body method may be expected to yield reasonable results.

The linearized method of characteristics does not agree with the data at small values of x/R where nose bluntness effects predominate (see fig. 2). The disagreement may be attributed to two separate phenomena, one dominant in the unperturbed nose region (see sketch (b)), and one applicable in the

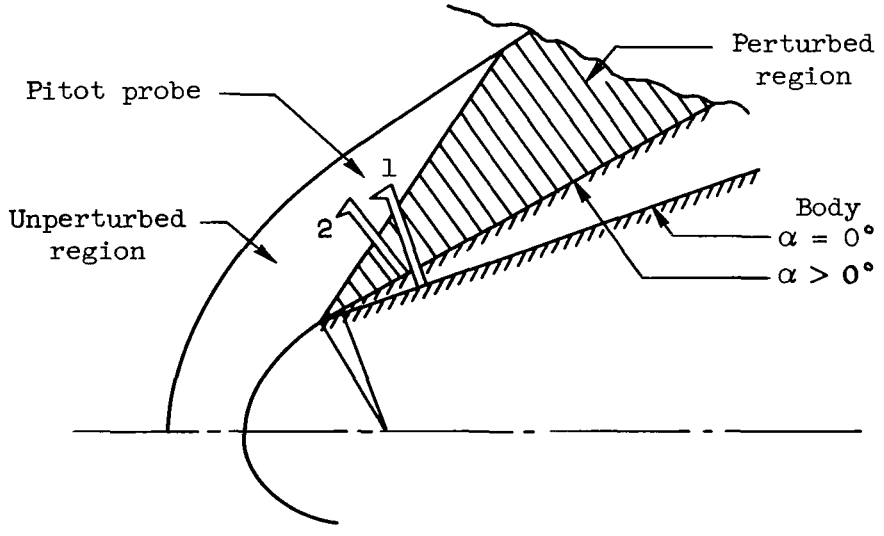

Sketch (b)

[1]The linearized method of characteristics is equivalent to the basic method of characteristics at zero angle of attack, since the p_1 term in equation (6) disappears when α becomes zero.

perturbed region. Near the nose two perturbations are calculated: First, perturbation parameters are calculated at points in the flow fixed with the wind axis (point 1, sketch (b)). Second, the wind-axis perturbations are then transformed to body axes (point 2) by means of a linearized coordinate rotation.

Near the spherical nose, wind-axis perturbations are zero. Thus much of the flow is not affected by a change in angle of attack. In this region, only the linearized rotation contributes to the theory.

It is not necessary to assume that the coordinate rotation is small, since the wind axis perturbations can be calculated at the exact coordinate location, that is, at point 2 in sketch (b). The theory will then properly give the axisymmetric zero angle-of-attack result in the unperturbed region near the spherical nose, and will also give a better approximation in the shaded region just downstream from the nose. The results of this calculation are shown in figure 2(a) as the modified linear characteristics method. Agreement with experiment is significantly improved by this modification. Farther downstream this modification, cannot be used, however, because the relatively large translation of the body in comparison with the shock-layer thickness places the body outside the original shock layer.

At the downstream station ($x/R = 16.67$, fig. 2(b)) the poor agreement between experiment and the linearized characteristics theory is attributed to the large entropy gradients produced by the blunt nose, which make the variations of pitot pressure highly nonlinear with angle of attack. Evidence of this may be seen in figure 3 which shows that on the compression or windward side, the experimental data exhibit a thinning or squeezing down of the entropy layer. It can be seen that at a given location in the shock layer the variation of pitot pressure with angle of attack may be extremely nonlinear. The linearized characteristics method cannot be expected to yield accurate results in these regions.

Ogive Cylinder

The linearized characteristics method describes a consistent first-order circumferential variation of all flow parameters including crossflow. This theory was compared with the data obtained from the wind-tunnel tests of an ogive cylinder of fineness ratio 8.5 at $M = 3.5$ reported in reference 11 (see fig. 4). Figures 5 to 7 show these comparisons of the circumferential distribution of pitot pressure, Mach number, and a transformed flow angle (see eq. (20)) at angles of attack of 5° and 10° at one longitudinal body station ($x/r = 15$) and three radial locations ($\eta/r = 0.39, 0.59, 0.79$), all relatively close to the body.[2]

[2]Communication with the author of reference 11 confirmed a typographical error which has been corrected in the Mach number data shown in figure 6(b).

The variations in the pitot pressure data at $\alpha = 10^{\circ}$ suggest a cosine dependency (fig. 5). Although the original linear theory of reference 6 assumed a cosine dependency, the present modification by including the crossflow velocity to obtain higher order terms, no longer has a cosine dependency (see eq. (12)). The crossflow velocity depends on a sine relationship, which, added to the other two velocity components, changes the circumferential dependency and causes a slight hump in the theoretical curves (see fig. 5).

Further insight into the theoretical circumferential distribution may be noted from figure 8, which shows the variation, normal to the surface, of pitot pressure, Mach number, and flow angle θ for various circumferential positions. It may be seen that the theoretical pitot pressures are relatively independent of circumferential position in the region near the body where the data were taken ($\eta/r = 0.39, 0.59, 0.79$). In this region the linear angle-of-attack perturbation is very small. For η/r greater than about 1.6, however, the linear perturbations are larger, and the circumferential distribution is more nearly a cosine. The circumferential variation in Mach number shows crossovers similar to the pitot pressure but less severe.

Figure 8 shows the flow angle has a strong circumferential variation even near the body. Because of the strong dependence on crossflow angle φ (see eq. (20)), the transformed flow angle has a circumferential variation which is nearly sinusoidal.

It should be noted that in figures 5 and 6 the 10° data on the leeward side ($\Phi \simeq 20^{\circ}$-40° on the figures) suggest a separated region associated with the shedding of vortices as described in reference 12. Where this viscous phenomenon is encountered, of course, correlation with inviscid theory is not expected.

It was necessary in comparing the data from reference 11 with the linear characteristics theory to make the flow angles compatible. The flow angle used in the data actually includes a component of crossflow angle as used in the convention of reference 7 and adopted herein. The theoretical results were transformed to be compatible with the experimental results by the equation

$$\cos \epsilon = \cos \theta \cos \varphi \tag{20}$$

where ϵ is the flow angle defined in reference 11, θ is the flow angle from reference 6, and φ is the crossflow angle of reference 6. It may be noted that by the definition adopted in reference 11, the transformed flow angle ϵ is always positive.

X-15 Airplane

One objective of this study was to obtain information about the flow field on the aft underside (compression surface $\Phi = 180^{\circ}$) of the X-15 airplane (fig. 9) for use in future airbreathing propulsion experiments. Pitot pressures from wind tunnel model tests (refs. 13 and 14) and from both the linearized characteristics method and the equivalent body method are

compared in figure 10. It may be noted that the equivalent body method (shown only for $\alpha = 10^{\circ}$) does not show the close agreement with data that the linearized method does for this slender body shape (fineness ratio $\simeq 10.5$). The linearized characteristics method also gives reasonable values for the flow angle (fig. 11).[3]

For the calculations, the X-15 shape was approximated by an ogive cylinder with a blunt nose. It is obvious from sketch (c) that this is a great simplification since the asymmetries due to wings, tail, cockpit, and other bulges are neglected. The protuberances neglected were felt to have the least effect in the region studied ($\Phi = 180^{\circ}$ compression surface). Therefore, the approximation used for body shape was felt to cause only minor discrepancies.

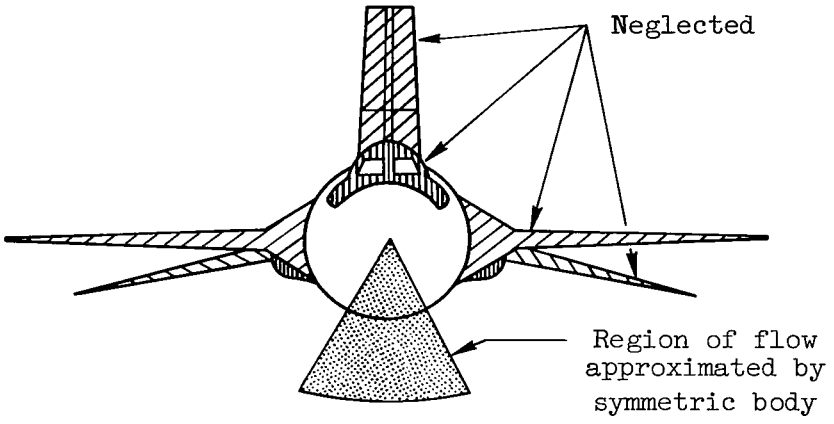

Sketch (c)

CALCULATED X-15 FLOW FIELD USING LINEARIZED CHARACTERISTICS THEORY

As part of the present study a more complete investigation was made of the X-15 aft underside region (in the plane of symmetry, $\Phi = 180^{\circ}$) using the linearized characteristics theory. Figure 12 indicates the bow shock location for Mach numbers of 4, 6, and 8 and at three angles of attack. Although the shock shapes are included for completeness, limited comparisons with experiment have indicated they are not accurate. It is felt that this reflects a strong sensitivity of shock position to second-order (α^2) terms which the present theory neglects. The surface static pressure for three Mach numbers ($M_{\infty} = 4, 6, 8$ at angles of attack of $0^{\circ}, 5^{\circ}, 10^{\circ}$) is given in figure 13. Note the overexpansion region (at $x/R = 70$) at the higher Mach number ($M_{\infty} = 8.0$). Figures 14 and 15 show predictions of the pitot pressure profiles at two body stations ($x/R = 64.0$ and 145.0). Station 64.0 represents the juncture of the ogive and cylinder and station 145.0 is a possible location for the propulsion package. For the three Mach numbers of 4, 6, and 8 at four angles of attack,

[3]Communication with Flight Research Center personnel concerning the wind tunnel flow angle data (fig. 11) indicated that close to the body, a disturbance due to either a local shock or probe interference effects could cause the variations shown between theory and data.

it is to be noted that as the Mach number is increased, the angle-of-attack effects are more pronounced. The theoretical bow shock position is noted on the curves.

Local Mach number profiles for stations 64.0 and 145.0 are shown in figures 16 and 17 for the previously considered free-stream Mach numbers and angles of attack. Flow-angle profiles at stations 64.0 and 145.0 are shown in figures 18 and 19 for the same variables in Mach number and angle of attack as shown on the previous figures. Whereas the gradients in flow angle at station 64.0 (fig. 18) appear rather strong near the surface, this effect again washes out further downstream as shown in figure 19.

CONCLUDING REMARKS

Two simplified methods for predicting the flow field about bodies of revolution at angle of attack have been compared with limited experimental data. Using experimental data from a spherically blunted 15° cone, an ogive cylinder, and the X-15 as a basis for evaluation, it was found that each theory studied was applicable to certain regions but neither theory was superior in all cases. The linear characteristics theory was found to be useful for predicting the flow fields about bodies of higher fineness ratio, such as the ogive cylinder and the X-15, at small angles of attack. Of particular interest was its ability to provide circumferential variations of certain flow quantities, especially flow angle, for bodies at angle of attack. Pressures were not predicted as well as Mach number and flow angles in the case studied.

In regions dominated by bluntness effects the linearized characteristics method agreed poorly with experiment. The nose bluntness strongly influenced the flow at least 16 nose radii downstream for the 15° sphere cone at a Mach number of 10.6. However, in the region of flow, less than about 4 nose radii downstream, modifications to the linearized characteristics method were shown to improve the agreement with experiment. The equivalent body method agreed well with experiment in these bluntness dominated regions but was restricted in the present report to the plane of flow symmetry.

The linear characteristics theory was employed to investigate the aft flow field of the X-15 airplane. The purpose was to provide flow quantities in a region where a scramjet inlet engine might be mounted.

Ames Research Center
National Aeronautics and Space Administration
Moffett Field, Calif., 94035, Jan. 24, 1967
126-15-03-01-00-21

APPENDIX

NUMERICAL INTEGRATION OF THE ENTROPY PERTURBATION

The present section describes a finite difference scheme developed for integrating equation (10). The differential equation for the entropy perturbation

$$\frac{\partial S_1}{\partial s_o} = -\theta_1 \frac{dS_o}{dn_o} \tag{A1}$$

describes the variation of entropy along the unperturbed streamlines which results from the conservation of entropy on the streamlines of the perturbed flow. It is assumed that S_1 is given on an initial data line between the body and shock wave, and that the following boundary conditions must be satisfied on the body.

$$S_B = S_{Initial} + (X-R_B)\cos\theta_o + r \sin\theta_o \frac{dS_o}{dn_o} \tag{A2}$$

The entropy perturbation is specified at the shock wave in terms of free-stream conditions and certain perturbation parameters, but these conditions need not be stated at this time (see ref. 6).

Equation (A2) makes use of the condition that the body is a streamline and S_B = constant; the dependence on dS_o/dn_o results from the transformation from body to wind reference axes. This quantity is easily evaluated at the body; therefore, the results of references 6 and 7, which were confined to the body surface, were correctly and accurately obtained. (One should note that the boundary condition was incorrectly stated in references 6 and 7 because of a typographical error.) During the present study it became apparent that the method used to integrate equation (A1) was introducing sizable errors off the body surface.

Two difficulties arise in integrating equation (A1). First, the entropy gradient dS_o/dn_o must be evaluated numerically, and this numerical differentiation becomes inaccurate as the entropy layer thins. The second difficulty is more basic to characteristics methods in general. It arises from the fact that the streamlines do not pass through the mesh points formed by intersecting Mach lines, and some form of interpolation becomes necessary. Just as with the first problem, numerical interpolation becomes inaccurate as the characteristic mesh opens up with respect to the scale of the entropy layer.

Using the stream function Ψ (i.e., mass flow function) in a manner similar to that described in reference 8 eliminated both of these problems in the present linearized characteristics program. The values of entropy S_o and entropy perturbation S_1 at each shock point are stored along with the corresponding value of stream function

$$\Psi = \rho_\infty V_\infty \pi r^2 \tag{A3}$$

These shock values of S_o, S_1, and Ψ, in addition to the values given along the input data line, form S_o-Ψ and S_1-Ψ tables which are retained as the computation proceeds downstream. Therefore, if the stream function is known at some point in the flow field, the entropy can be found from these tables with an accuracy comparable to that of the shock point calculation. The important difference in the present method is that the stream function can be determined more accurately than the entropy at downstream points near the body surface. The stream function is found at a typical mesh point by a quadratic interpolation in the same way that entropy is found in a standard characteristics scheme (see refs. 4 and 15). However, interpolating for Ψ is more accurate because the stream function is an increasing function and is much smoother than the entropy. For the same reasons the entropy gradient can be determined more accurately if $dS_o/d\Psi$ is evaluated by numerical differentiation of the data in the S_o-Ψ table, and the following relation is used

$$\frac{dS_o}{dn_o} = \frac{d\Psi}{dn_o}\frac{dS_o}{d\Psi} \equiv \rho V r \frac{dS_o}{d\Psi} \tag{A4}$$

Since S_o is constant on streamlines Ψ = constant, the values in the S_o-Ψ table are determined by the shock conditions. However, the entropy perturbation depends also on a streamline dimension through equation (A1); that is, $S_1 = f(\Psi, s_o)$. Therefore, as each new characteristic line is computed, the values of S_1 in the S_1-Ψ table must be changed in accordance with equation (A1).

The procedure used to perform this calculation is described briefly with the help of sketch (d).

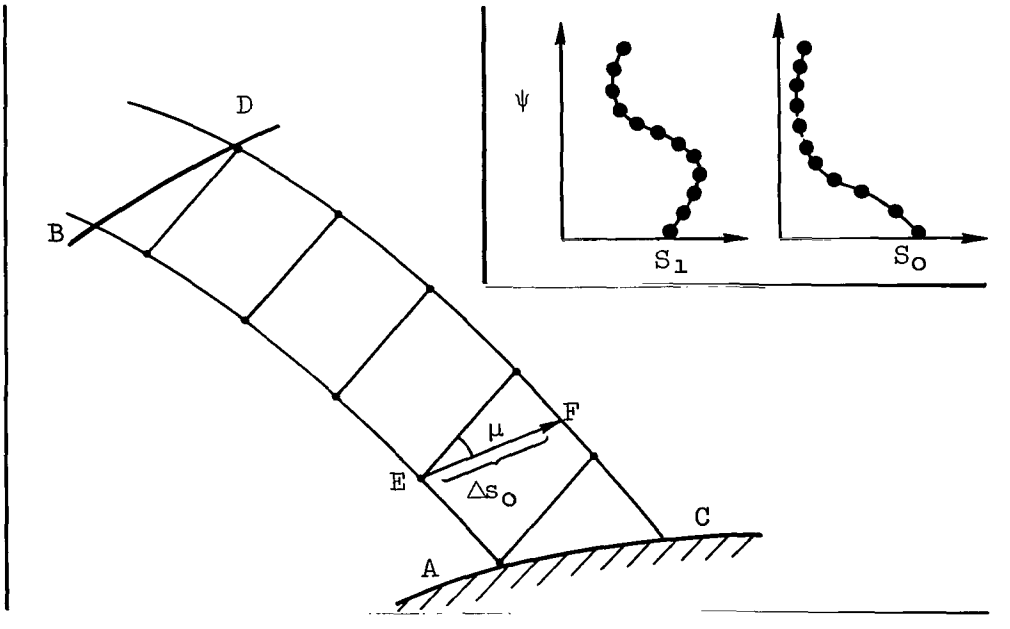

Sketch (d)

It is assumed that the characteristic mesh for zero angle of attack is known, and it is necessary to calculate the change in S_1 in going from line $\overline{AB}$ to $\overline{CD}$ in the sketch. The distance along streamlines, Δs_o, is calculated between these lines (shown as $\overline{EF}$ for a typical point) for all the mesh points along $\overline{AB}$. With the known stream function on this line, one has

$$\theta_1 \Delta s_o = f(\Psi)$$

on line $\overline{AB}$. This quantity is then calculated, by means of quadratic curve fits, at those values of Ψ for which S_1 is stored. The entropy gradient is evaluated in a similar way with the help of equation (A4) and the S_o-Ψ table. New values of S_1 are then computed by means of equation (A1). These are the values of entropy perturbation that apply on the characteristic line $\overline{DC}$. In this manner the entropy perturbation is integrated on a scale that is much finer than the basic characteristic mesh.

In figure 20 the results of this method are compared to the original scheme used in reference 6 which was based only on characteristic mesh points. The example shown is a sphere ogive cylinder for a free-stream Mach number of 10. The entropy perturbation is plotted along several right running characteristic rays; the distance is normalized to be $\xi = 0$ on the shock and $\xi = 1$ on the body. It is seen that the two methods give substantially the same results up to the 60th ray ($x_B/R = 8.97$), but large differences start to show up at the 80th ray. Near the end of the body, the results of the standard interpolation scheme are very irregular and differ from the results of the new method over most of the shock layer. Along the last ray, the new method gives a large variation of S_1 in a layer near the body, and a relatively constant value in the remaining 80 percent of the shock layer. This is consistent with the physics of the flow which require (by continuity of mass) that the large entropy variations caused by the blunt nose must be confined to a layer near the body.

REFERENCES

1. Moretti, Gino, et al.: Flow Field Analysis of Reentry Configurations by a General Three Dimensional Method of Characteristics. ASD TR-61-727, vol. 3, Feb. 1962.

2. Jenkins, B. Z.: Real Gas Flow Properties Around Blunt Cones. U. S. Army Missile Command Rep. RF-TR-63-18, vol. 1, Aug. 19, 1963.

3. Pridmore, Brown B. N.; and Franks, W. J.: A Method of Characteristics Solution in Three Independent Variables. ARL 65-124, June 1965.

4. Inouye, Mamoru; and Lomax, Harvard: Comparison of Experimental and Numerical Results for the Flow of a Perfect Gas About Blunt-Nosed Bodies. NASA TN D-1426, 1962.

5. Cleary, Joseph W.: An Experimental and Theoretical Investigation of the Pressure Distribution and Flow Fields of Blunted Cones at Hypersonic Mach Numbers. NASA TN D-2969, 1965.

6. Rakich, John V.: Numerical Calculation of Supersonic Flows of a Perfect Gas Over Bodies of Revolution at Small Angles of Yaw. NASA TN D-2390, 1964.

7. Rakich, John V.: Calculation of Hypersonic Flow Over Bodies of Revolution at Small Angles of Attack. AIAA J., vol. 3, no. 3, Mar. 1965, pp. 458-464.

8. Powers, S. A.; and O'Neill, J. B.: Determination of Hypersonic Flow Fields by the Method of Characteristics. AIAA J., vol. 1, no. 7, July 1963, pp. 1693-1694.

9. Keener, Earl R.: Prediction of Ogive-Forebody Pressures at Angles of Attack. J. Aerospace Sci., vol. 29, no. 8, Aug. 1962, pp. 1013-1014.

10. Eggers, A. J., Jr.; and Savin, Raymond C.: A Unified Two-Dimensional Approach to the Calculation of Three-Dimensional Hypersonic Flows, With Application to Bodies of Revolution. NACA Rep. 1249, 1955.

11. Lankford, J. L.: Preliminary Results of Flow Surveys About an Inclined Body of Revolution at Mach Number 3.5. NAVORD Rep. 6708, Jan. 6, 1960.

12. Allen, H. Julian; and Perkins, Edward W.: A Study of Effects of Viscosity on Flow over Slender Inclined Bodies of Revolution. NACA Rep. 1048, 1951.

13. Rippy, J.: Flow Field Investigation of a .0667 Scale Model of the X-15 Research Vehicle at Mach 4, 6, and 8. AEDC TDR-64-201, Oct. 1964.

14. Palitz, Murray: Measured and Calculated Flow Conditions on the Forward Fuselage of the X-15 Airplane and Model at Mach Numbers From 3.0 to 8.0. NASA TN D-3447, 1966.

15. Inouye, Mamoru; Rakich, John V.; and Lomax, Harvard: A Description of Numerical Methods and Computer Programs for Two-Dimensional and Axisymmetric Supersonic Flow Over Blunt-Nosed and Flared Bodies. NASA TN D-2970, 1965.

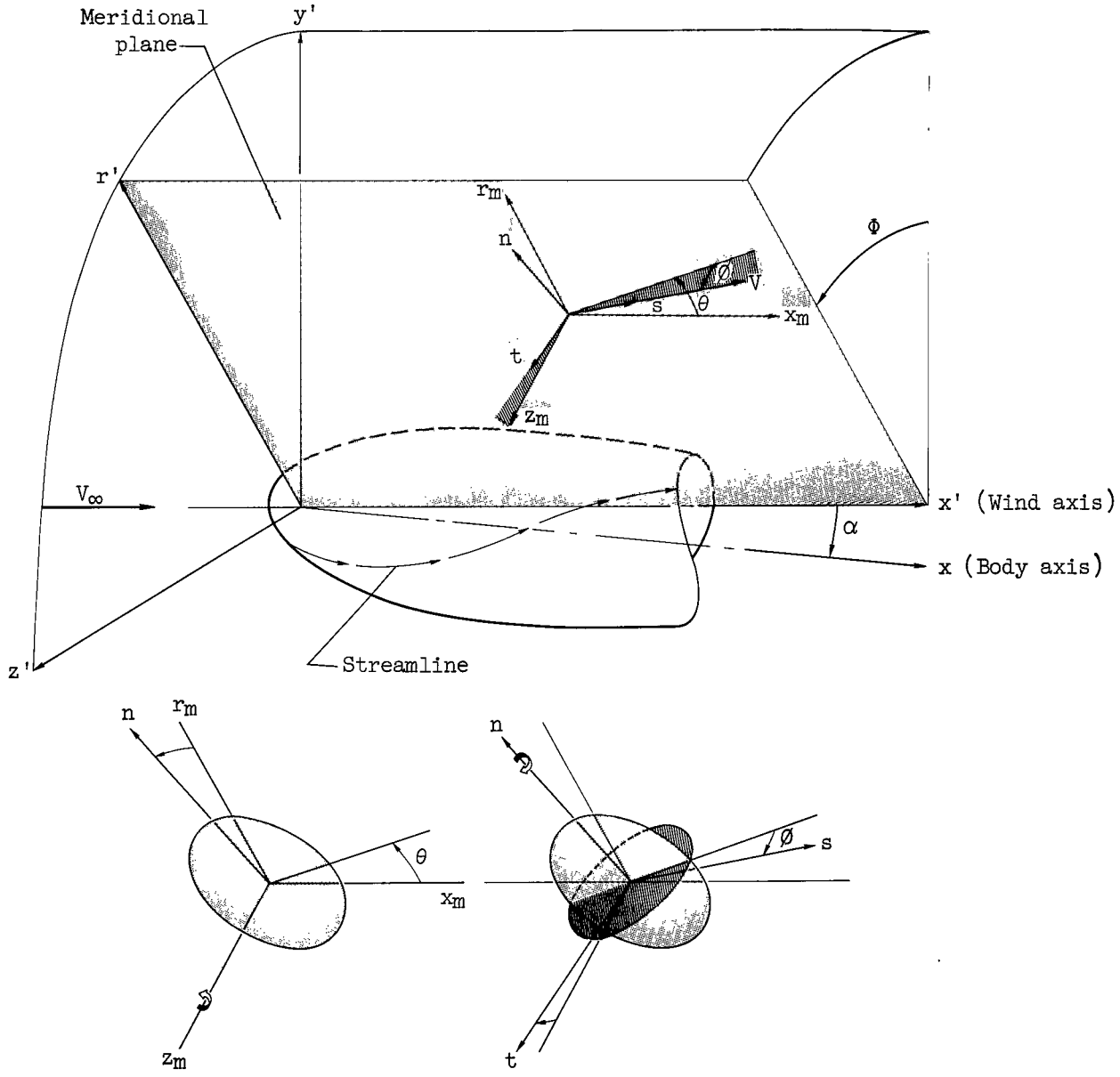

(a) Rotation about z_m (b) Rotation about n

Figure 1.- Coordinate systems.

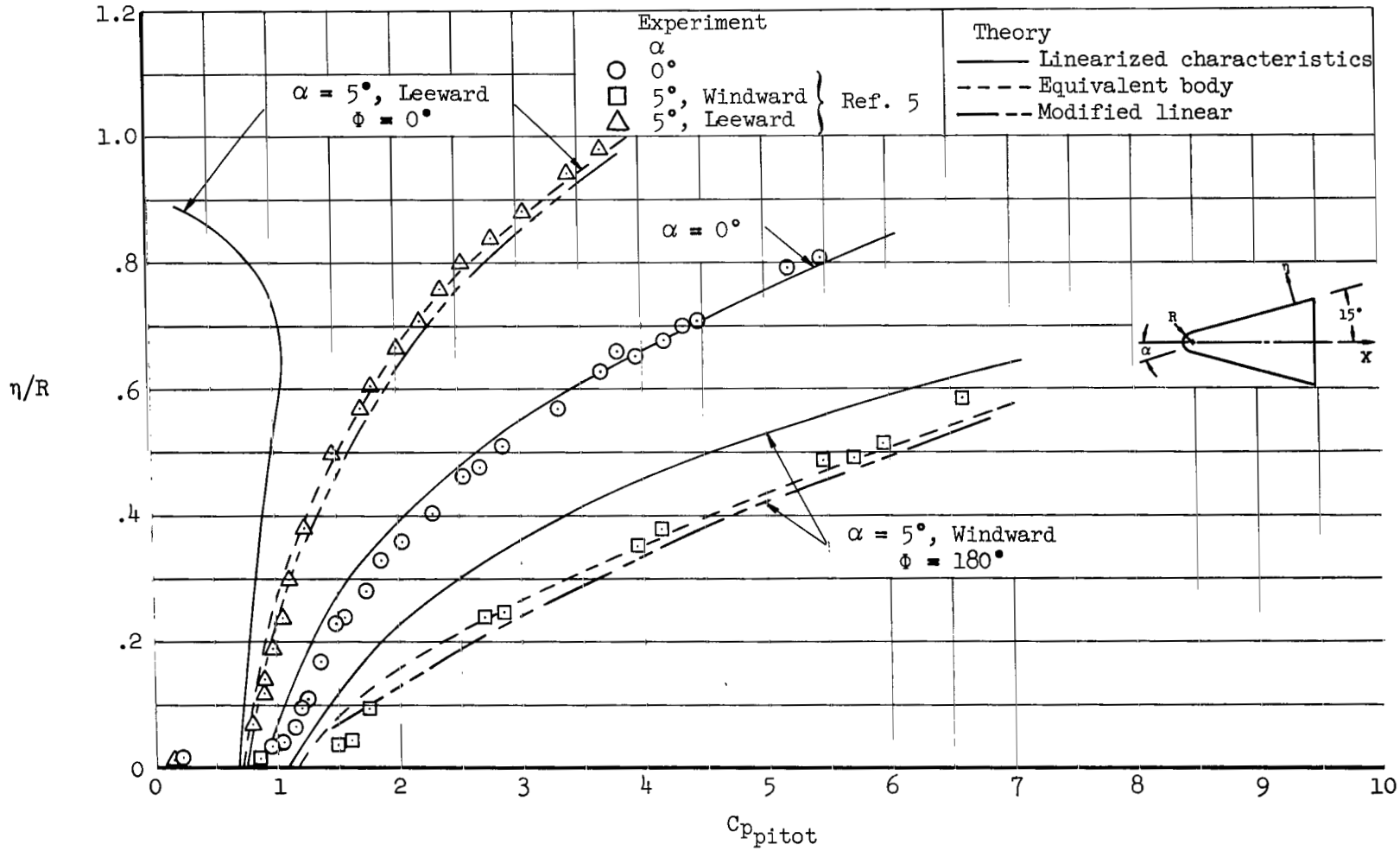

(a) x/R = 3.59

Figure 2.- Pitot pressure in the shock layer for a 15° half-angle spherically blunted cone; M_∞ = 10.6.

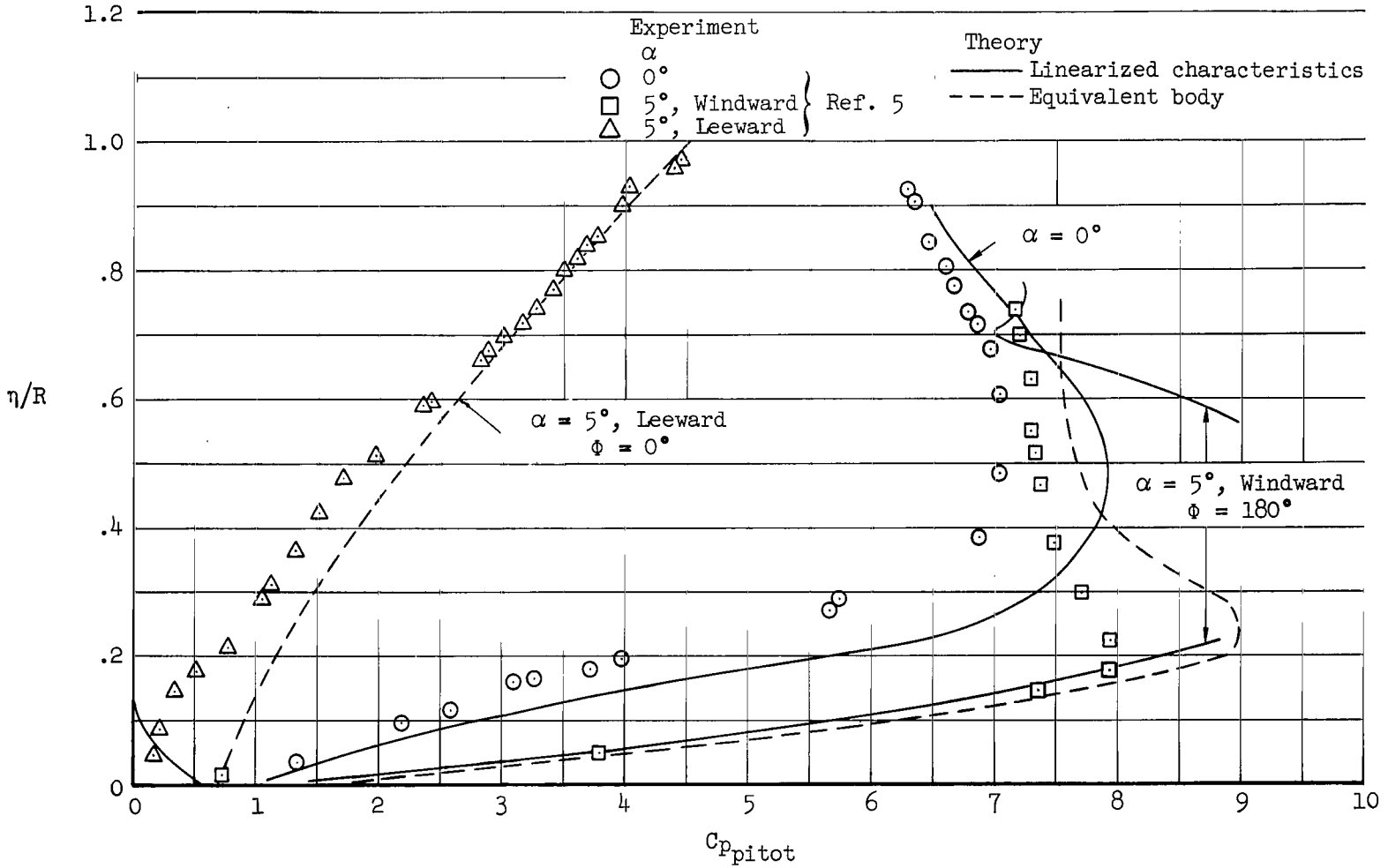

(b) x/R = 16.67

Figure 2.- Concluded.

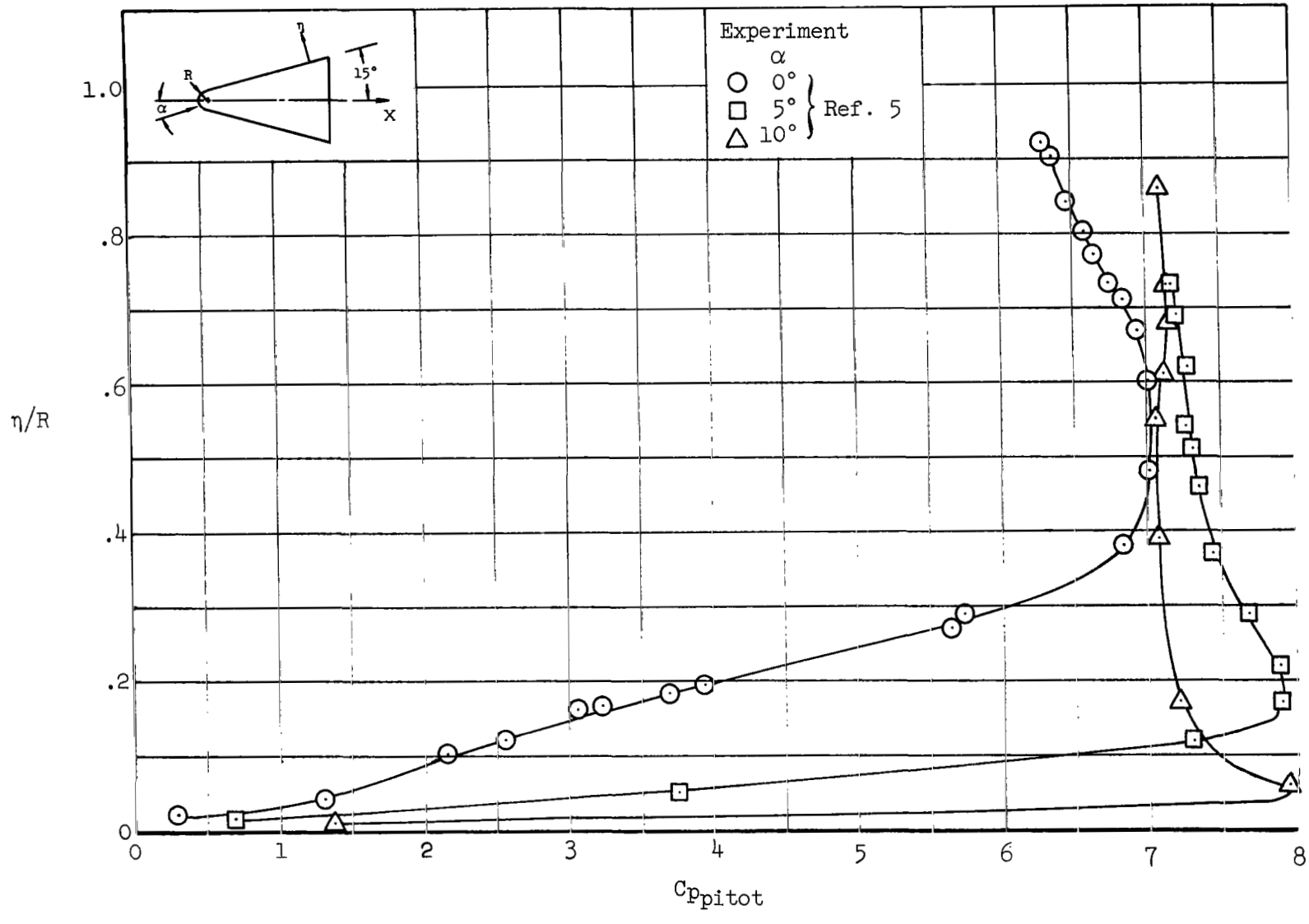

x/R = 16.67

Figure 3.- Effect of angle of attack on pitot pressure distribution, for the windward side (Φ = 180°) of a 15° half-angle spherically blunted cone; M_∞ = 10.6.

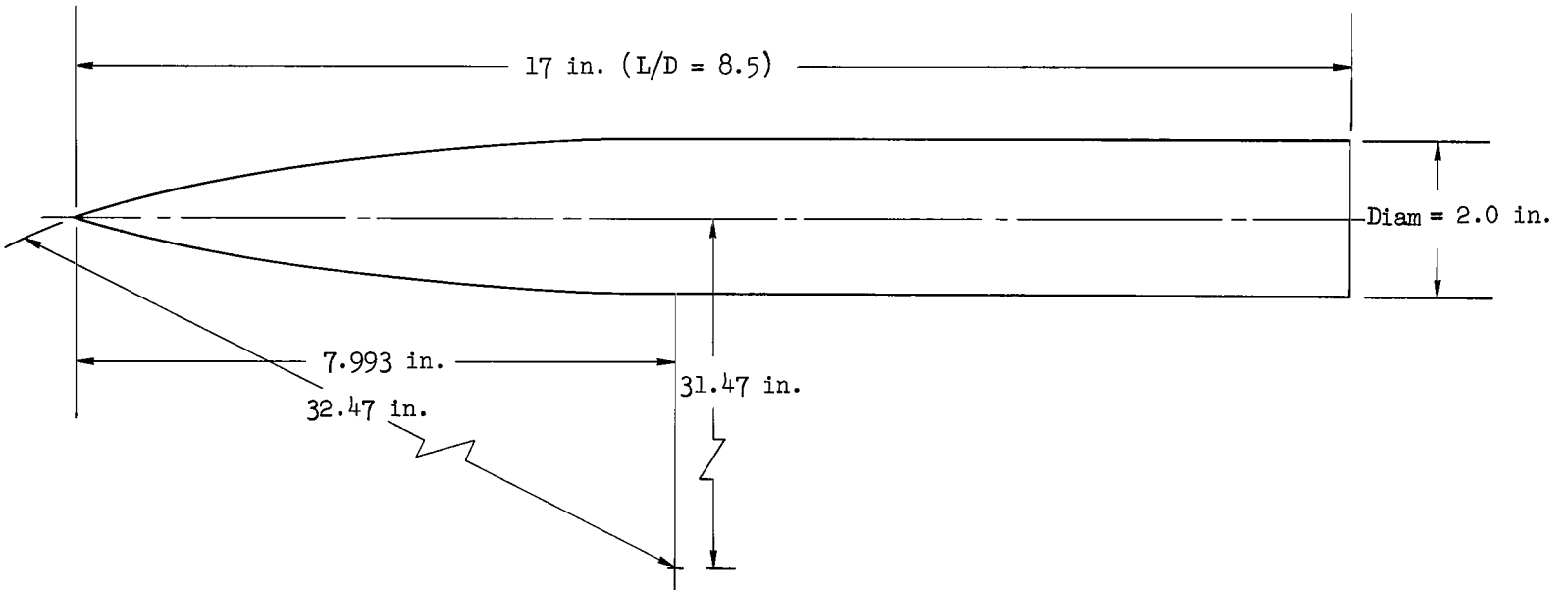

Figure 4.- Ogive-cylinder from reference 11.

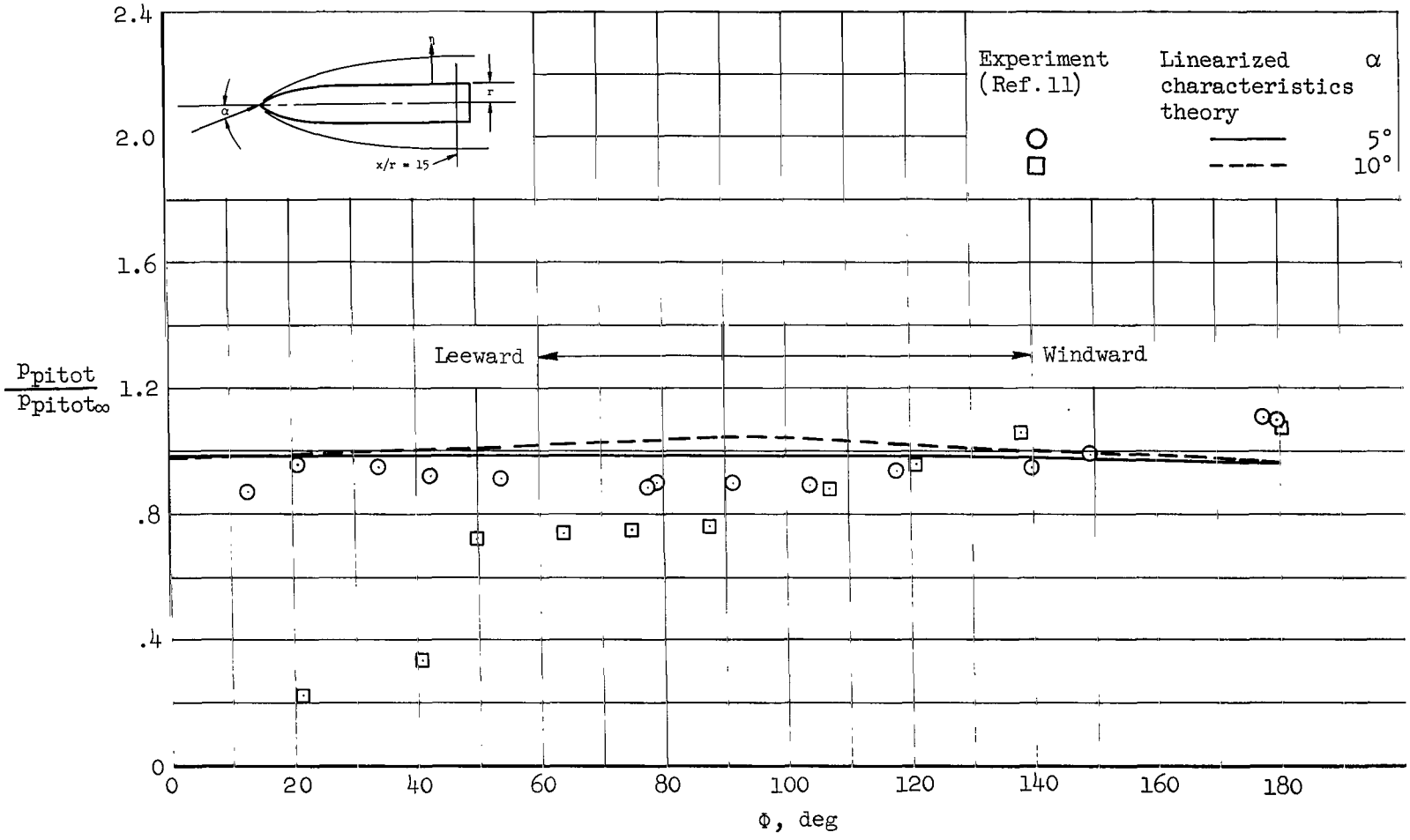

(a) $\eta/r = 0.39$

Figure 5.- Circumferential pitot pressure distribution, ogive-cylinder; $M_\infty = 3.5$, $x/r = 15.0$.

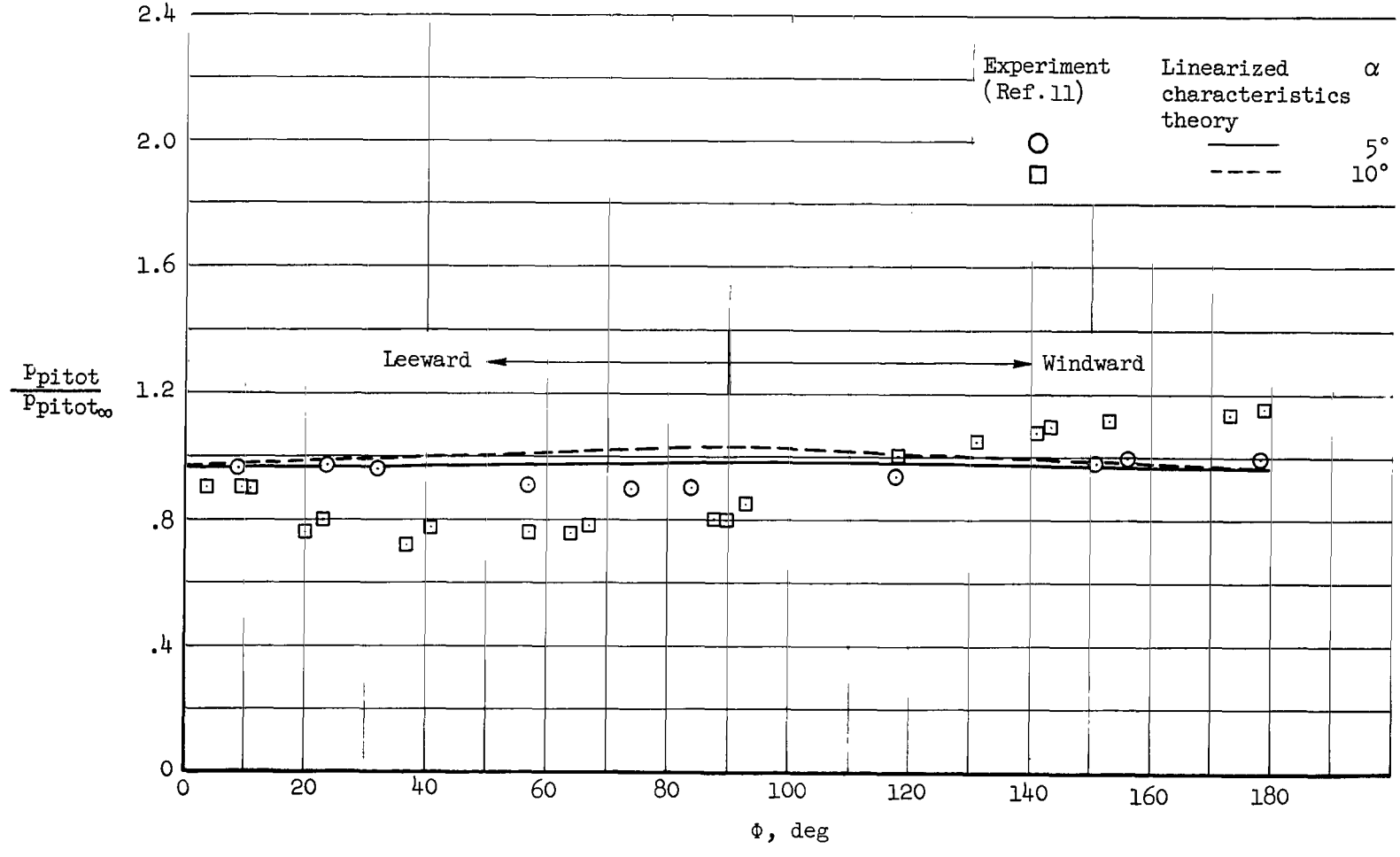

(b) $\eta/r = 0.59$

Figure 5.- Continued.

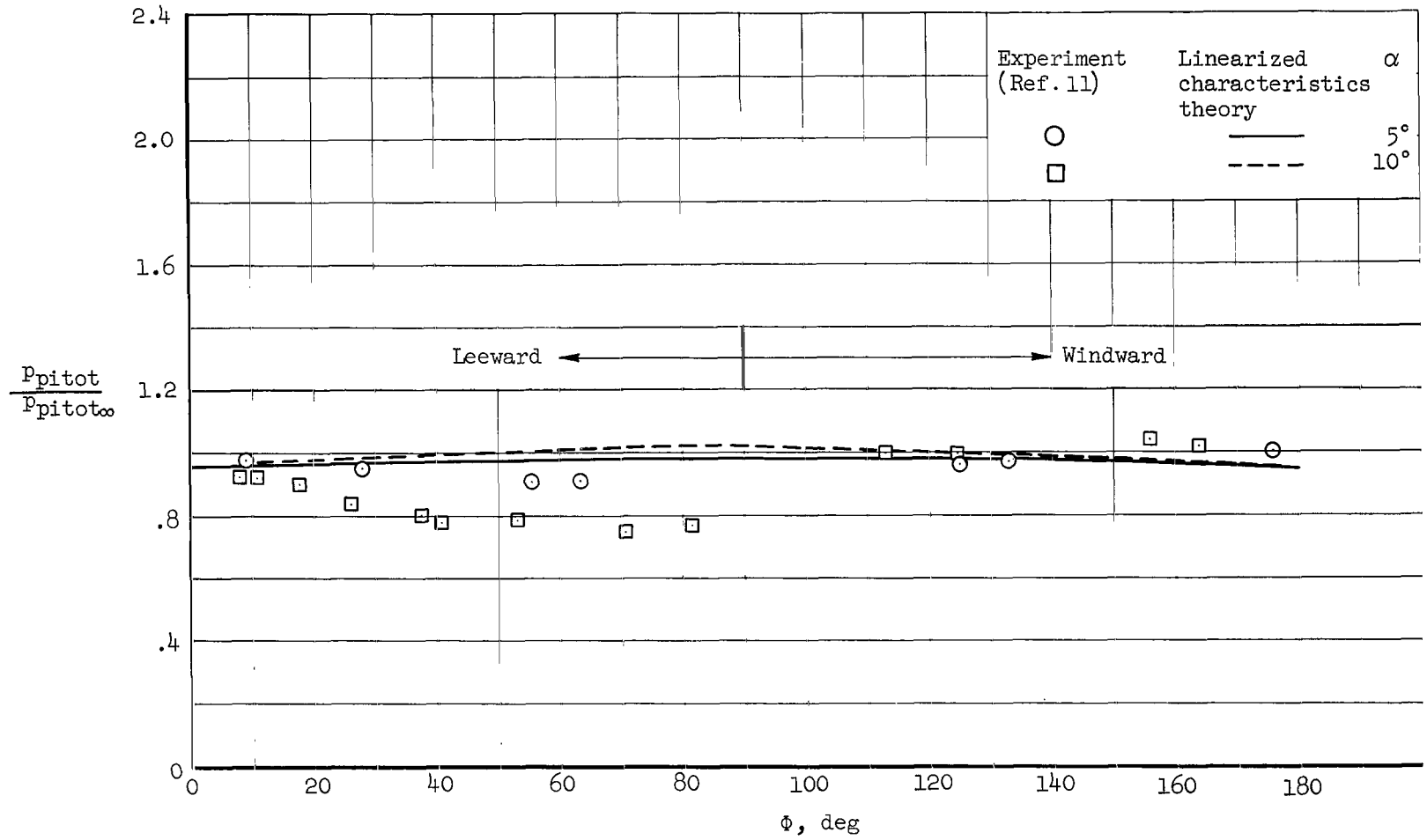

(c) $\eta/r = 0.79$

Figure 5.- Concluded.

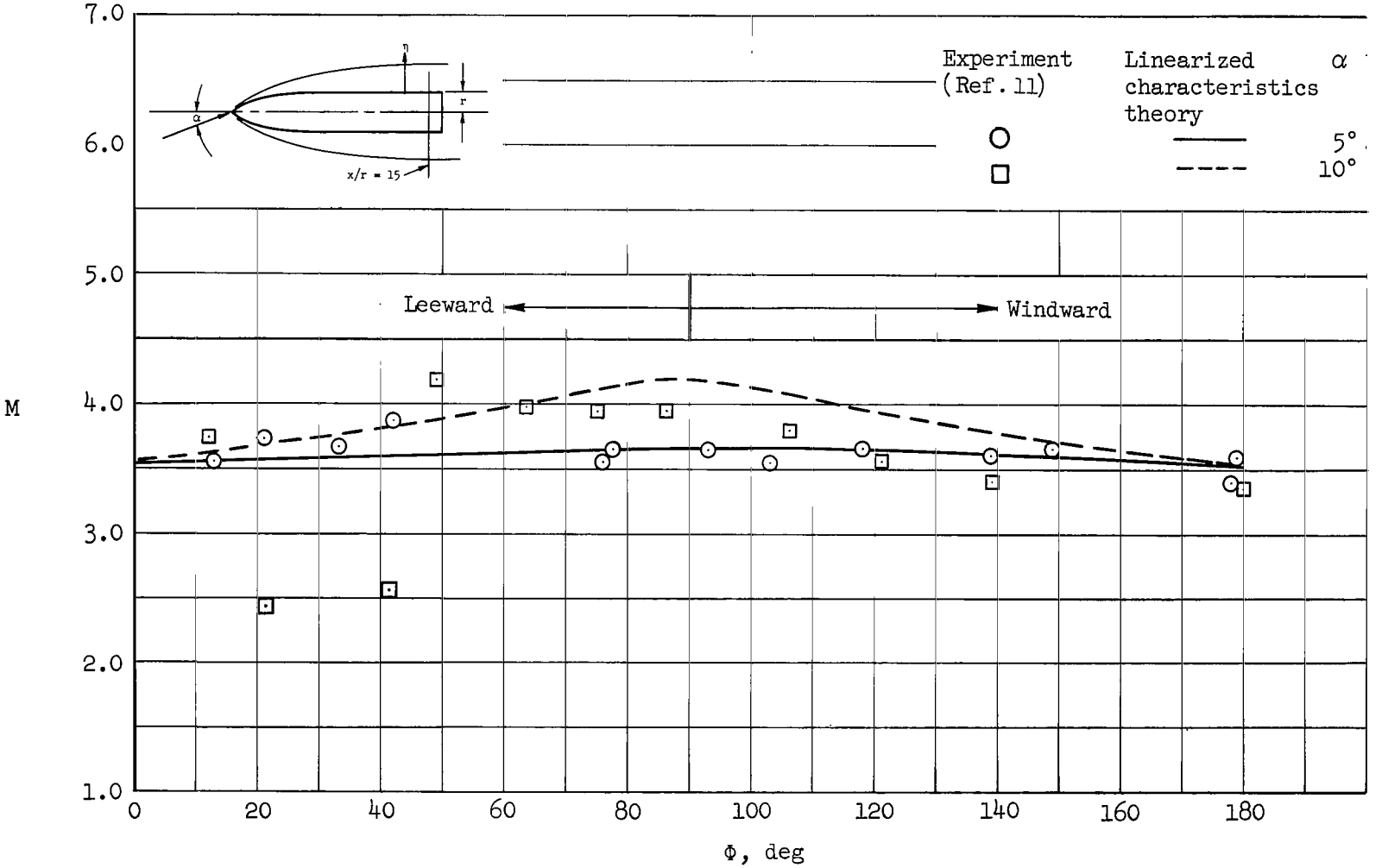

(a) $\eta/r = 0.39$

Figure 6.- Circumferential Mach number distribution; ogive-cylinder, $M_\infty = 3.5$, $x/r = 15.0$.

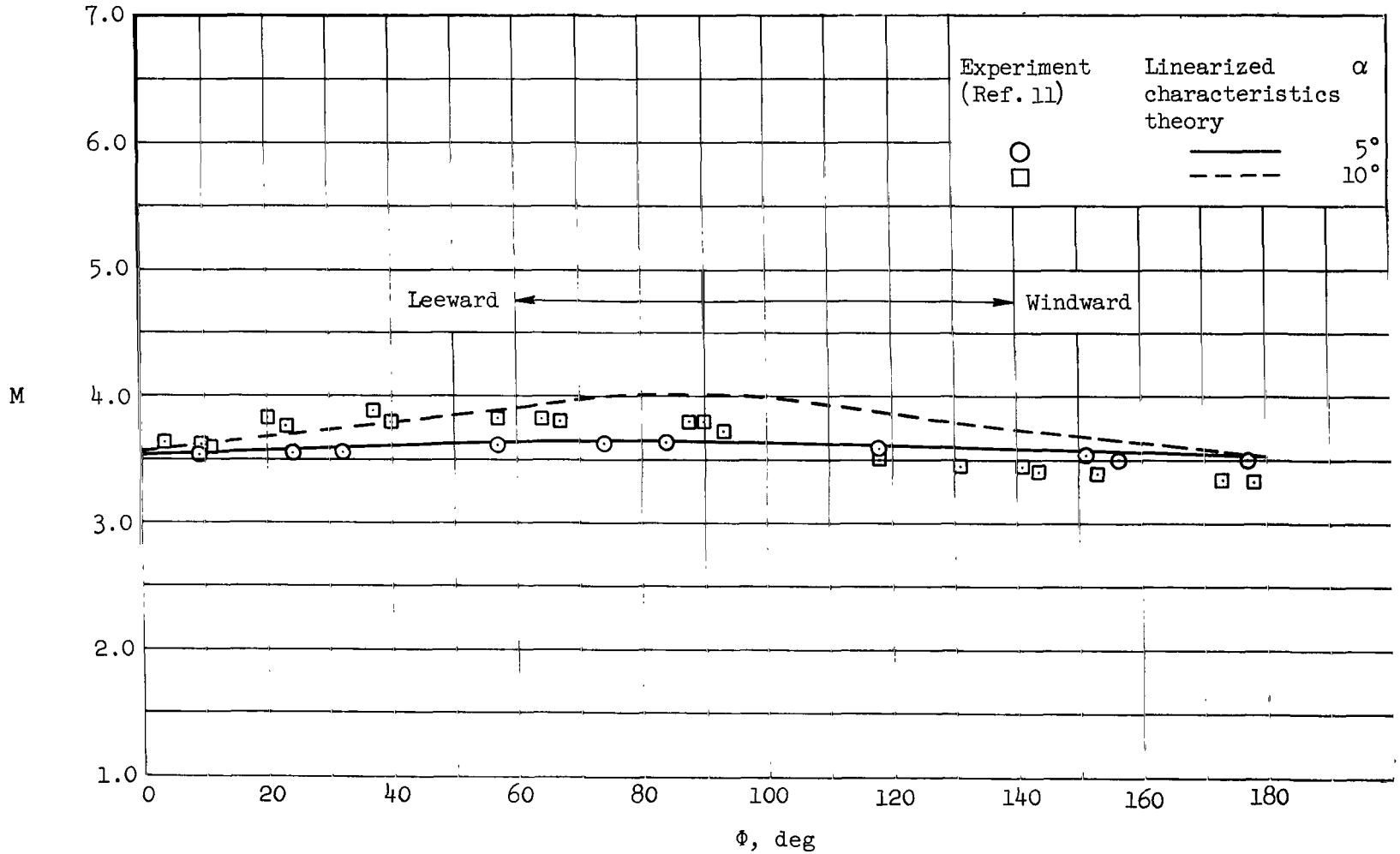

(b) $\eta/r = 0.59$

Figure 6.- Continued.

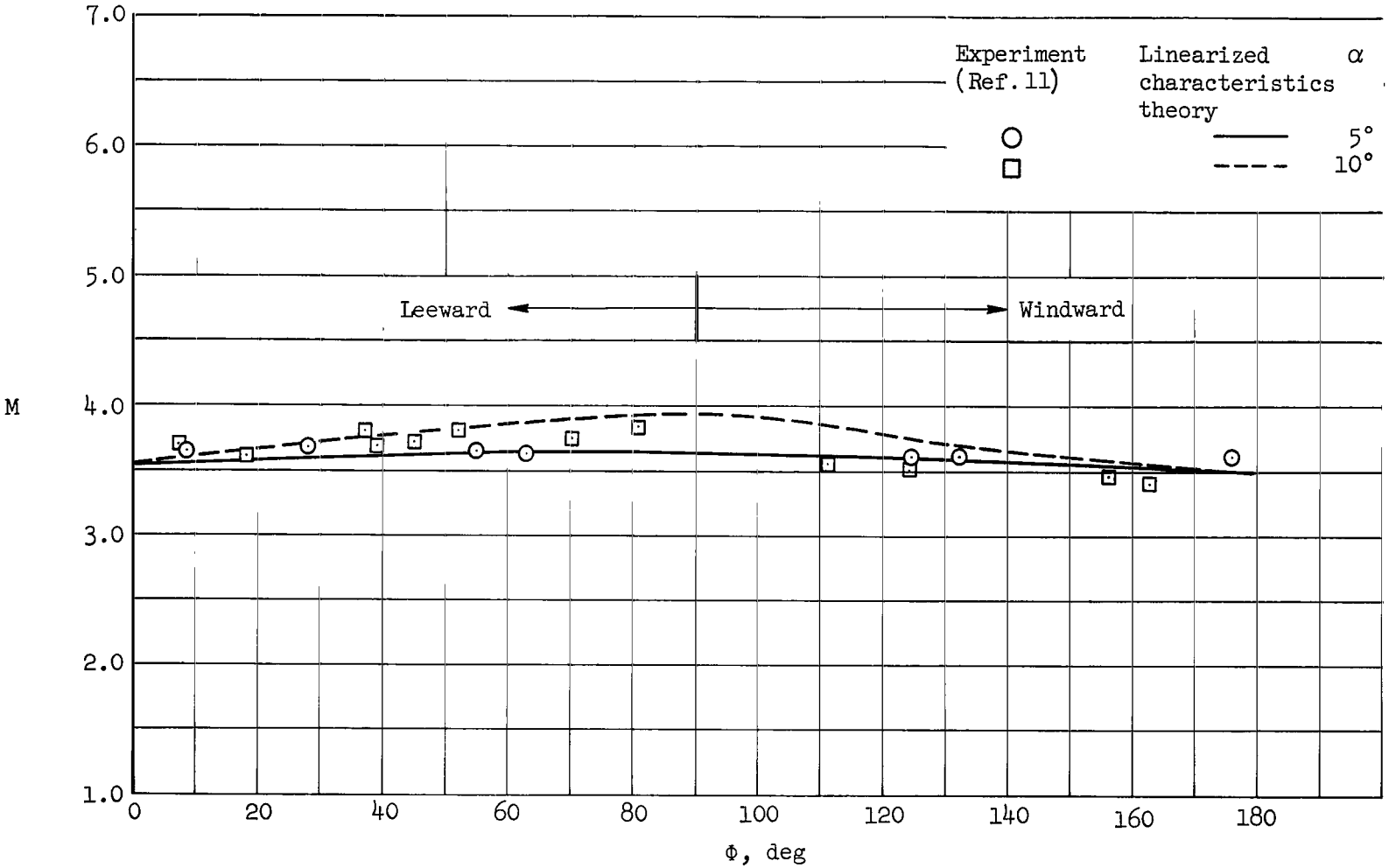

(c) $\eta/r = 0.79$

Figure 6.- Concluded.

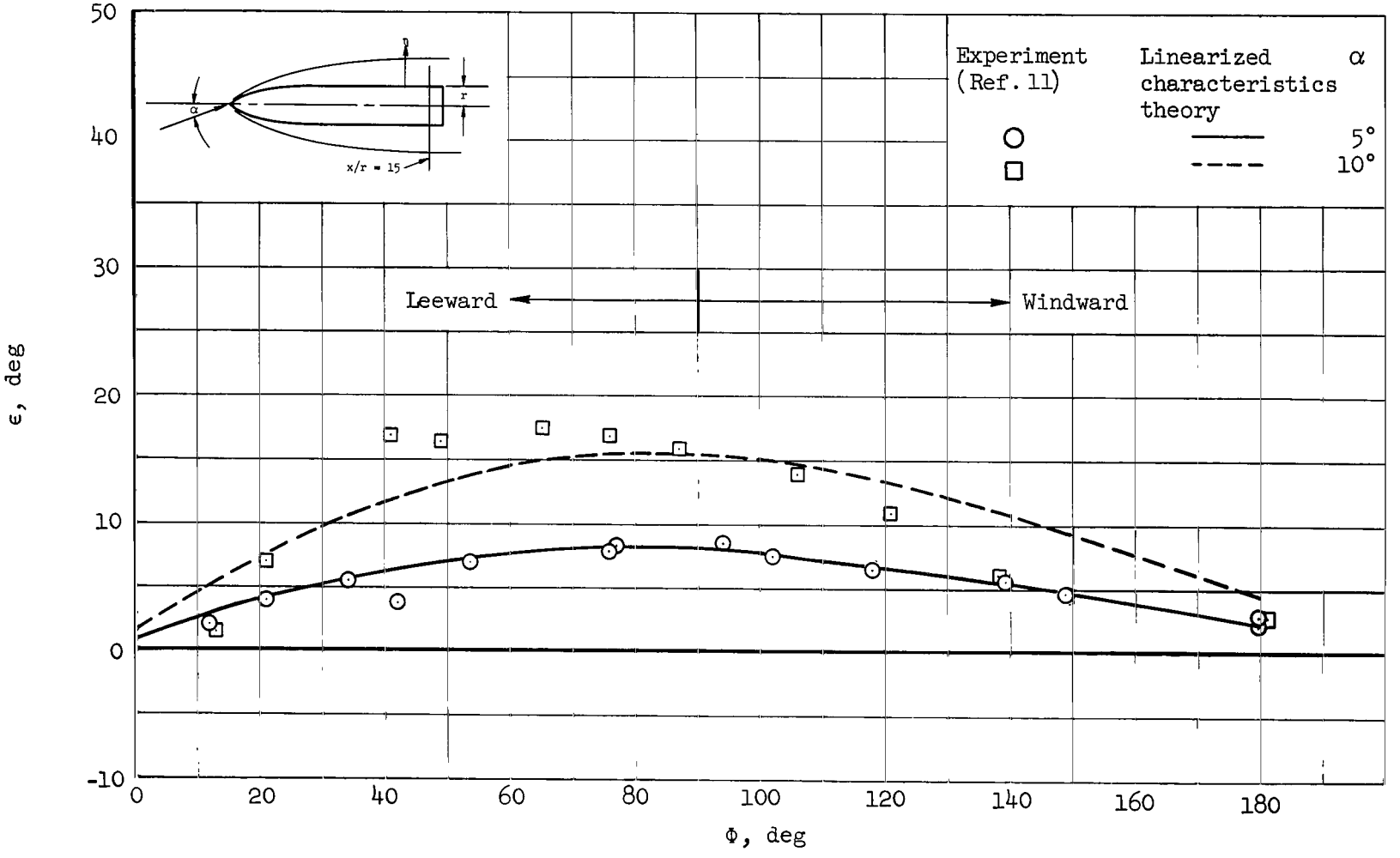

(a) $\eta/r = 0.39$

Figure 7.- Circumferential variation of flow angle; ogive-cylinder, $M_\infty = 3.5$, $x/r = 15.0$.

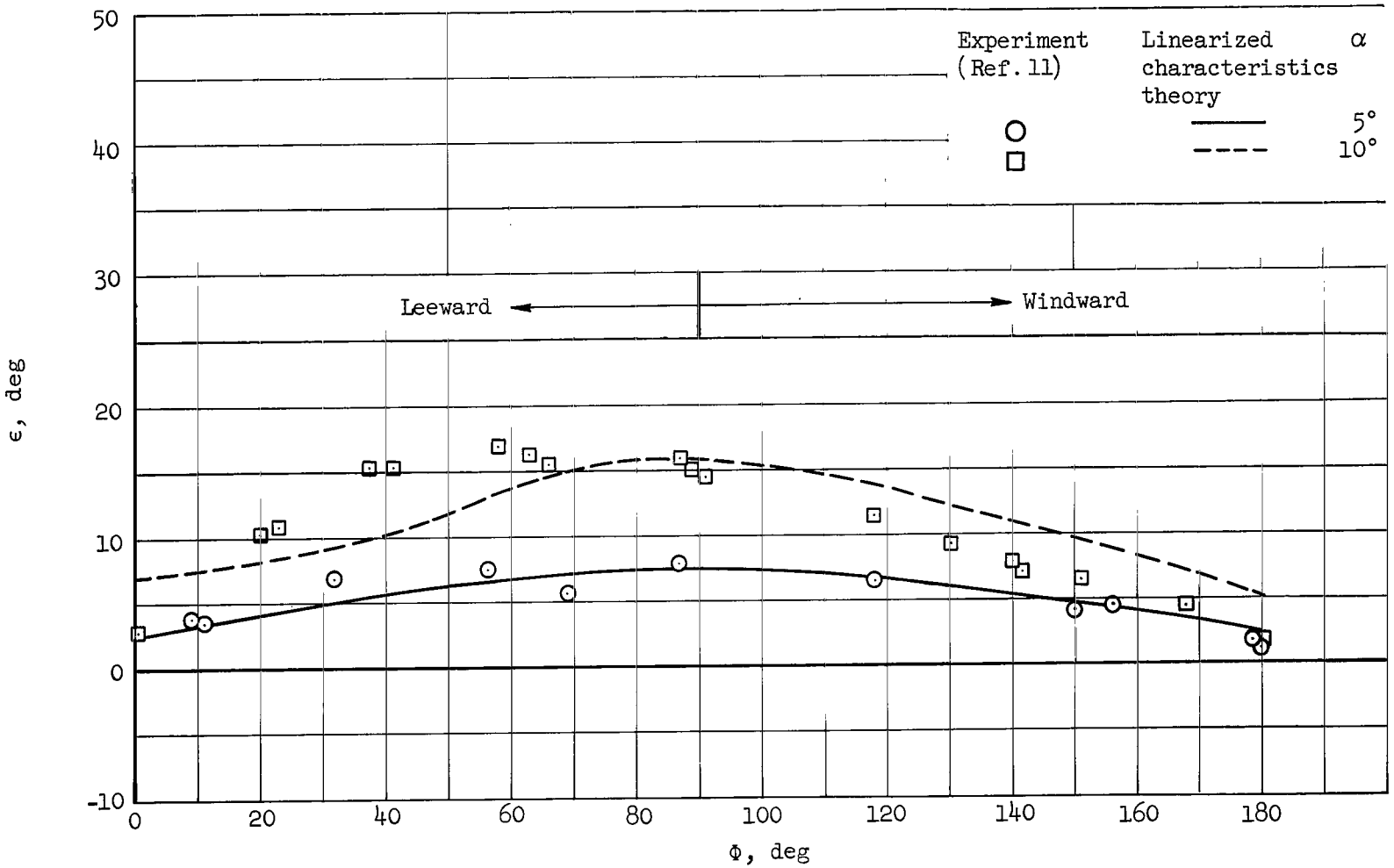

(b) $\eta/r = 0.59$

Figure 7.- Continued.

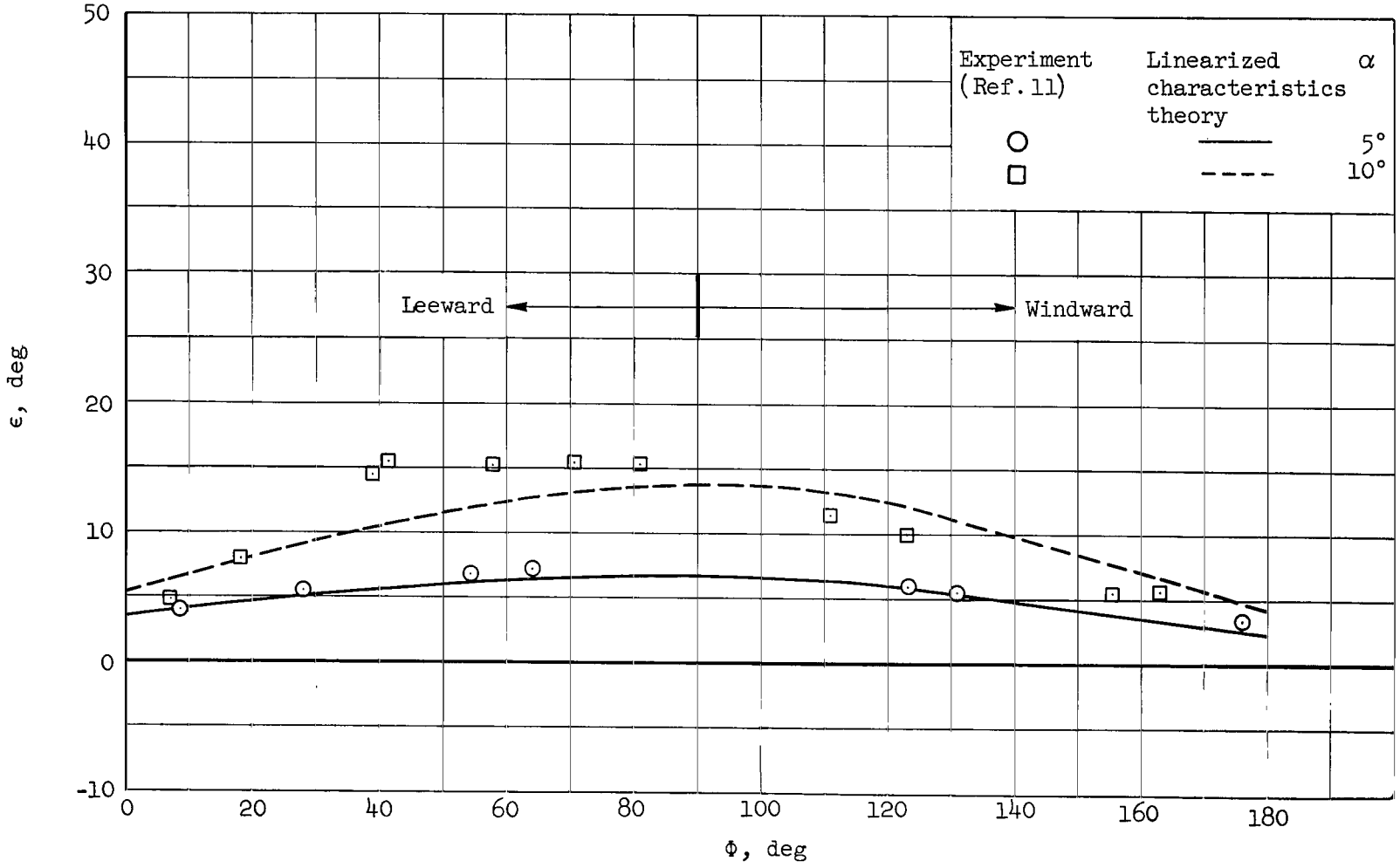

(c) $\eta/r = 0.79$

Figure 7.- Concluded.

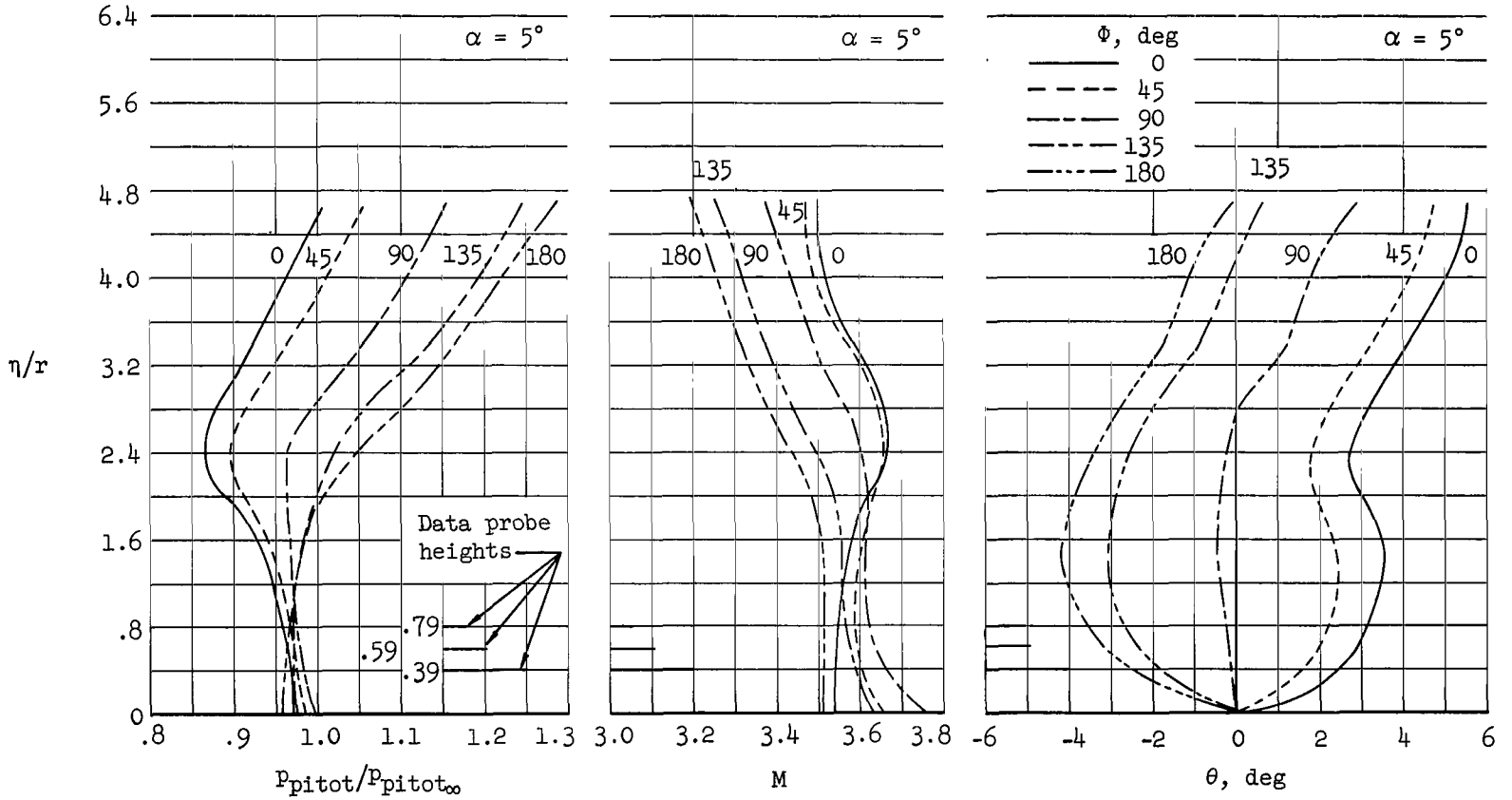

Figure 8.- Radial profiles from the linearized method of characteristics on an ogive-cylinder, $x/r = 15.0$, $M_\infty = 3.5$.

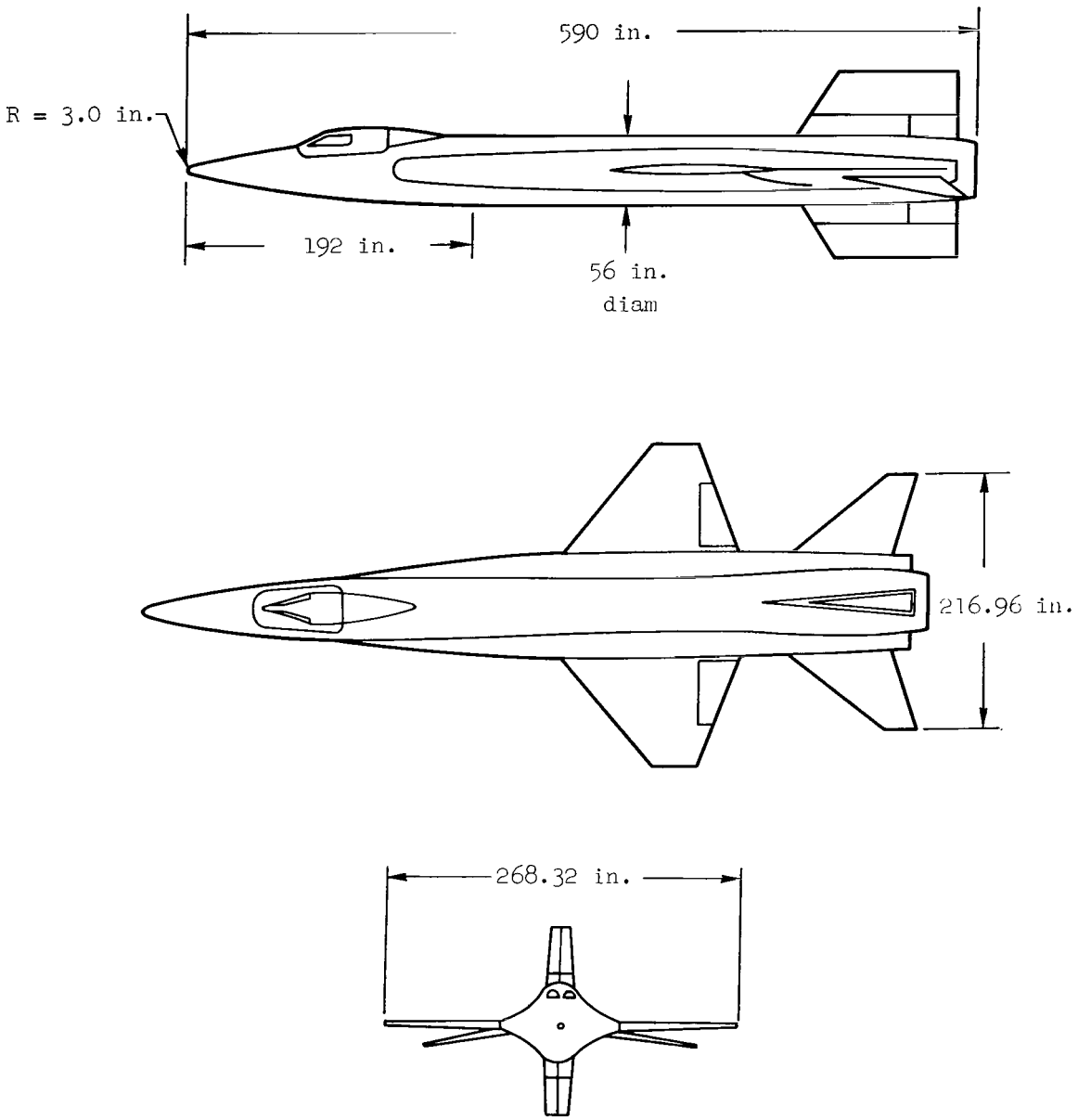

Figure 9.- X-15, three-view drawing.

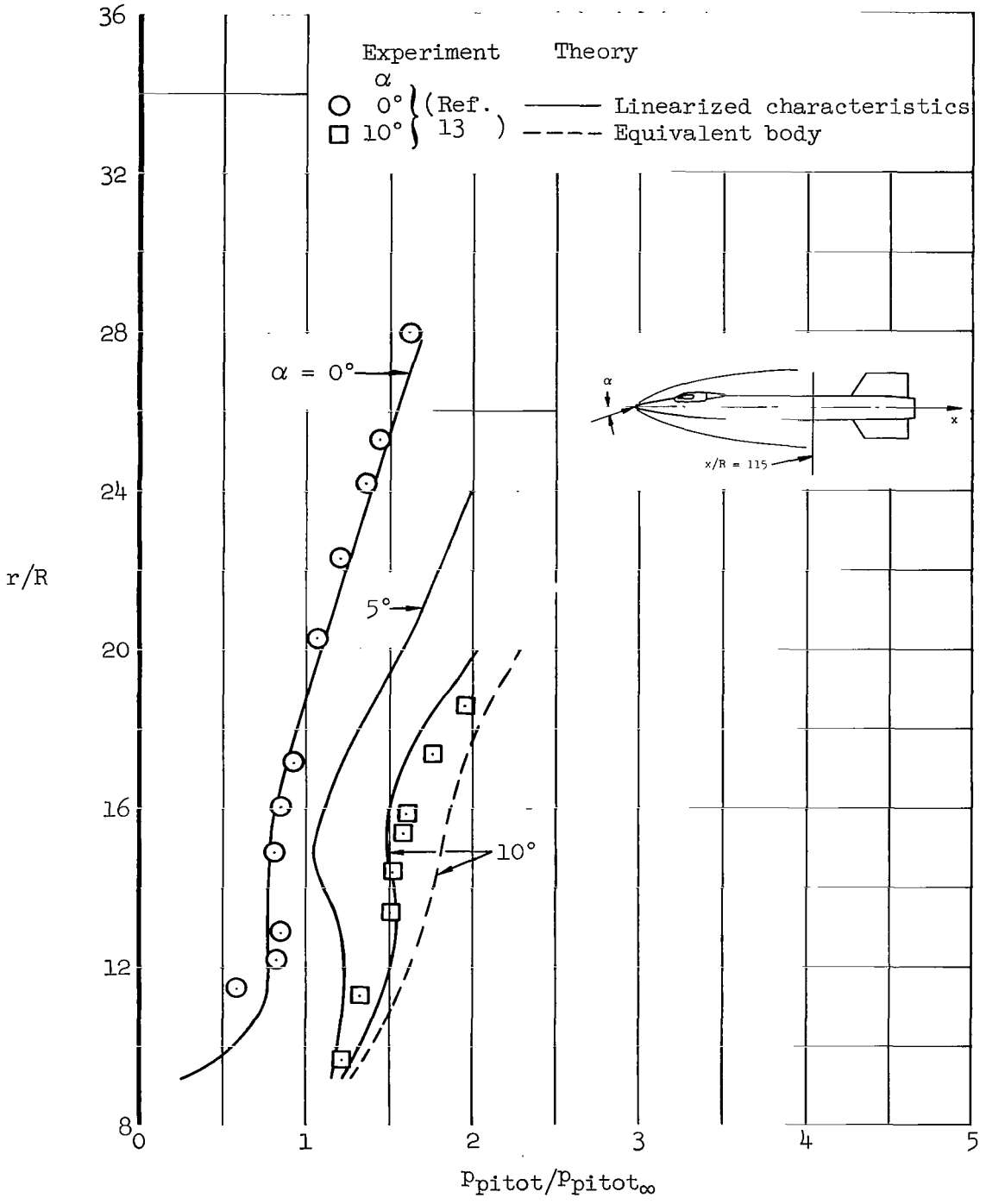

(a) x/R = 115

Figure 10.- Pitot pressure profile in shock layer; X-15, $\Phi = 180°$, $M_\infty = 8.0$.

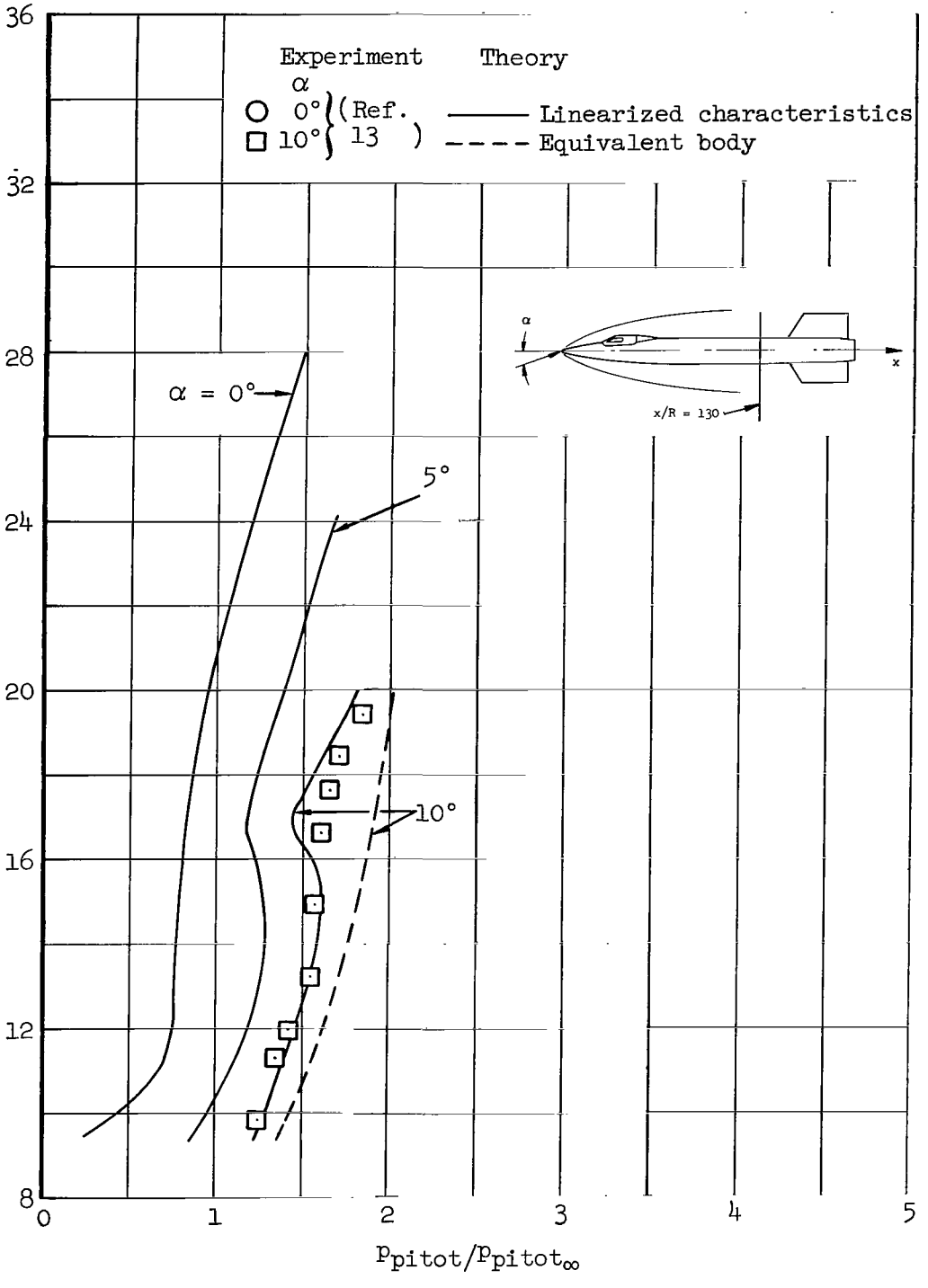

(b) x/R = 130

Figure 10.- Continued.

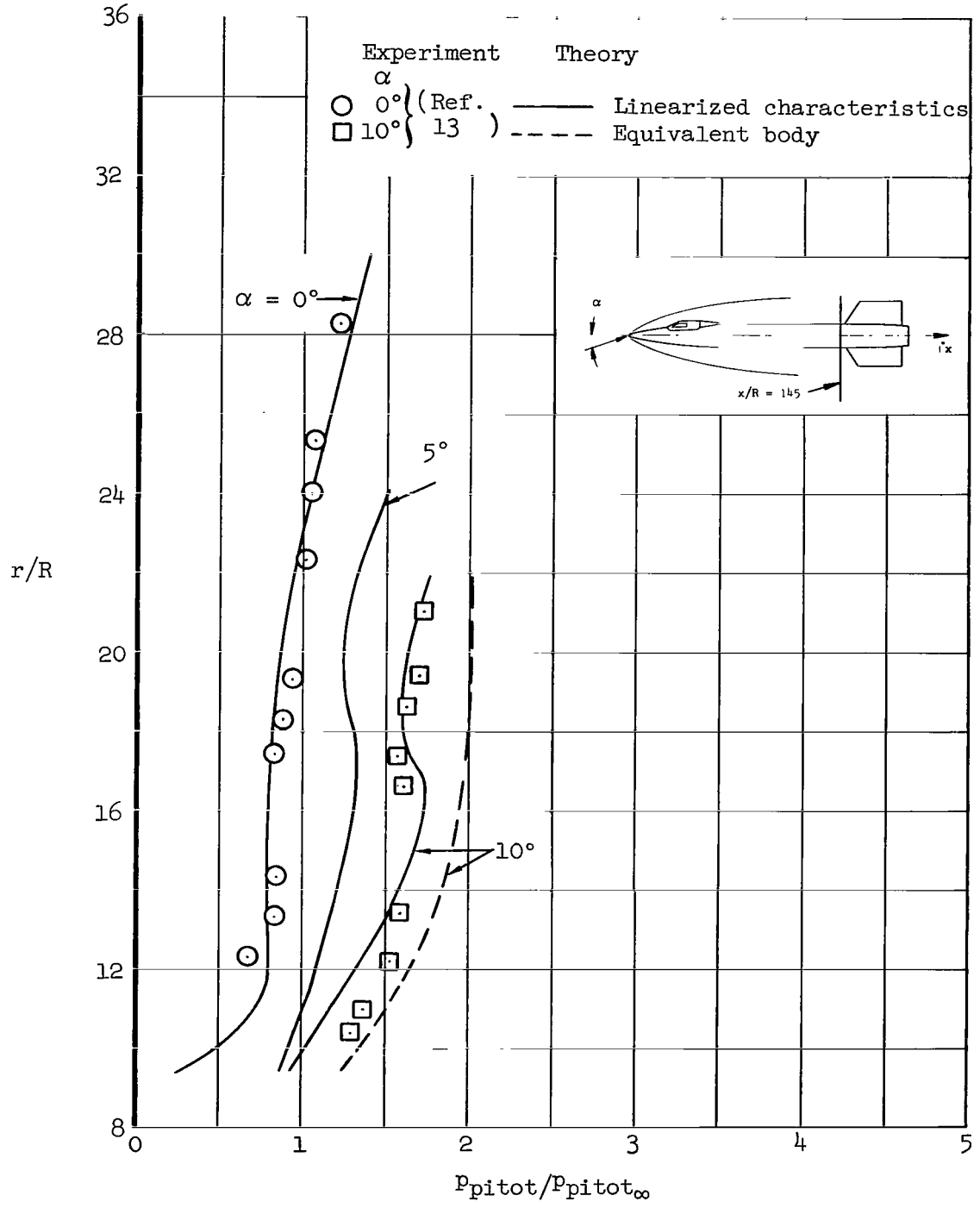

(c) x/R = 145

Figure 10.- Concluded.

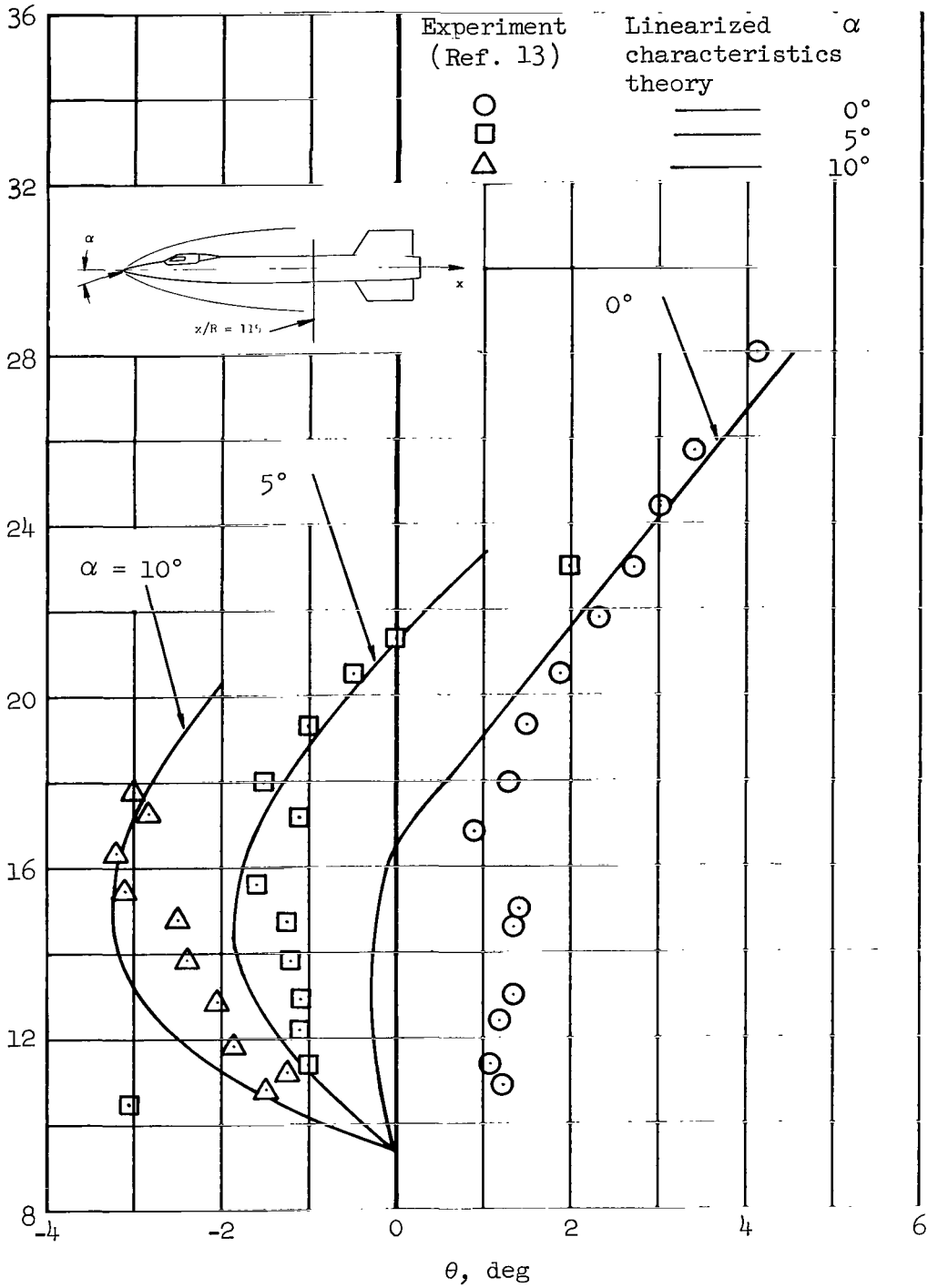

(a) x/R = 115

Figure 11.- Flow angle profiles; X-15, $\Phi = 180°$, $M_\infty = 8.0$.

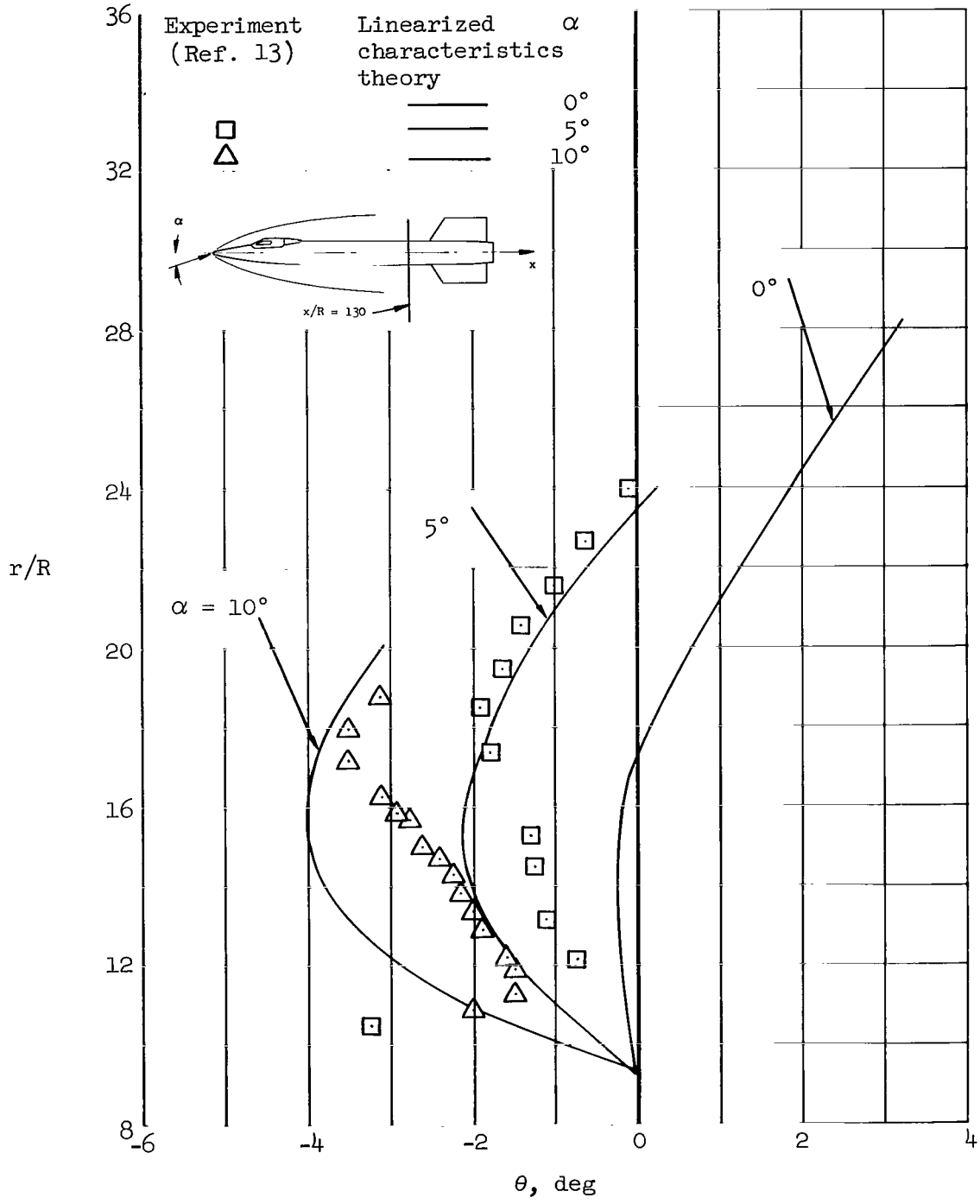

(b) x/R = 130

Figure 11.- Continued.

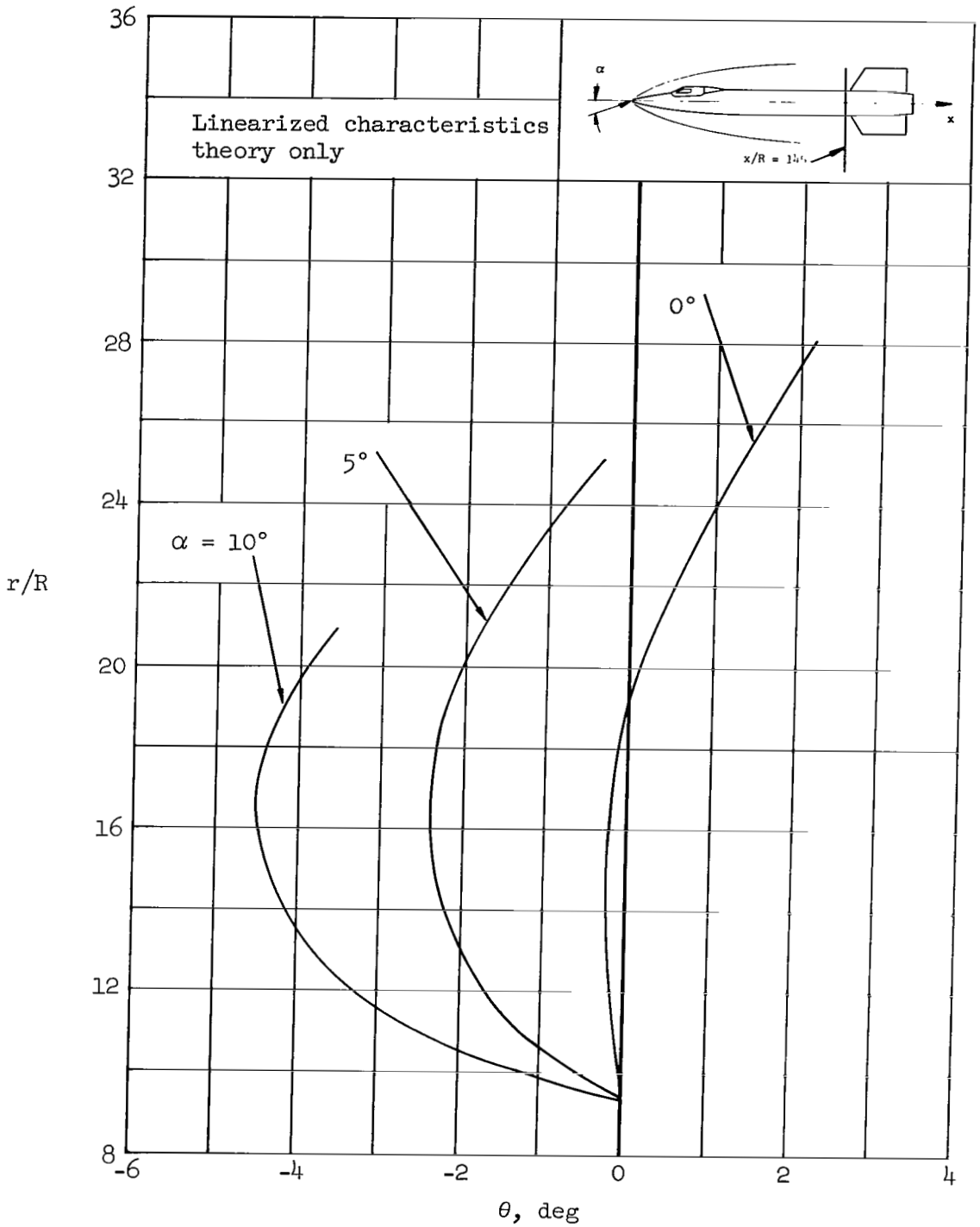

(c) x/R = 145

Figure 11.- Concluded.

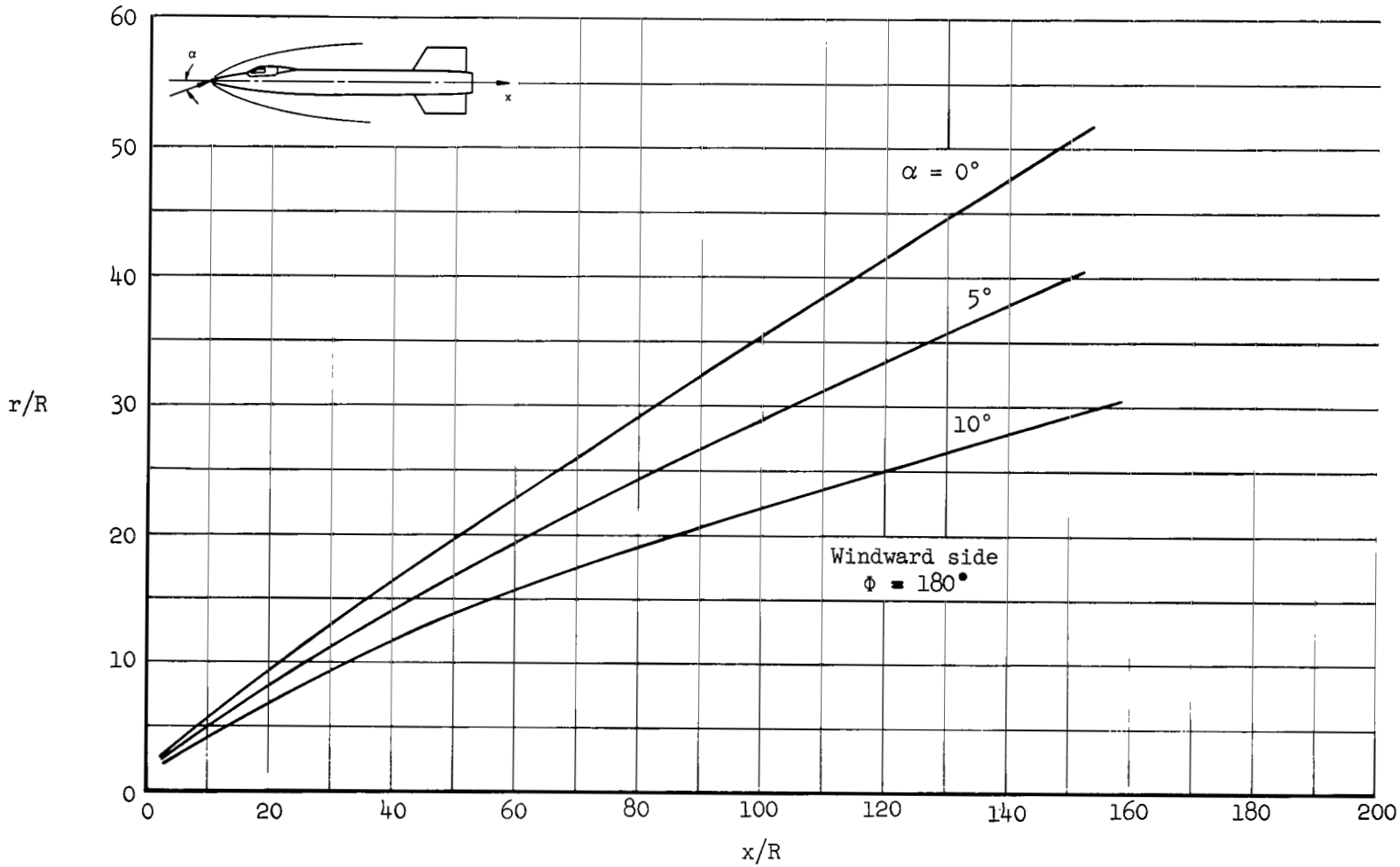

(a) $M_\infty = 4.0$

Figure 12.- Bow-shock location on the X-15.

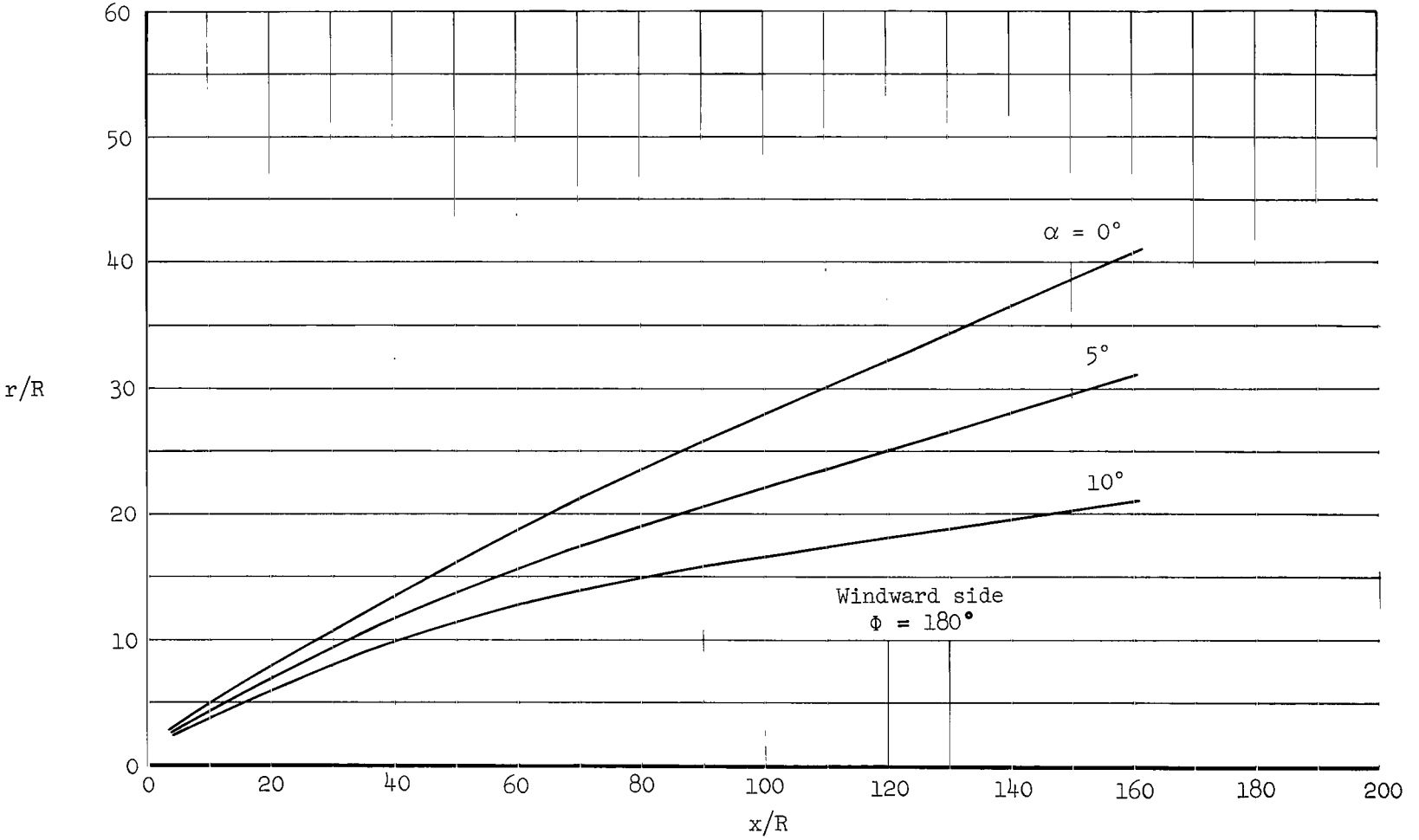

(b) $M_\infty = 6.0$

Figure 12.- Continued.

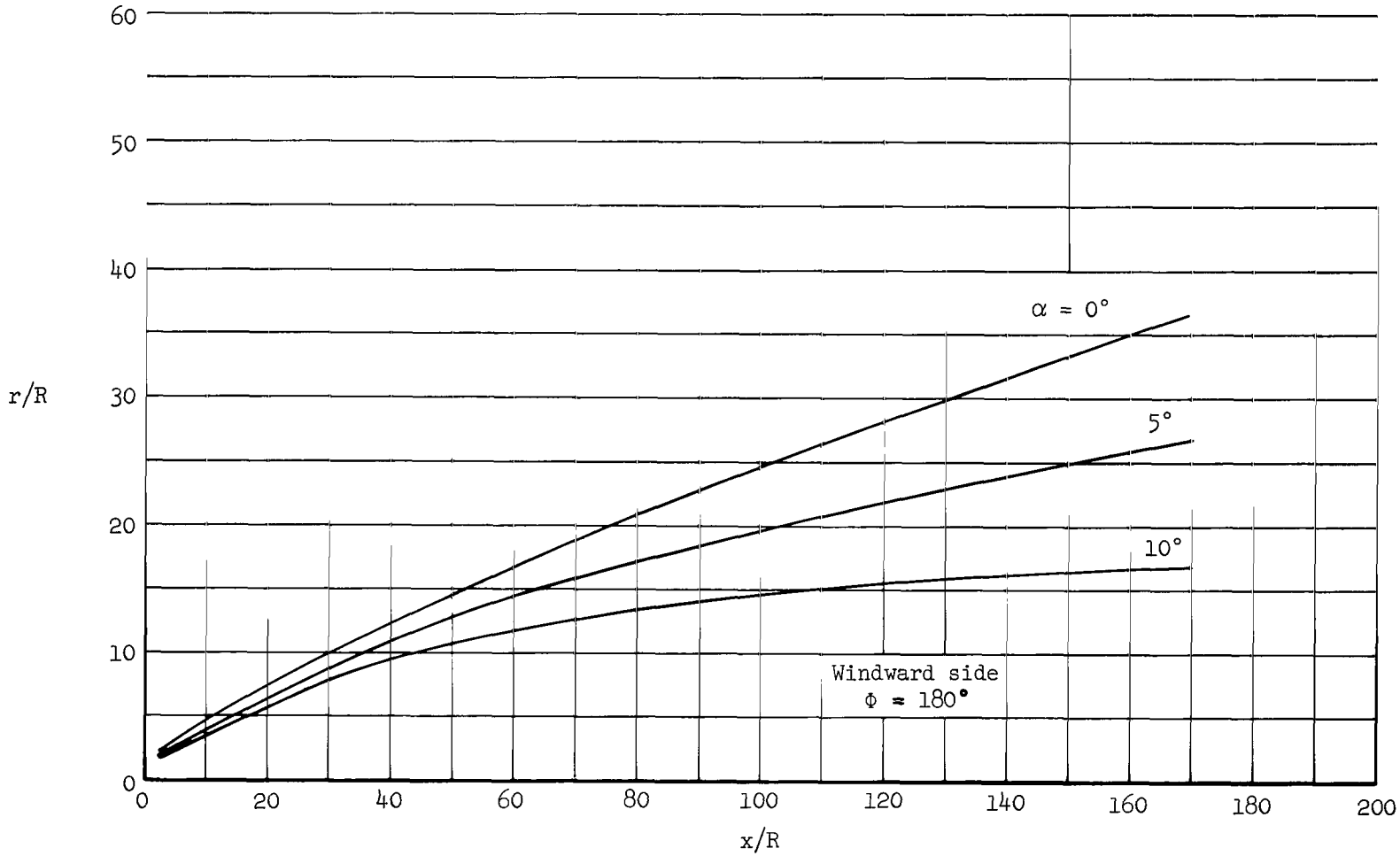

(c) $M_\infty = 8.0$

Figure 12.- Concluded.

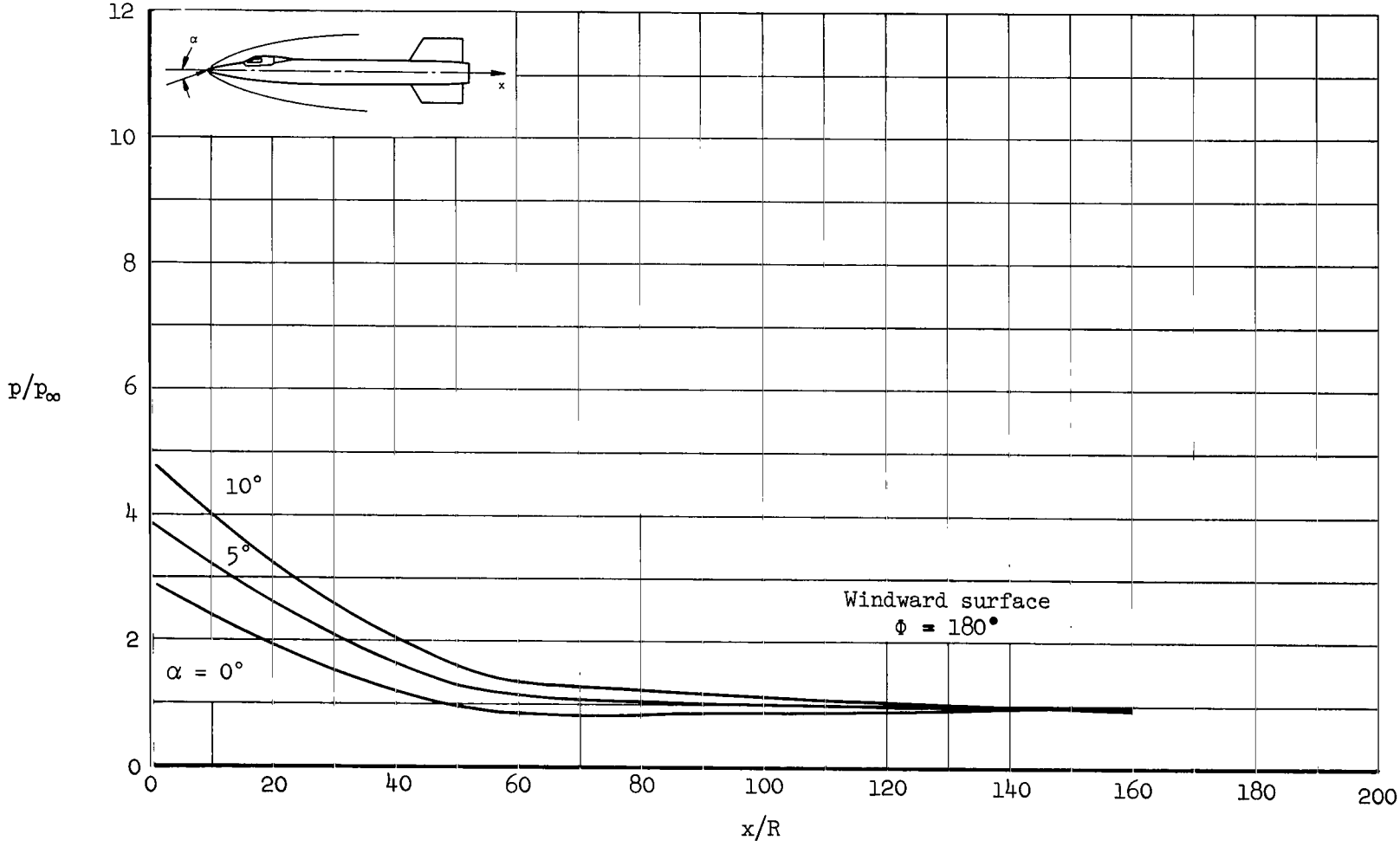

(a) $M_\infty = 4.0$

Figure 13.- Longitudinal surface static pressure distribution on the X-15.

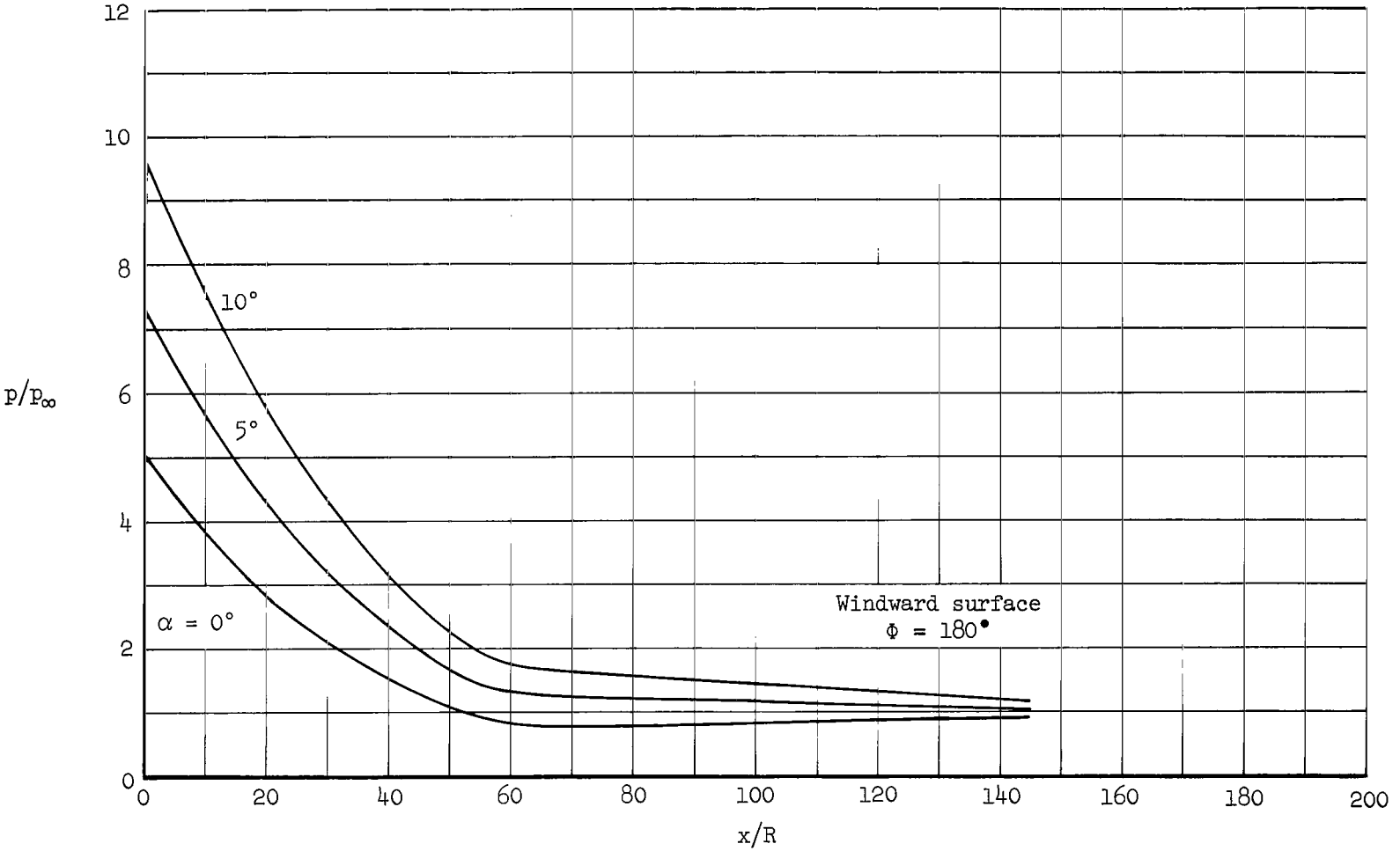

(b) $M_\infty = 6.0$

Figure 13.- Continued.

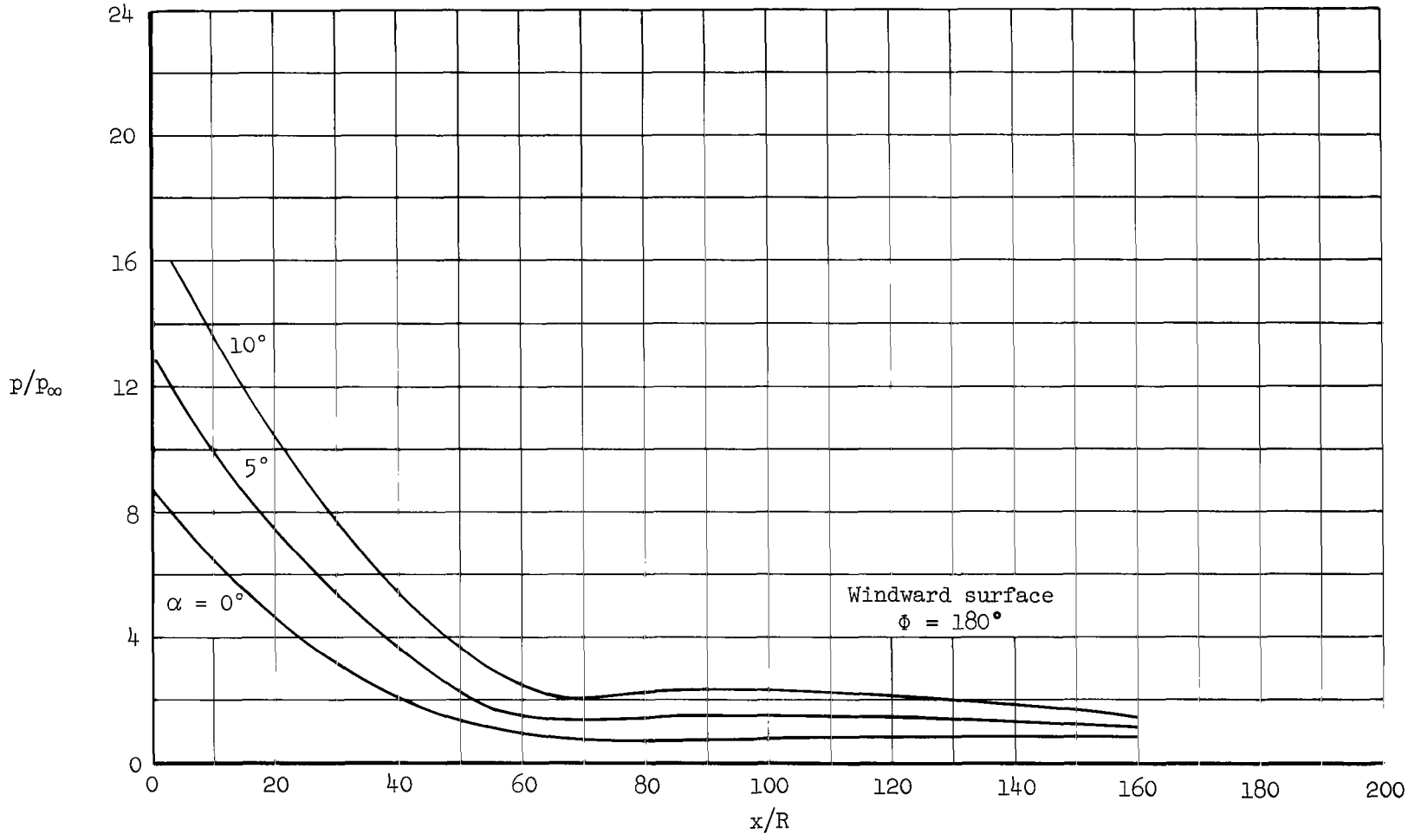

(c) $M_\infty = 8.0$

Figure 13.- Concluded.

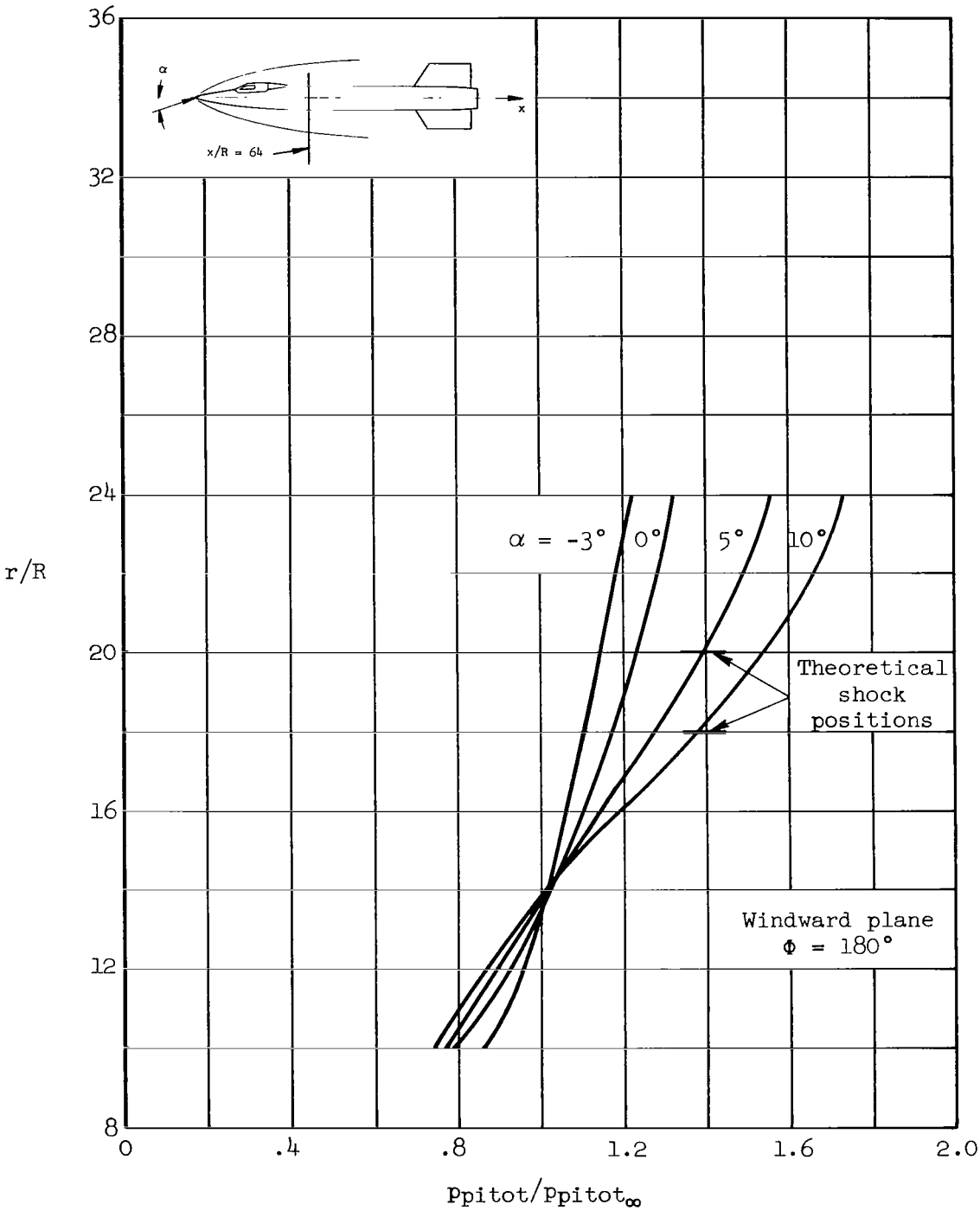

(a) $M_\infty = 4.0$

Figure 14.- Pitot pressure profiles on the X-15 at x/R = 64.0.

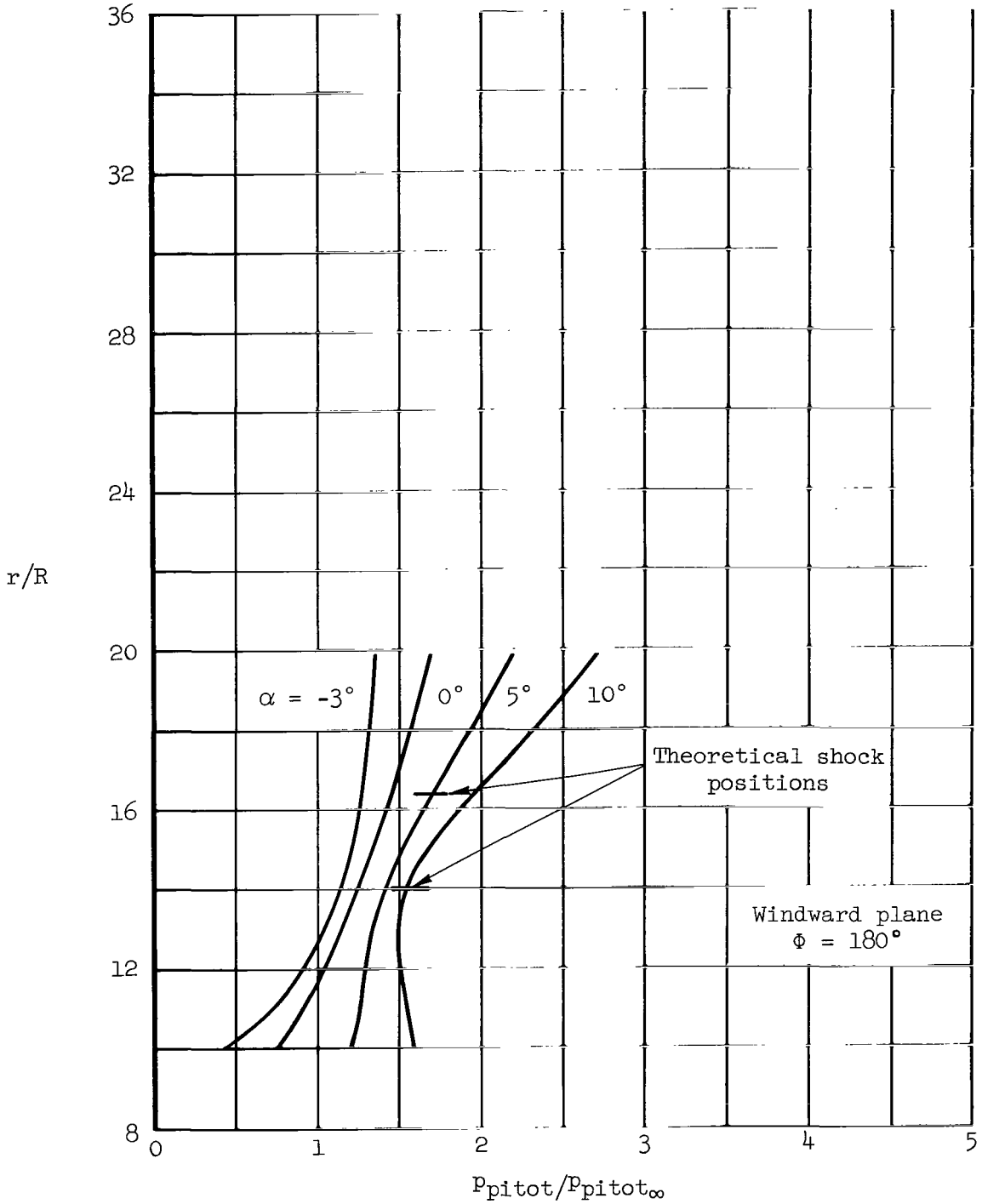

(b) $M_\infty = 6.0$

Figure 14.- Continued.

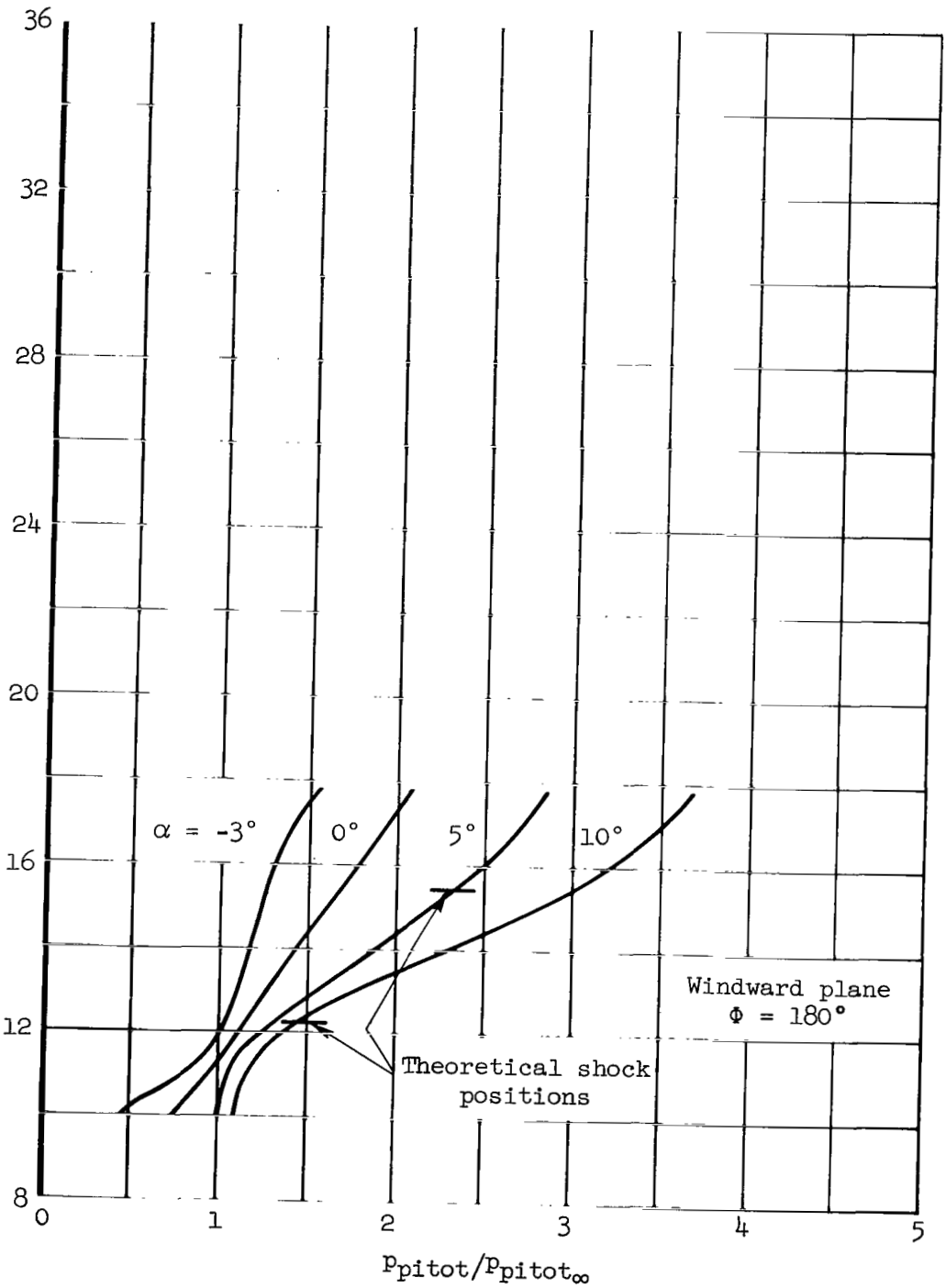

(c) $M_\infty = 8.0$

Figure 14.- Concluded.

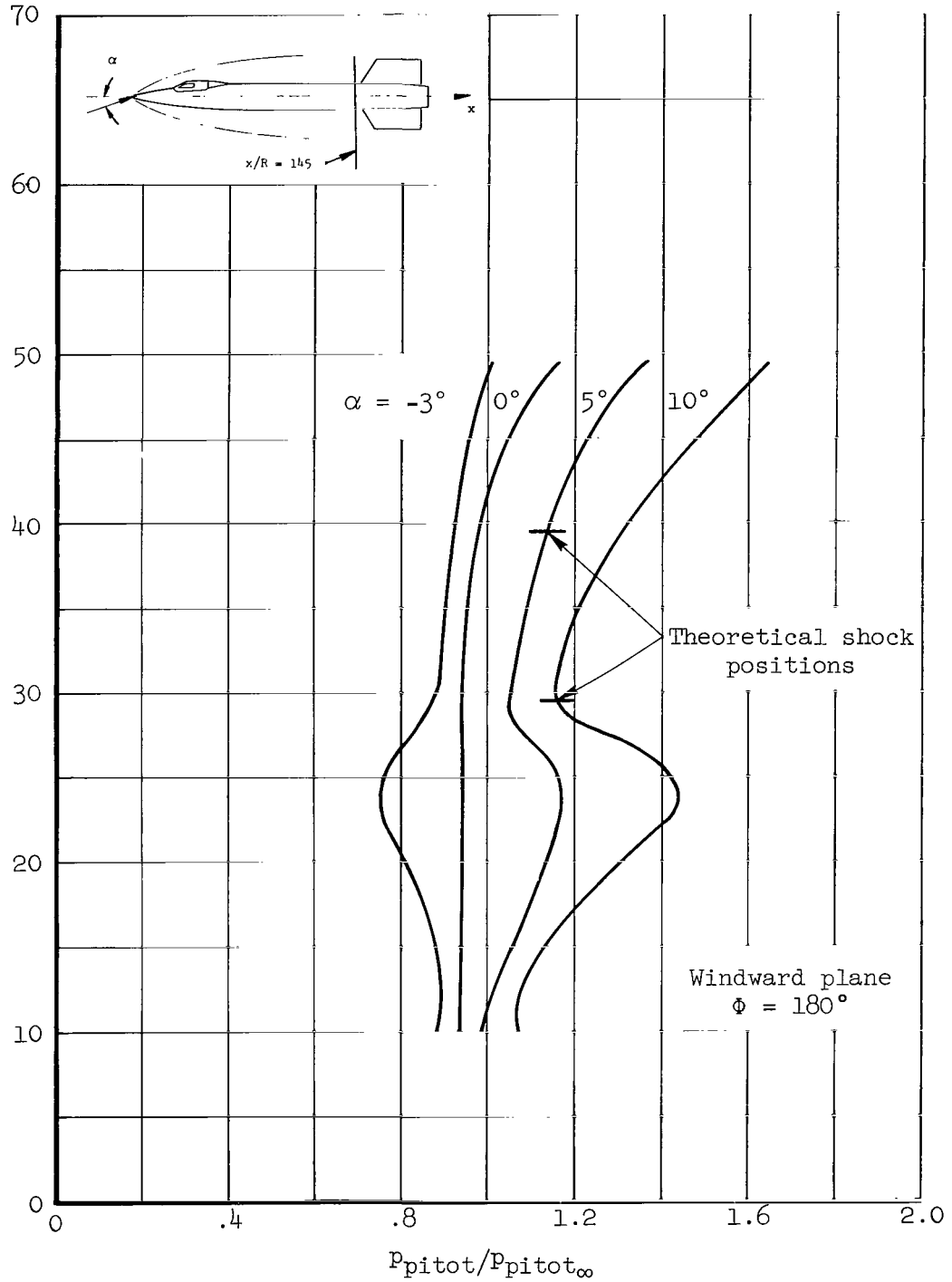

(a) $M_\infty = 4.0$

Figure 15.- Pitot pressure profiles on the X-15 at x/R = 145.0.

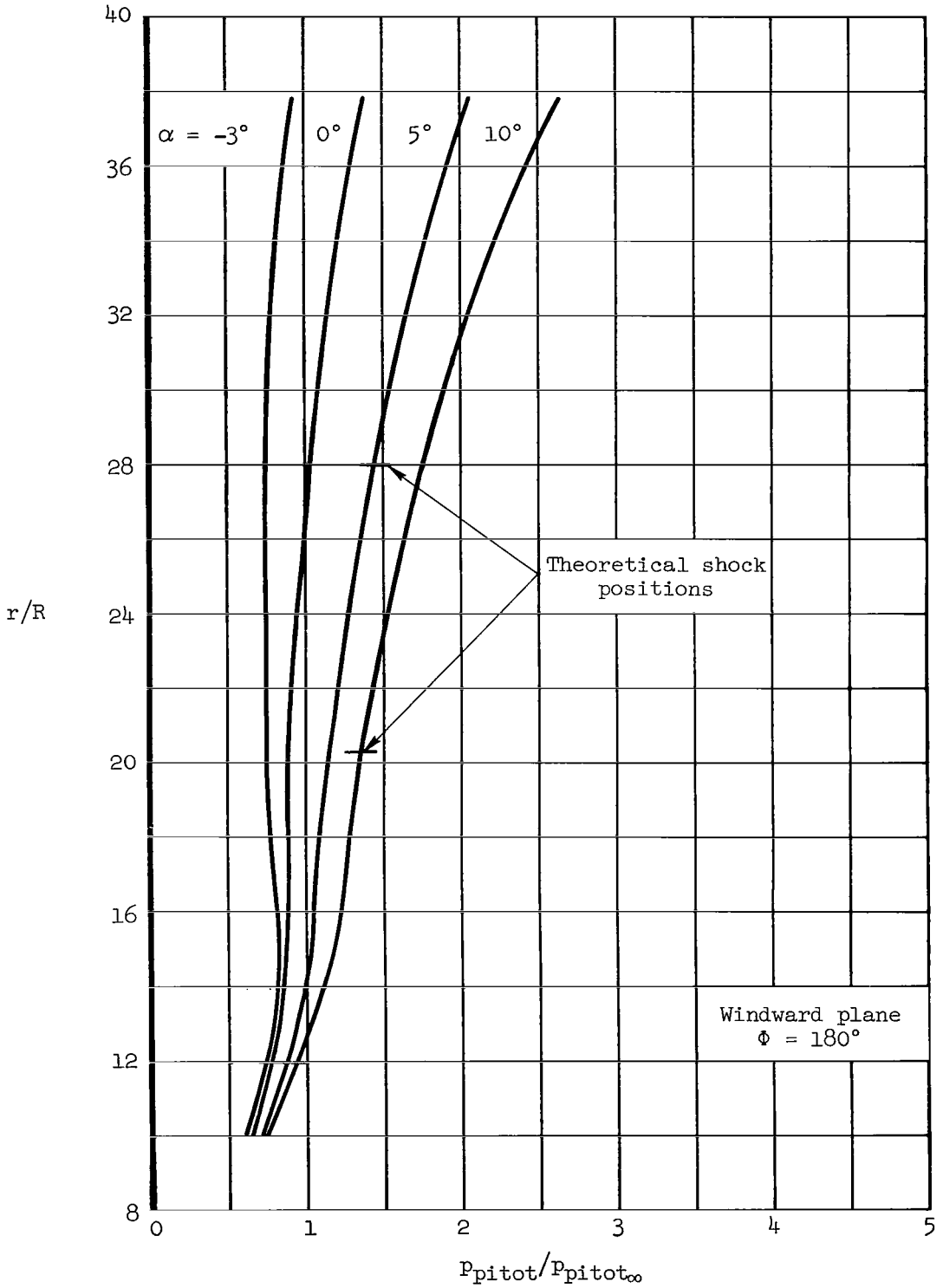

(b) $M_\infty = 6.0$

Figure 15.- Continued.

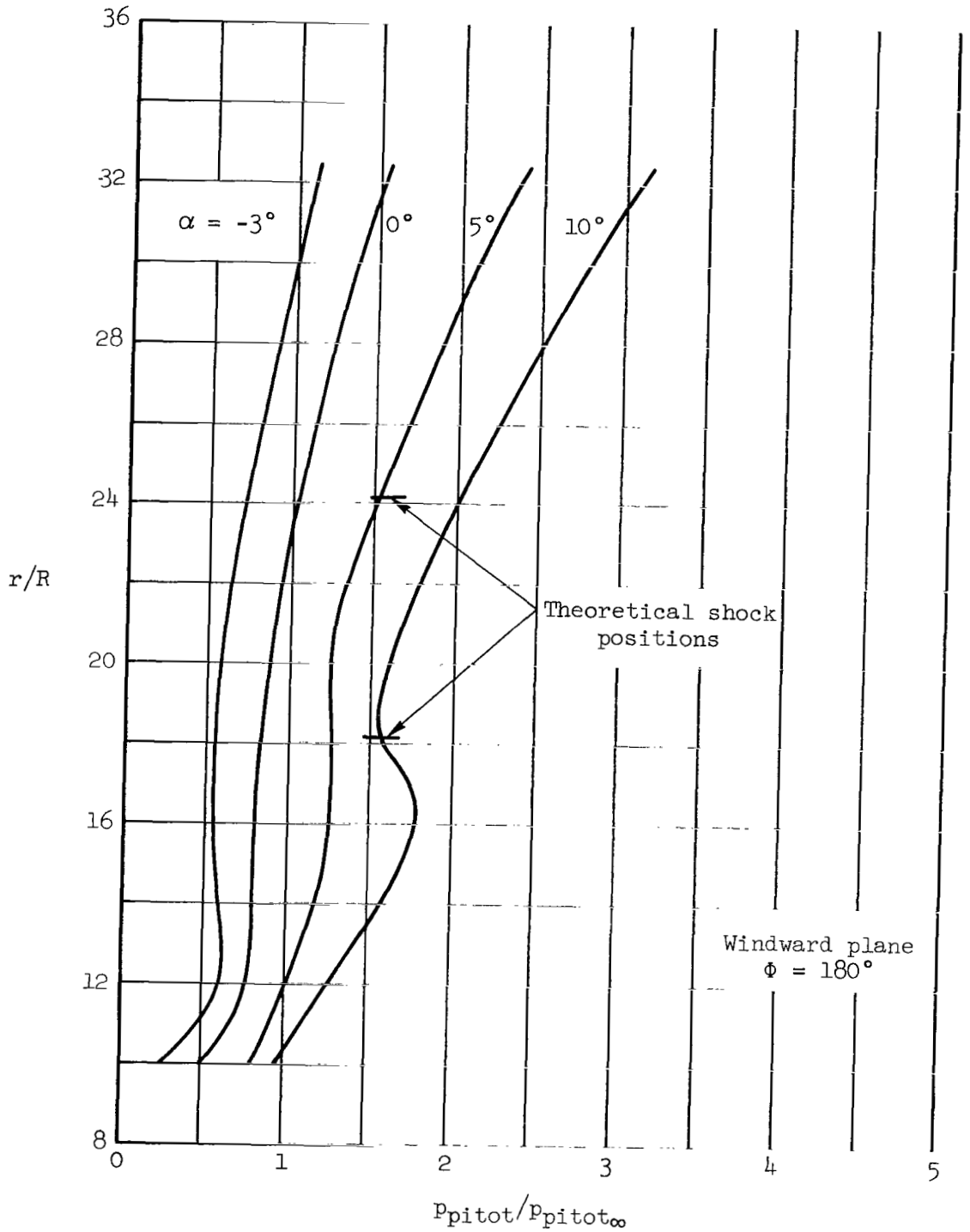

(c) $M_\infty = 8.0$

Figure 15.- Concluded.

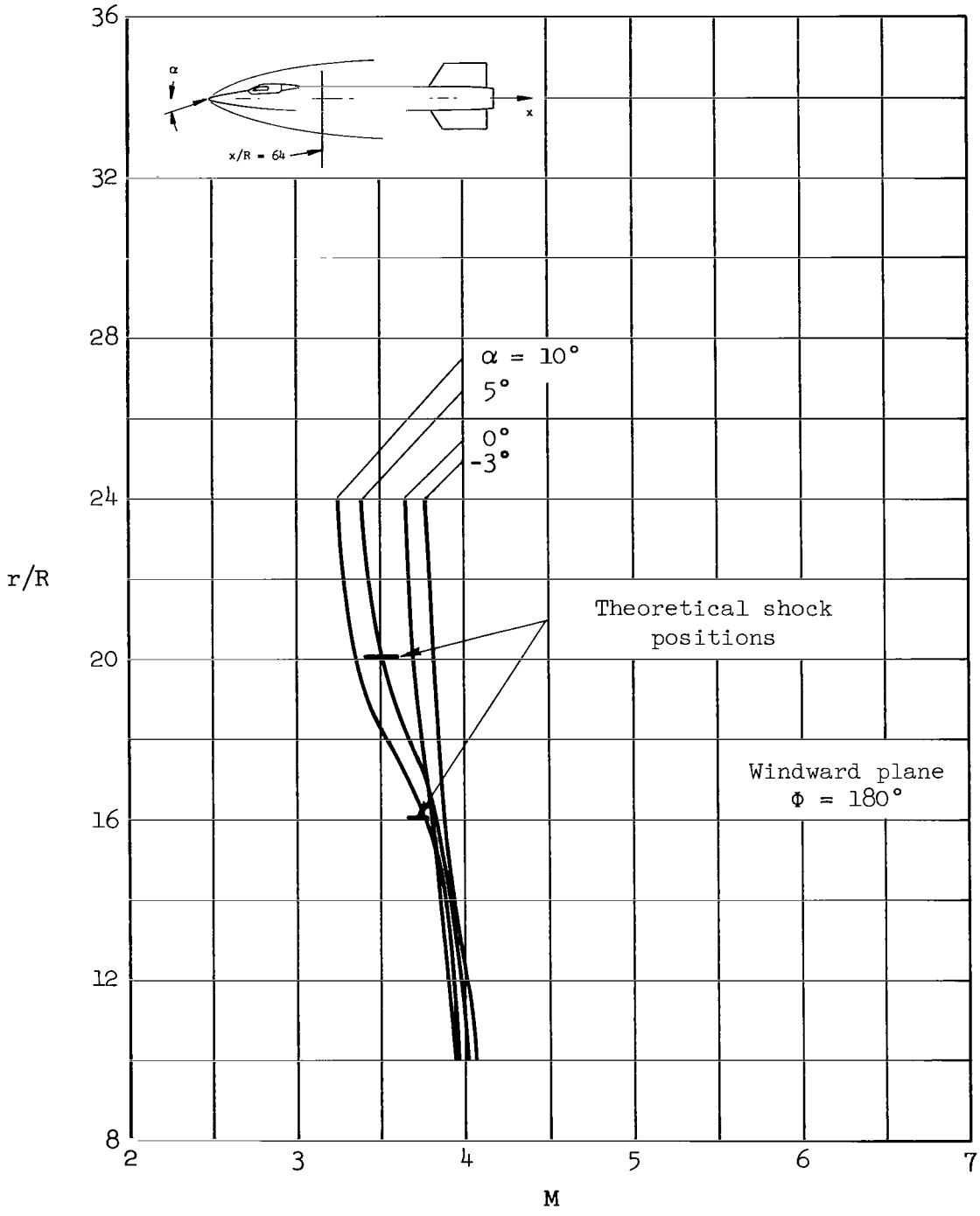

(a) $M_\infty = 4.0$

Figure 16.- Local Mach number profiles on the X-15 at x/R = 64.0.

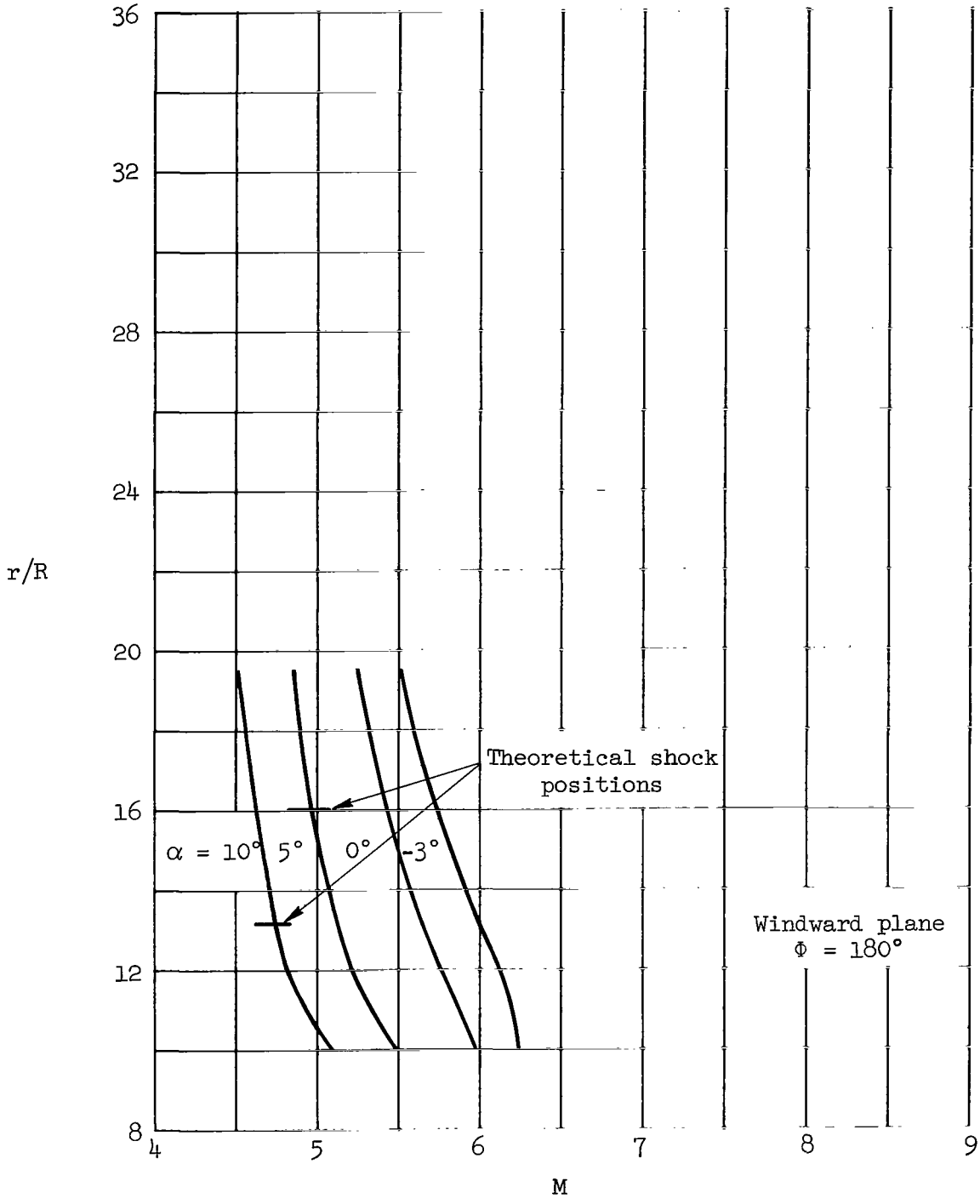

(b) $M_\infty = 6.0$

Figure 16.- Continued.

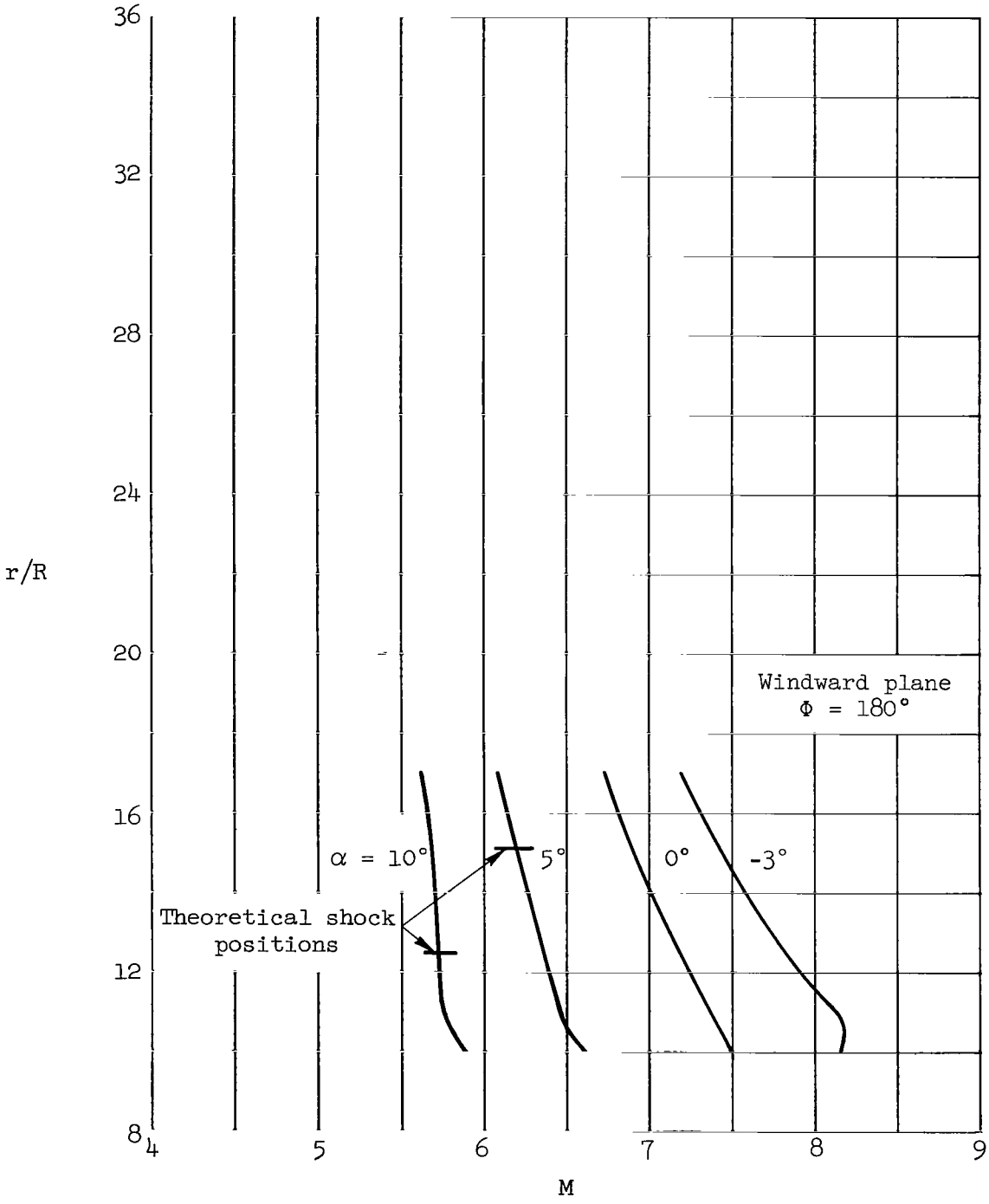

(c) $M_\infty = 8.0$

Figure 16.- Concluded.

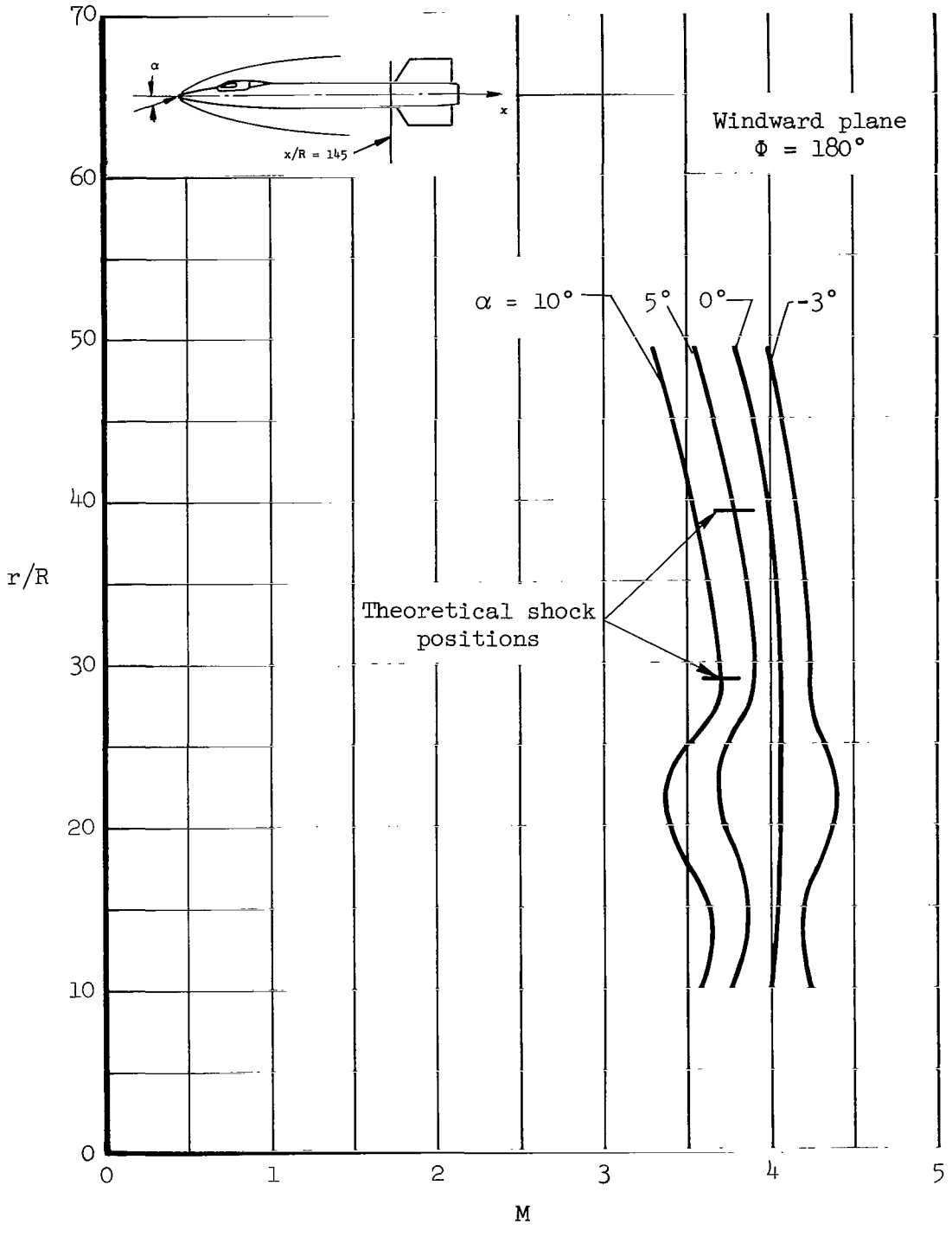

(a) $M_\infty = 4.0$

Figure 17.- Local Mach number profiles on the X-15 at x/R = 145.0.

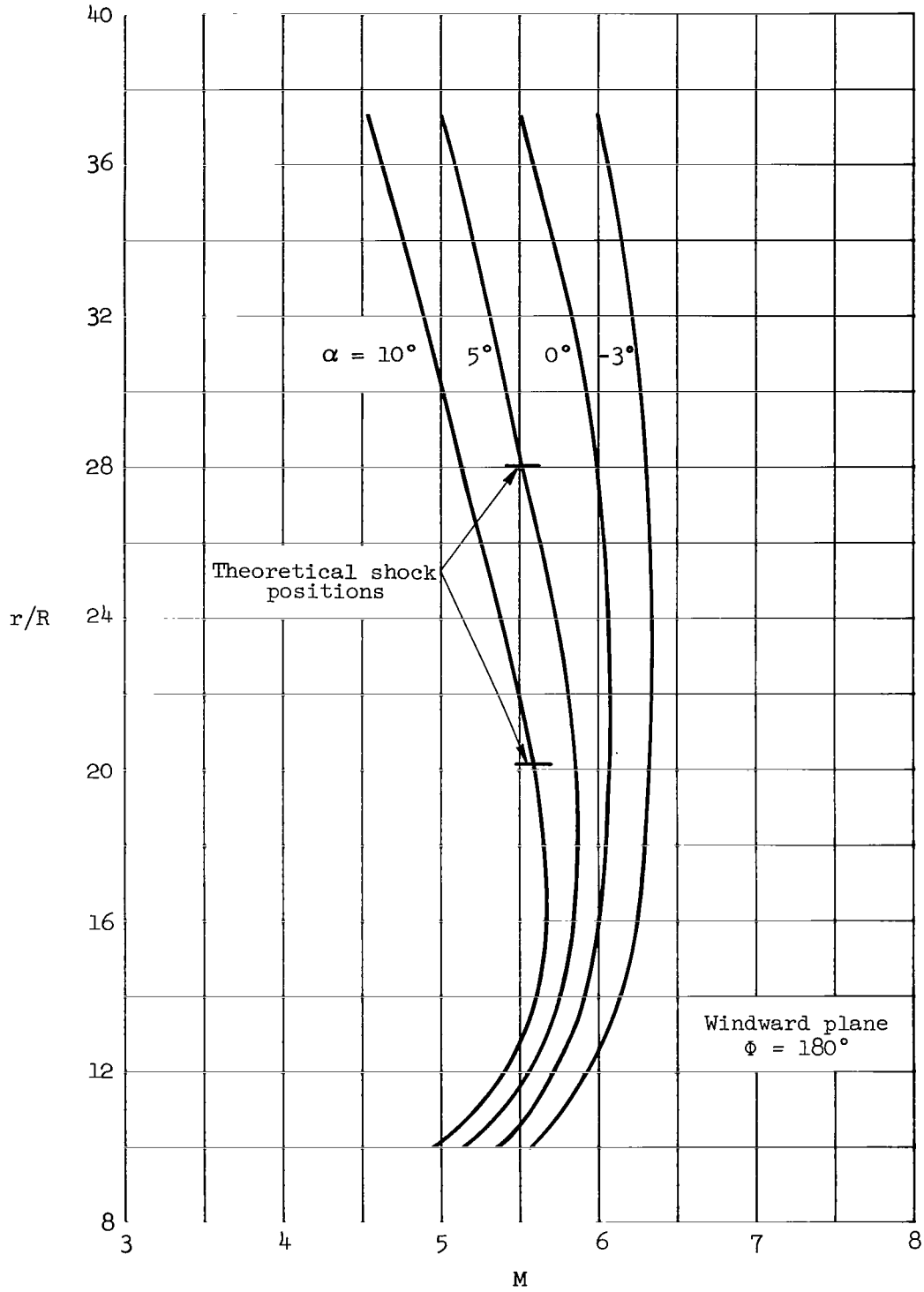

(b) $M_\infty = 6.0$

Figure 17.- Continued.

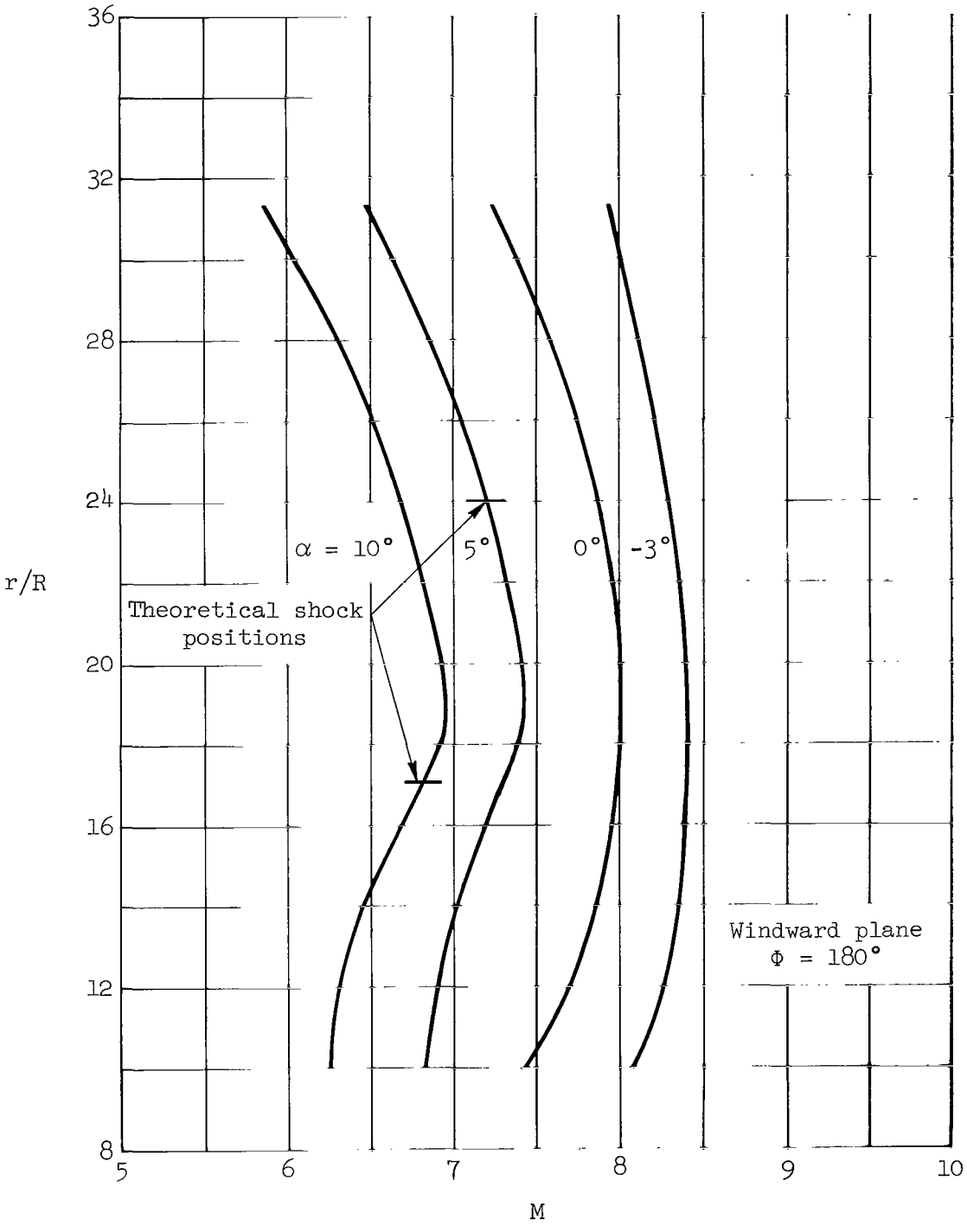

(c) $M_\infty = 8.0$

Figure 17.- Concluded.

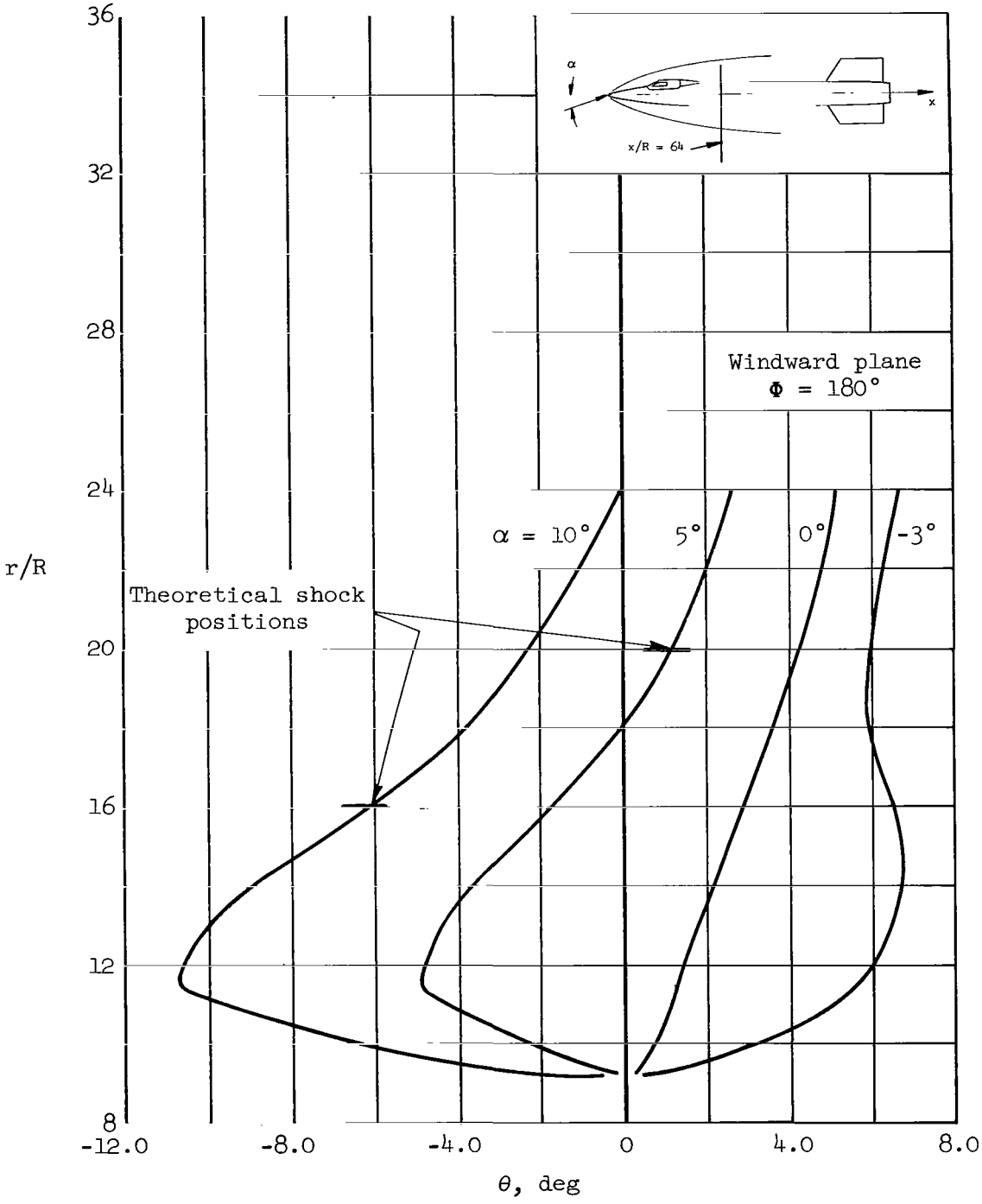

(a) $M_\infty = 4.0$

Figure 18.- Flow angle profiles on the X-15 at x/R = 64.0.

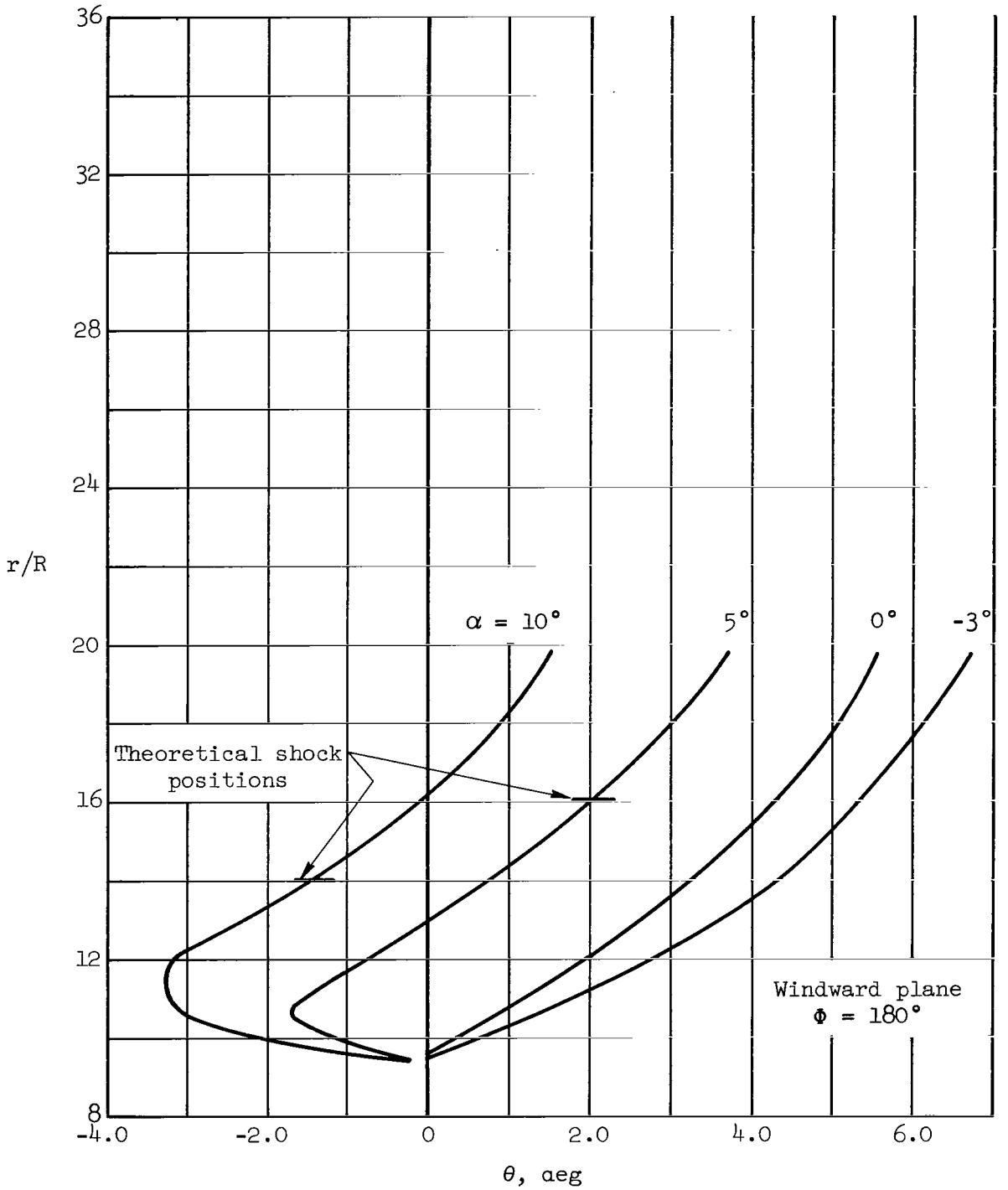

(b) $M_\infty = 6.0$

Figure 18.- Continued.

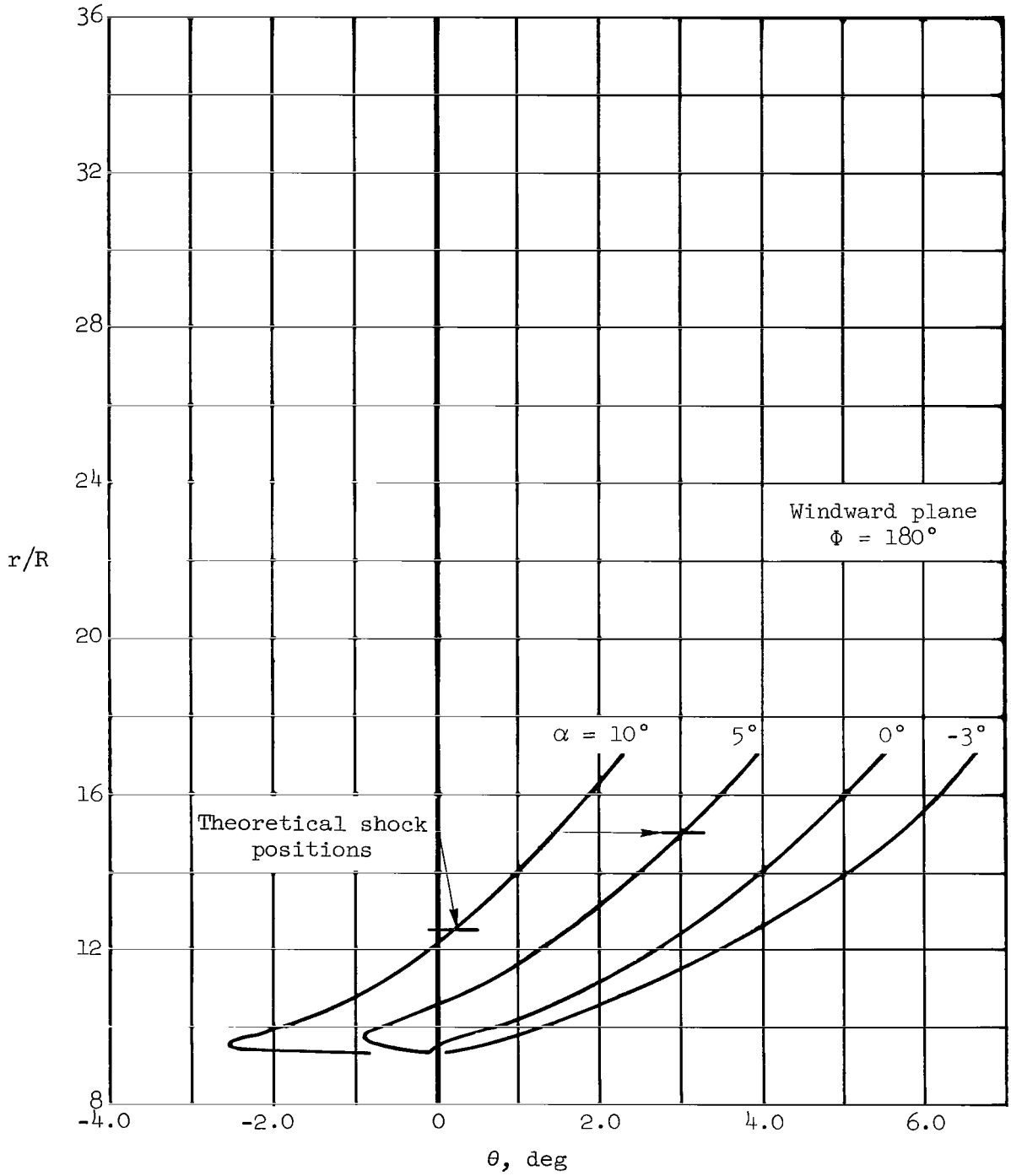

(c) $M_\infty = 8.0$

Figure 18.- Concluded.

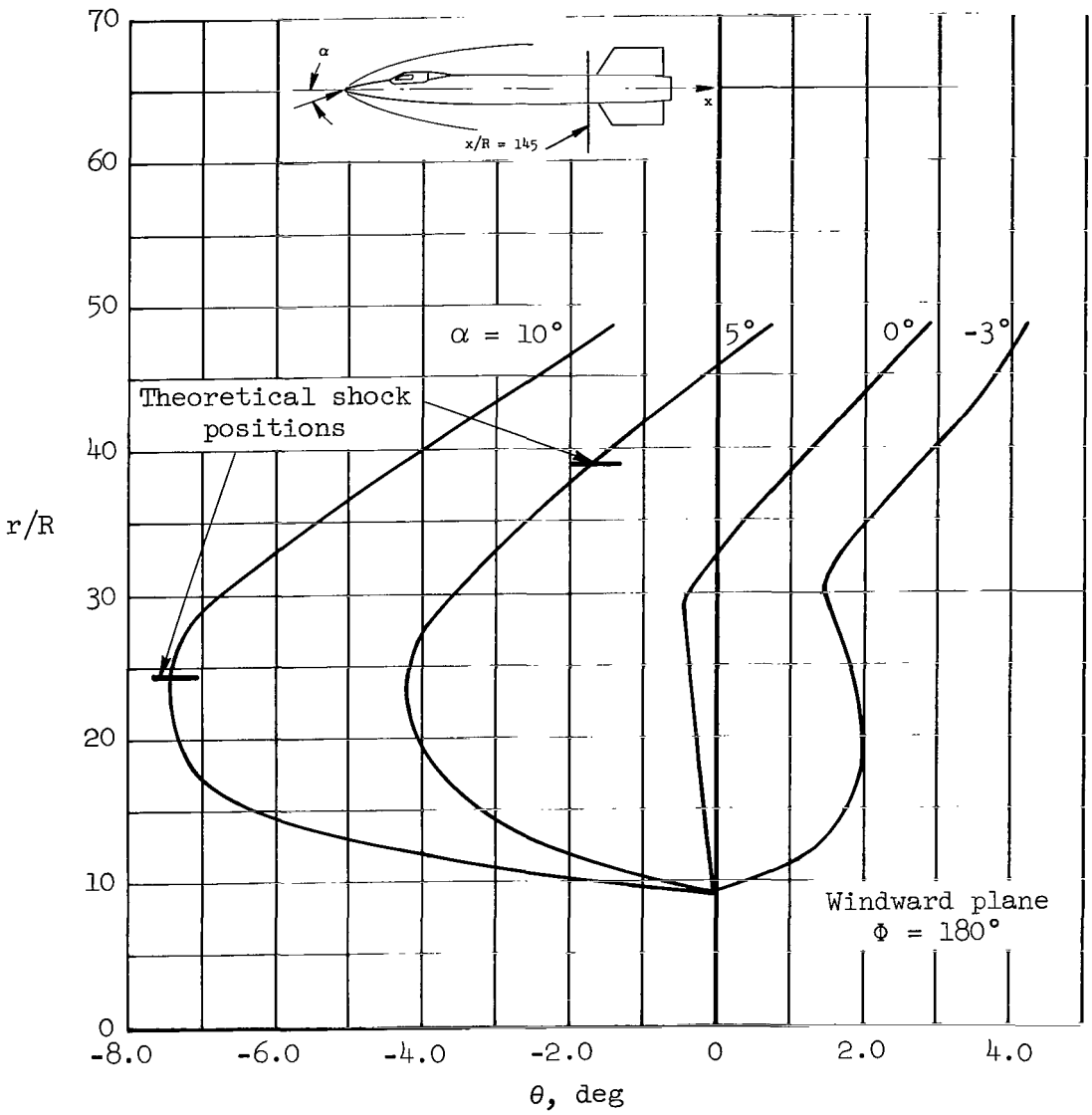

(a) $M_\infty = 4.0$

Figure 19.- Flow angle profiles on the X-15 at x/R = 145.0.

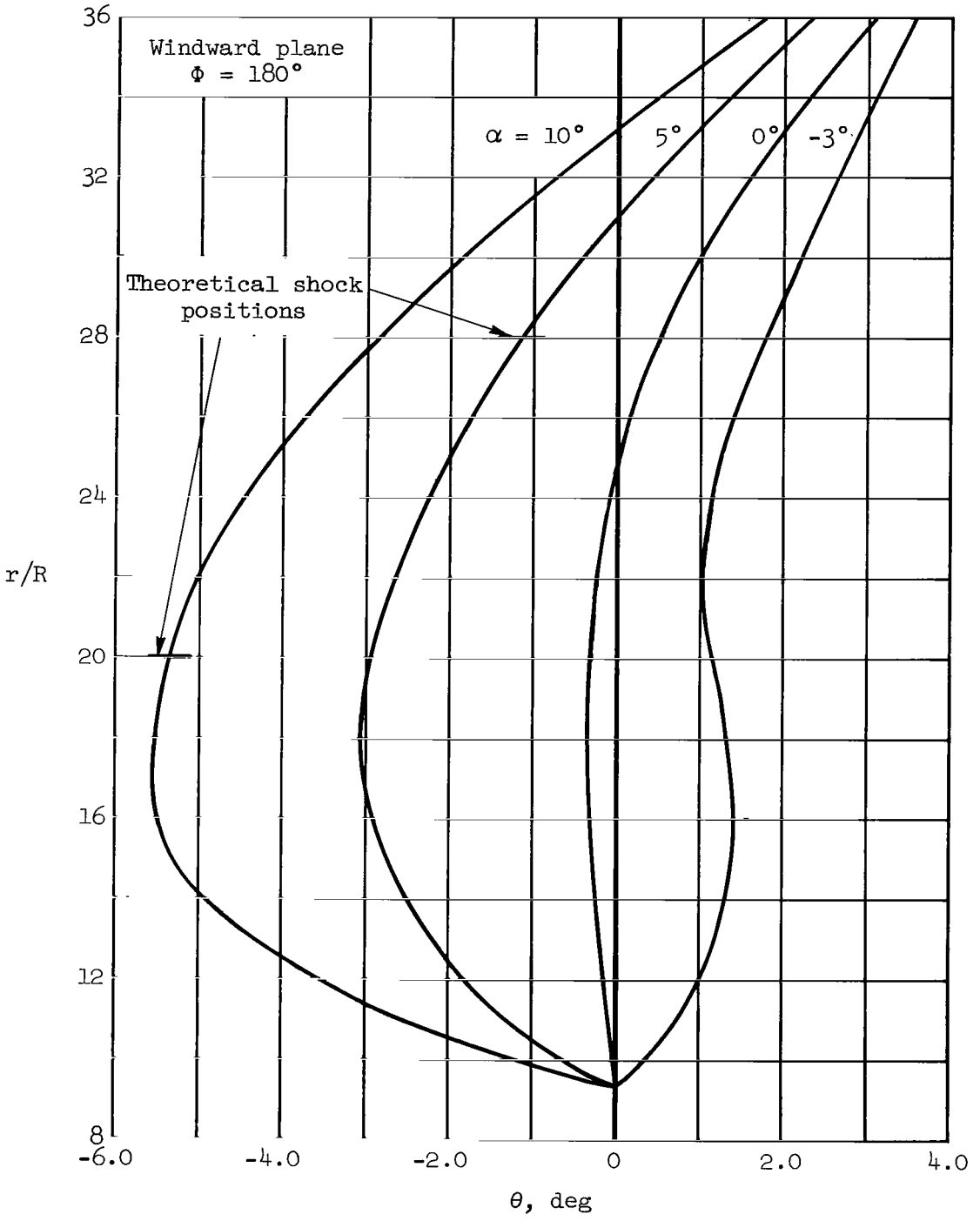

(b) $M_\infty = 6.0$

Figure 19.- Continued.

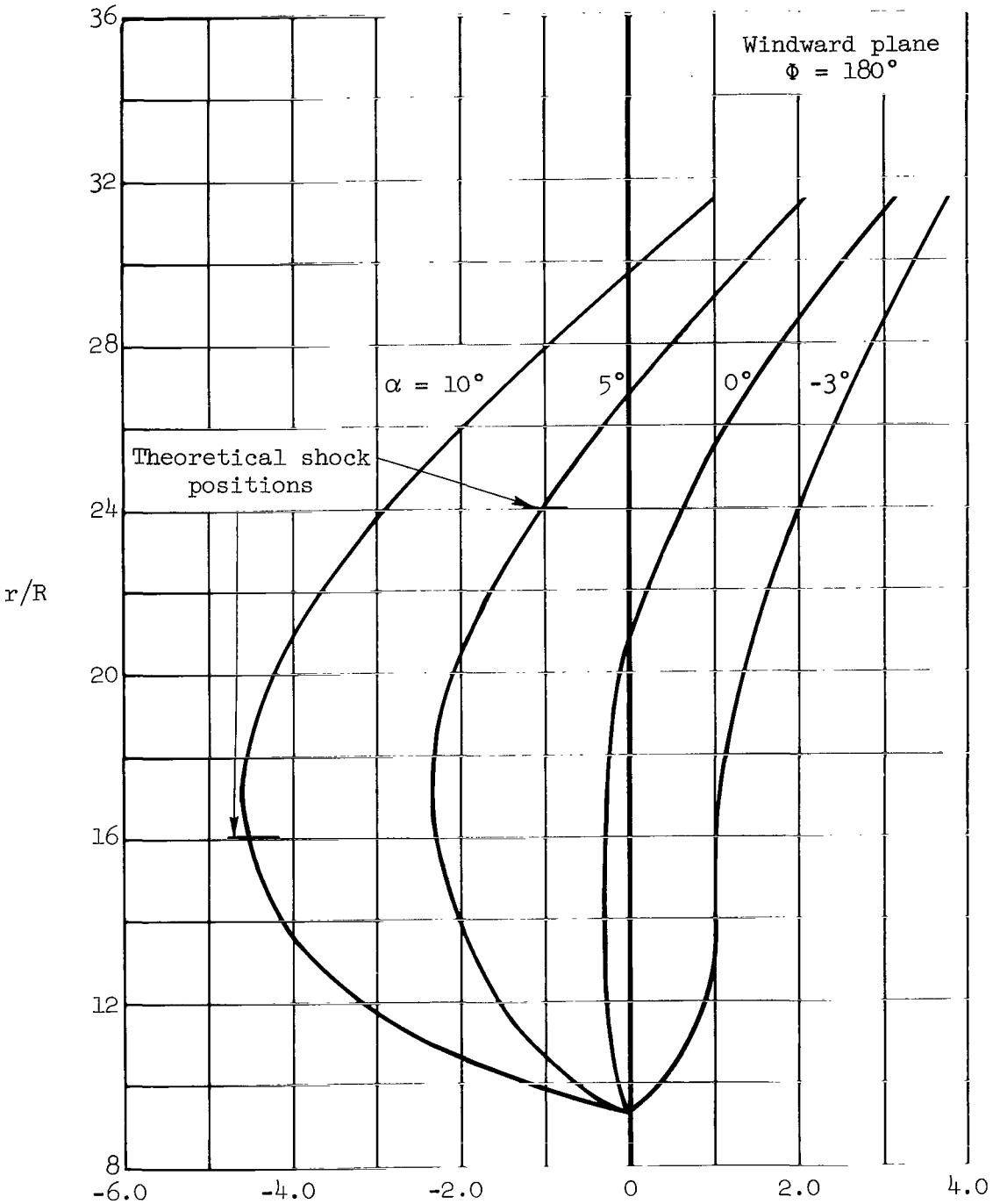

(c) $M_\infty = 8.0$

Figure 19.- Concluded.

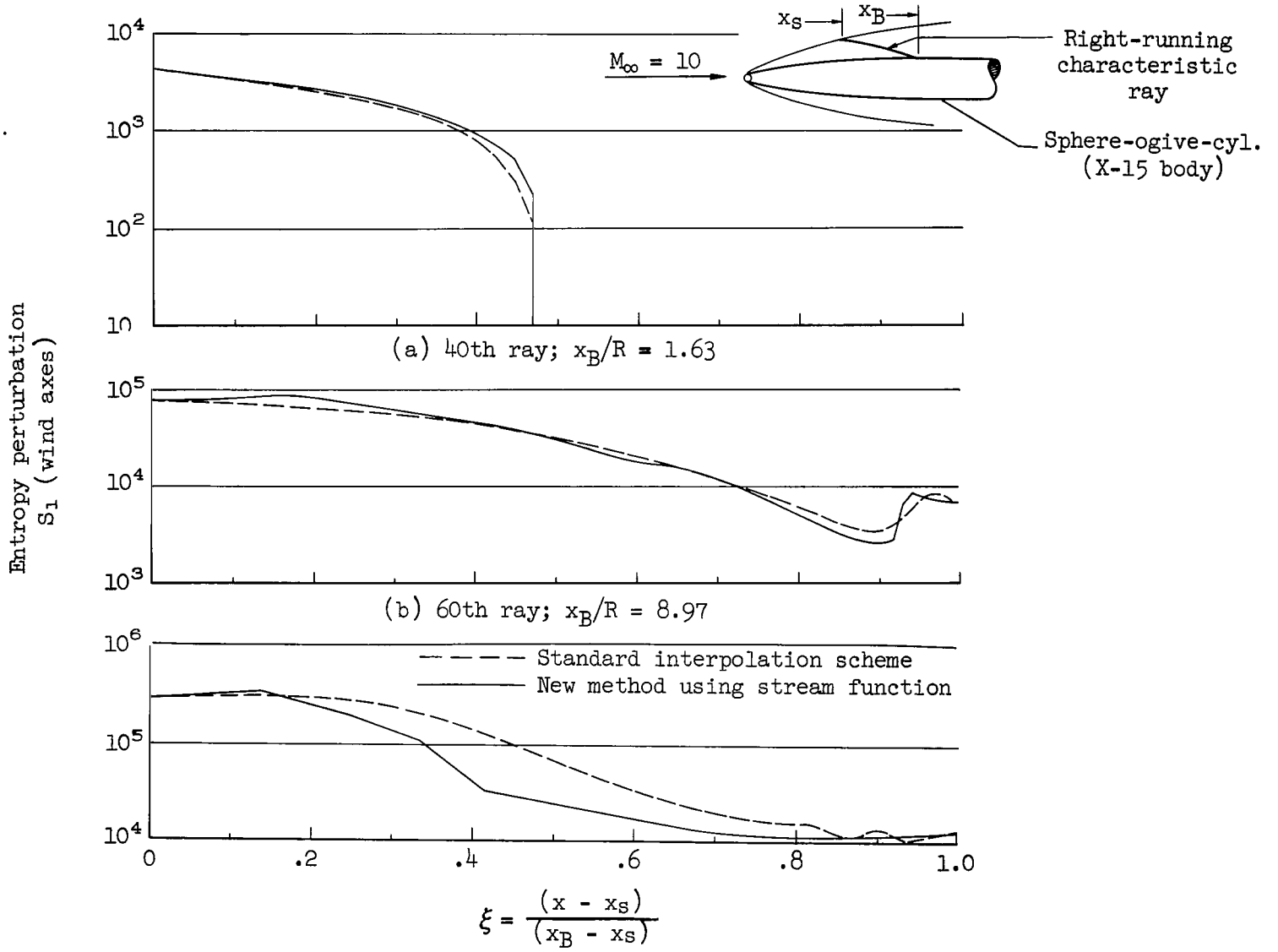

Figure 20.- Entropy perturbation in the shock layer for a sphere-ogive-cylinder; $M_\infty = 10$.

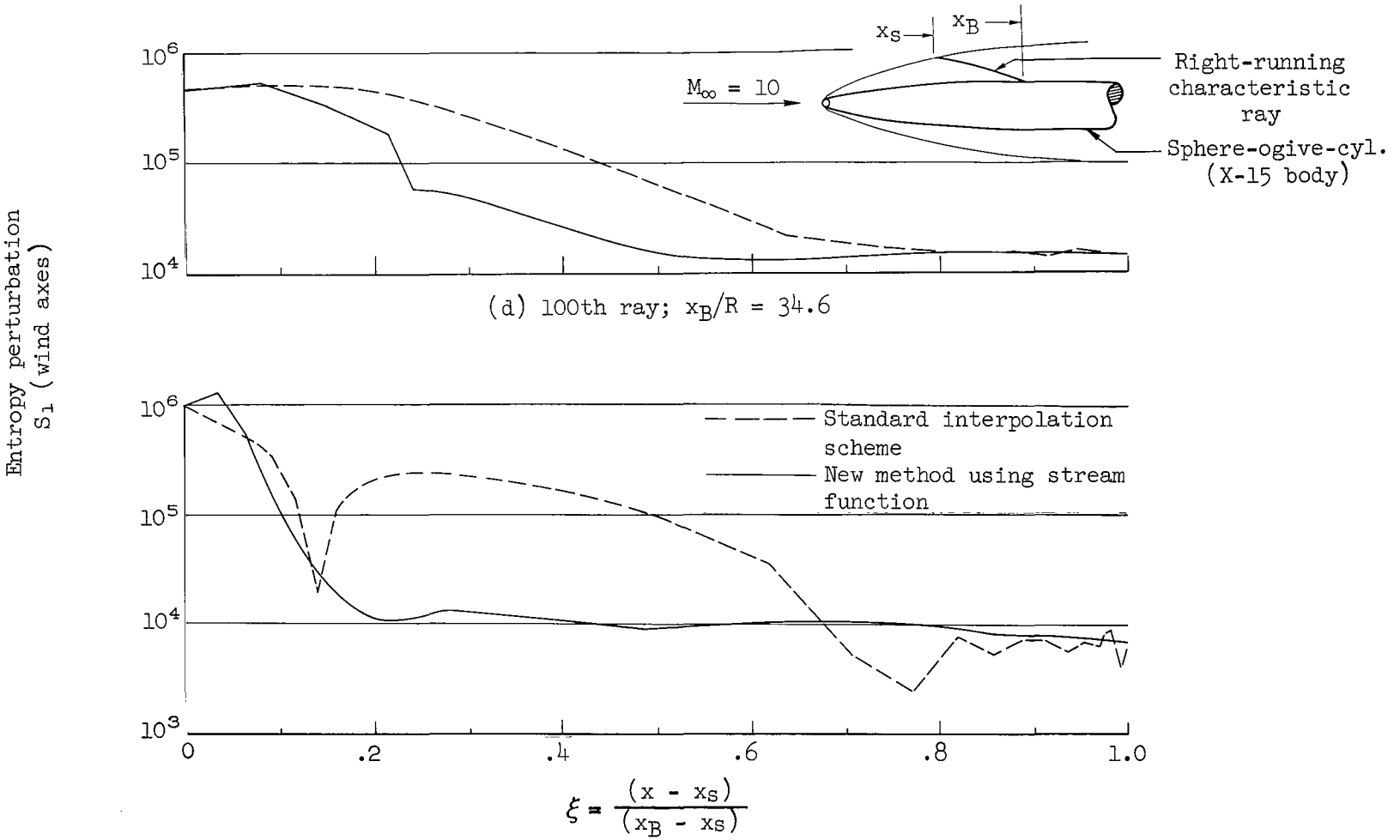

Figure 20.- Concluded.

"The aeronautical and space activities of the United States shall be conducted so as to contribute . . . to the expansion of human knowledge of phenomena in the atmosphere and space. The Administration shall provide for the widest practicable and appropriate dissemination of information concerning its activities and the results thereof."

—NATIONAL AERONAUTICS AND SPACE ACT OF 1958

NASA SCIENTIFIC AND TECHNICAL PUBLICATIONS

TECHNICAL REPORTS: Scientific and technical information considered important, complete, and a lasting contribution to existing knowledge.

TECHNICAL NOTES: Information less broad in scope but nevertheless of importance as a contribution to existing knowledge.

TECHNICAL MEMORANDUMS: Information receiving limited distribution because of preliminary data, security classification, or other reasons.

CONTRACTOR REPORTS: Scientific and technical information generated under a NASA contract or grant and considered an important contribution to existing knowledge.

TECHNICAL TRANSLATIONS: Information published in a foreign language considered to merit NASA distribution in English.

SPECIAL PUBLICATIONS: Information derived from or of value to NASA activities. Publications include conference proceedings, monographs, data compilations, handbooks, sourcebooks, and special bibliographies.

TECHNOLOGY UTILIZATION PUBLICATIONS: Information on technology used by NASA that may be of particular interest in commercial and other non-aerospace applications. Publications include Tech Briefs, Technology Utilization Reports and Notes, and Technology Surveys.

Details on the availability of these publications may be obtained from:

SCIENTIFIC AND TECHNICAL INFORMATION DIVISION

NATIONAL AERONAUTICS AND SPACE ADMINISTRATION

Washington, D.C. 20546